

Volume 4 • Issue 1 June 2021

 sciendo



"GEORGE EMIL PALADE"
UNIVERSITY OF MEDICINE,
PHARMACY, SCIENCE AND TECHNOLOGY
OF TÂRGU MUREȘ

ACTA BIOLOGICA MARISIENSIS



ISSN 2601 - 6141 (Print)
ISSN-L 2601 - 6141 (Online)
ISSN - 2668 - 5124 (Online)

www.abmj.ro

ACTA BIOLOGICA MARISIENSIS

Official Journal of the George Emil Palade University of Medicine, Pharmacy, Science, and Technology
of Târgu Mureș

Acta Biologica Marisiensis

ISSN: 2601 – 6141 (Print)

ISSN-L: 2601 – 6141

ISSN: 2668 – 5124 (Online)

Published by University Press Târgu Mureș in cooperation with Sciendo by De Gruyter

Contact information:

George Emil Palade University of Medicine, Pharmacy, Science, and Technology of Târgu Mureș

Gheorghe Marinescu street no. 38, Târgu Mureș, 540139, ROMANIA

Phone: +40-265-21 55 51, fax +40-265-21 04 07

E-mail: abmjournal@umfst.ro



EDITORIAL BOARD

EDITOR IN CHIEF

Corneliu Tanase

George Emil Palade University of Medicine, Pharmacy, Science, and Technology of Târgu Mureș, Romania

MANAGING EDITOR

Domokos Erzsébet

George Emil Palade University of Medicine, Pharmacy, Science, and Technology of Târgu Mureș, Romania

ASSOCIATE EDITORS

John R. Akeroyd

Plant Talk, Lawn Cottage, West Tisbury, Salisbury, Wiltshire, United Kingdom

Andreea Letiția Arsene

"Carol Davila" University of Medicine and Pharmacy Bucharest, Romania

Tatiana Calalb

"Nicolae Testemițanu" State University of Medicine and Pharmacy of the Republic of Moldova

Gianina Crișan

"Iuliu Hațieganu" University of Medicine and Pharmacy Cluj-Napoca, Romania

Manuela Claudia Curticăpean

George Emil Palade University of Medicine, Pharmacy, Science, and Technology of Târgu Mureș, Romania

Monica Hăncianu

"Grigore Popa" University of Medicine and Pharmacy Iași, Romania

Kohut Erzsébet

Ferenc Rákóczi II. Transcarpathian Hungarian Institute, Ukraine

Luigi Menghini

Università degli Studi G. D'Annunzio Chieti e Pescara, Chieti, Italia

Andrei Marius Mocan

"Iuliu Hațieganu" University of Medicine and Pharmacy Cluj-Napoca, Romania

Molnár Zsolt

Hungarian Academy of Sciences, Centre for Ecological Research, Hungary

Daniela Lucia Muntean

George Emil Palade University of Medicine, Pharmacy, Science, and Technology of Târgu Mureș, Romania

Anatolie Nistoreanu

"Nicolae Testemițanu" State University of Medicine and Pharmacy of the Republic of Moldova

Silvia Oroian

George Emil Palade University of Medicine, Pharmacy, Science, and Technology of Târgu Mureș, Romania

Papp Nóra

University of Pécs, Faculty of Pharmacy, Hungary

Stanislav Yanev

Bulgarian Academy of Sciences, Sofia, Bulgaria

Zhao-Jun Wei

Hefei University of Technology, School of Food and Biological Engineering, Hefei, China

Gökhan Zengin

Selçuk University, Faculty of Science, Konya, Turkey

Copyright © 2019 by Acta Biologica Marisiensis. All rights reserved.

No part of this publication may be reproduced, stored in a retrieval system, or transmitted in any form or by any means, electronic, mechanical, photocopying, recording or otherwise without either the prior written permission of the Publisher.

Disclaimer

Although each paper has been reviewed by a peer-reviewer, the authors take full responsibility for the scientific content. The views expressed in this journal represent those of the authors or advertisers only. In no way can they be construed necessarily to reflect the view of either the Editors or Publishers.

AIM AND SCOPE

Acta Biologica Marisiensis (ABM) is an official Journal of the George Emil Palade University of Medicine, Pharmacy, Science, and Technology of Târgu Mureș, Romania and is published twice a year. The peer-reviewed journal is dedicated to the life sciences and publishes articles in the following fields: biochemistry, botany, cell biology and molecular biology, biotechnology, ecology, genetics, microbiology, pharmacognosy, phytochemistry.

The journal is published in every year since 1964 under the name *Note Botanice*. Since 2018 it is published with a new name, *Acta Biologica Marisiensis*, included as a new series in *Acta Marisiensis*. Both original research papers and reviews are welcomed. The journal addresses the entire academic community of

specialists and researchers activate in different fields of life sciences and pharmacy, and its goal is to provide them the latest research developments in their field of activity.

Abstracting & Indexing

Acta Biologica Marisiensis is covered by the following services: Baidu Scholar, CNKI Scholar (China National Knowledge Infrastructure), CNPIEC - cnpLINKer, Dimensions, EBSCO Discovery Service, Google Scholar, J-Gate, KESLI-NDSL (Korean National Discovery for Science Leaders), Naviga (Softweco), Primo Central (ExLibris), ReadCube, Semantic Scholar, Summon (ProQuest), TDNet, WanFang Data, WorldCat (OCLC).

EDITORIAL PROCESS

Submitted manuscripts are first checked to ensure that they comply with instructions to authors and that all references, figures and tables meet the journal's requirements.

All manuscripts sent to the journal are routinely screened using specialized anti-plagiarism soft-wares. In all cases where any possible irregularity exists, the editorial office will follow the principles stated in COPE (Committee on publication ethics) guidelines. Only manuscripts complying with the above requirements and free of possible irregularities will be entered into the review process. The author(s) will be informed that the manuscript has been accepted for review.

Authors are invited to suggest the names of potential reviewers and the Editor may choose, without obligation or explanation, to use one or more of these. Authors may also specify the names of a person(s) which they do not wish to review their manuscript, in which case a brief explanation should be given. All articles will be reviewed by at least two colleagues with expertise in the manuscript's subject matter. The identities of the reviewers, chosen by the editor, will not be disclosed to

the authors. The average time from submission to a decision following the first review is approximately 4-6 weeks.

Based on the reviewers' opinion, the Editor will choose one of the following alternatives:

- Accepted;
- Minor revisions required;
- Major revisions required;
- Rejected.

In cases where revision is required, the authors will be invited to amend their manuscript, which should be resubmitted as soon as possible, but not later than 4 weeks. The revised manuscript will be reappraised by the initial reviewers and notification of a final decision will be sent to the author in approximately 14 days.

After acceptance and prior to publication, authors will receive a PDF file with the edited version of their manuscript for final proofreading and will be asked to carefully check the completeness and accuracy of the text, tables and figures. Accepted articles will receive a DOI code and will be published ahead of print immediately after acceptance.

SUBMISSIONS GUIDELINES

Publication fee

The journal does not have article processing charges, neither article submission charges.

Manuscript submission

All prepared manuscripts should be submitted to the following E-mail address: abmjjournal@umfst.ro

Download *Acta Biologica Marisiensis* manuscript template from <https://abmj.ro/instructions-for-authors/submissions-guidelines/>

Cover letter and an open access license

All manuscripts should be submitted together with a cover letter and an open access license attached as a separate file. Download *Acta Biologica Marisiensis* cover letter template and open access license from <https://abmj.ro/instructions-for-authors/submissions-guidelines/>

Online manuscript submission

<https://abmj.ro/instructions-for-authors/submit-a-manuscript/>

Supplementary material

Acta Biologica Marisiensis do not support pushing important results and information into supplementary sections. However, data that are not of primary importance to the text, or which cannot be included in the article because it is too large can be sent via E-mail (abmjjournal@umftgm.ro) and will be displayed online along with the published article. The Supplementary material can be sent in Microsoft Office Word 97-2003 Document. Supplementary material is not typeset so please ensure that all information is clearly presented, the appropriate caption is included in the file and not in the manuscript, and that the style conforms to the rest of the article.

CONTENTS

MICRO-ANATOMICAL CHARACTERIZATION OF AFRICAN NATIVE MONOTYPIC GENERA - <i>ANOGEISSUS</i> (DC.) GUILL AND <i>QUISQUALIS</i> LINN (COMBRETACEAE) Opeyemi Philips AKINSULIRE, Olaniran Temitope OLADIPO, Aderemi Lucas AKOMOLEDE.....	1
INVESTIGATION OF HRP2 GENE DELETION IN <i>PLASMODIUM FALCIPARUM</i> IN NORTHWESTERN NIGERIA Dayyabu SHEHU, Farida Muhammad AMINU, Shehu DANLAMI, Jamila Ahmed MASHI.....	10
EFFECT OF LIGHT-EMITTING DIODES (LEDs) ON SOME PHYSICAL AND BIOACTIVE COMPOUNDS OF 'ICEBERG' LETTUCE (<i>LACTUCA SATIVA</i> L.) Asmaa Sayed AHMED, Arshad Abdulkhalq YASEEN, Triska Dlshad BAKR.....	21
HOMAGE TO GEORGE E. PALADE CELL PROTEIN SECRETION IN VASCULAR BIOLOGY: OVERVIEW AND UPDATES George N. CHALDAKOV, Luigi ALOE, Anna KÁDÁR, Peter GHENEV, Marco FIORE, Rouzha Z. PANCHEVA, Plamen PANAYOTOV	31
PERSPECTIVES ON ANTIVIRAL DRUGS DEVELOPMENT IN THE TREATMENT OF COVID-19 Aura RUSU, Eliza-Mihaela ARBĂNAȘI, Ioana-Andreea LUNGU, Octavia-Laura MOLDOVAN.....	44
ECOSYSTEM SERVICES OF HOSPITAL GARDENS - BASED ON MICROCLIMATE ANALYSES OF GREEN AND BLUE GARDEN ELEMENTS Vera Takácsné ZAJACZ, Kinga M SZILÁGYI.....	60
THE EFFECT OF DIFFERENT SUBSTRATE ON THE MORPHOLOGICAL CHARACTERISTICS OF HUNGARIAN <i>TAGETES PATULA</i> CULTIVARS Máté ÖRDÖGH.....	73
INCLUSION COMPLEX OF GEDUNIN-2-HYDROXYPROPYL-B-CYCLODEXTRIN PREPARED BY KNEADING AND FREEZE-DRYING METHODS: SYNTHESIS AND STRUCTURAL CHARACTERIZATION Mary Olufunmilayo OLOGE, Adedibu Clement TELLA, Olubunmi ATOLANI, Olajire Aremu ADEGOKE, Olusegun George ADEMOWO.....	83

MICRO-ANATOMICAL CHARACTERIZATION OF AFRICAN NATIVE MONOTYPIC GENERA - *ANOGEISSUS* (DC.) GUILL AND *QUISQUALIS* LINN (COMBRETACEAE)

Opeyemi Philips AKINSULIRE^{1*}, Olaniran Temitope OLADIPO¹, Aderemi Lucas AKOMOLEDE²

^{*1}Department of Botany, Obafemi Awolowo University, Ile – Ife, Nigeria

²Forestry Research Institute of Nigeria, Jericho Hill, Ibadan, Nigeria

*Correspondence:

Opeyemi Philips AKINSULIRE

opeyemibotanist@gmail.com, opeyemiakinsulire@gmail.com

Received: 20 January 2021; **Accepted:** 28 February 2021; **Published:** 30 June 2021

Abstract: This study was designed to explore the micro-anatomical characteristics of leaf and petiole of two unstudied West African native monotypic genera - *Anogeissus* and *Quisqualis* in Combretaceae with a view to characterizing the taxa, providing useful research-based information for identification. The samples were prepared following standard procedures. The light microscopic study of the transverse sections of the leaves in *A. leiocarpus* revealed a thick upper and lower cuticle while the cuticle on both leaf surfaces in *Q. indica* remain thin. The midrib vascular bundle of the leaf in *Q. indica* is characterized by arc-shape and starch grains were observed in the parenchyma cells of the ground tissue. The uniseriate rows of lamina epidermis were oval, squared, rectangular or polygonal in *Q. indica* while it was rectangular or slightly oval in *A. leiocarpus*. Vascular bundle in the leaves and petioles of both taxa were collateral. Simple, slender and short unicellular non-glandular trichomes were also observed in the leaf and petiole micro-anatomy of both taxa. It was concluded that the micro-anatomical features of the leaves and petioles are important parameters of characterization, used in the identification of the studied taxa.

Keywords: *Anogeissus leiocarpus*, Combretaceae, Ground tissue, Monotypic, Palisade, *Quisqualis indica*.

1. Introduction

The genus *Anogeissus* and the genus *Quisqualis* belong to the subtribe Combretinae in the family Combretaceae (Maurin et al., 2010) and according to Mann et al., (2009), *Anogeissus* is a genus of trees which are native to South Asia, the Arabian Peninsula, and Africa. The genus has been reported to consist of eight species. Of these, five are native to South Asia, two are endemic to the Southern Arabian Peninsula, and only one species is native to Africa namely- *Anogeissus leiocarpus* (Hutchinson and Dalziel, 1958). Previous researches of Andary et al., (2005) and USDA,

(2010) revealed that "in Africa, *A. leiocarpus* spreads over a large range of ecosystems, from dry savannah to wet forest borders, in wooded grassland and bushland, and on riverbanks in Ethiopia, Sudan, Cameroon, Congo-Kinshasa, Benin, Cote d'Ivoire, Gambia, Ghana, Guinea, Mali, Niger, Senegal, and Nigeria."

The leaves of *Anogeissus* serve several economic importances. It can be used as a yellow dye in ancestral Bogolan textile techniques in Mali and Burkina-Faso (Heuze et al., 2016). According to Andary et al., (2005), "the wood makes an excellent fuel and yields

good charcoal. Similarly, the barks, leaves and roots have ethno-medicinal properties (antimicrobial and anthelmintic activity) as they are usually taken as decoctions or aqueous extracts (Andary et al., 2005). Derivatives of ellagic acids ("anogelline") extracted from the bark have been shown to delay the degradation of collagen and the tree is grown commercially since 2000 for the production of cosmetics in the Koro region of Burkina Faso (Jansen and Cardon, 2005). "

The inner bark is used as chewing sticks in Nigeria while extracts of the bark show antibacterial properties. Reported as being very sensitive to fire, *A. leiocarpus* can serve reforestation purposes (Andary et al., 2005). The leaves of this taxa are rich in tannin: they contain ellagic, gallic and gentisic acids, derivatives of gallic and ellagic acid, and several flavonoids (derivatives of quercetin and kaempferol) that have been investigated to be very useful for dyeing (Andary et al., 2005), but that may have deleterious effects on nutritive value. The leaf have also been reported as having a relatively low protein content of about 12-14% (Fall Toure, 1991), and the leaf/stem ratio is also quite low (0.4) (Yahaya et al., 2000).

The genus *Quisqualis*, established by Linnaeus (1762), is an extremely shrubby vine or liana, found in thickets or secondary forests of Philippines, India, Malaysia, and Africa. It is a climbing, mesophytic to xerophytic, or helophytic genus (Akinsulire et al., 2018a). "Lawson (1871) and Brandis (1898) separated *Quisqualis* from the genus *Combretum* on the basis of such characteristics as its elongated, tubular, upper hypanthium which is however, subterete throughout and not constricted towards the base - a character-state absent in typical *Combretum*." According to Hutchinson and Dalziel (1958), the genus consists of three species with only one species native to West

Africa - *Quisqualis indica*, also called Rangoon creeper.

The relevance of *Q. indica* in traditional medicine cannot be overemphasized (Sahu et al., 2012). Decoction of the roots, seeds or fruits can be used as anti-helmintic to expel parasitic worms or for alleviating diarrhoea. Fruit decoction can also be used for gargling against toothache as well as combating nephritis while the leaves can be used to relieve pain caused by fever. The roots are used to treat rheumatism. *Quisqualis* are also used as a cough cure. Decoction of boiled leaves is used to relieve flatulent distention of the abdomen. Leaves and fruits are reported to be anthelmintic and also used for nephritis. Dried seeds are preferred for deworming and roasted seeds for diarrhoea and fever. Seeds can be given with honey as electuary, and the preparation used for the expulsion of parasitic worms in children. Seeds are also vermifuge; destroying intestinal worms in children. Seeds macerated in oil are applied for parasitic skin diseases. Seeds are also used for diarrhoea and leucorrhoea discharge in female children (Sahu et al., 2012).

Some research works have been carried out on these two African monotypic genera – *Anogeissus* and *Quisqualis*, which include the work of Oladipo et al. (2016) on the species' wood anatomy, and Akinsulire et al. (2018a) on their vegetative and reproductive morphology, but investigating the leaf and petiole micro-anatomy of the taxa becomes imperative. *Quisqualis* have been known for its taxonomic complexity (Jordaan et al., 2011), while several literature surveys showed a few or no review which correlates the data of the micro-anatomy of the transverse sections of the leaves and petioles of both genera together, hence this study. The choice of the two plant species was also owing to the fact that the two taxa are the only West African monotypic genera in the family Combretaceae and yet unstudied.

2. Materials and methods

Three apparently healthy *Quisqualis indica* samples were collected from three different locations within Obafemi Awolowo University, Ile-Ife (OAU) campus, Osun state, while due to its distribution; the sample of *Anogeissus leiocarpus* was collected at the University of Ibadan campus, Oyo state. All collection sites were geo-referenced using a GPS device (Garmin nuvi 2597LMT) (**Table 1**). Ten mature leaves were harvested from each of the accessions for leaf and petiole micro-anatomical investigations and were preserved in formalin acetic-alcohol (FAA). For leaf micro-anatomy, each of the leaves and midribs was cut at approximately halfway between the base and the apex, while due to the subsessile natures of the petiole (Akinsulire et al., 2018a), transverse sections of the median portions were considered. All leaf and petiole samples were sectioned using Reichert Sliding Microtome (Reichert Austria Nr. 367 019) and at a thickness of 8 to 10 microns. The sections were stained with Safranin O for 3 to 5 minutes, rinsed with 4 to 5 changes of water to remove excess stain and counterstained with Toluidine Blue for 3 to 5 minutes as well. The sections were then rinsed thoroughly with 4 to 5 changes of water and treated in series of ethanol dilutions (50%, 70%, 80%, 90%, and 100%) to enhance dehydration process. The dehydrated sections were then transferred into absolute xylene to remove any remaining trace of water and ethanol. These made the sections clearer and prevented cloudiness of the slide. Sections were afterwards mounted in 25% glycerol containing thymol crystals to prevent fungal attack on a clean glass slide for light microscopy (Sonibare et al., 2014; Akinsulire et al., 2018b; Jainab and Kensa, 2018; Priya and Hari, 2018).

2.1. Light Microscopy

Quantitative leaf anatomical parameters such as thickness of upper and lower cuticle, thickness of upper and lower epidermis, length of palisade layers all at 40 measurements per parameter ($n = 40$), as well as qualitative leaf and petiole micro-anatomical characters such as nature of spongy layers, nature of ground tissues, types of trichomes were all observed and documented using light microscope (Leica Galen III). All quantitative parameters were taken with the aid of ocular micrometre. Photomicrographs of the transverse sections of the leaves and petioles were made with the aid of "Accu-scope Trinocular Microscope (Accu-scope 33001 LED Trinocular Microscope fixed with 3.2 MP CMOS Digital Camera)."

2.2. Data Analysis

In order to shed light on the dimensions of cells and tissues of the two taxa, "quantitative data generated in the study were subjected to One Way Analysis of Variance (ANOVA)."

3. Results and discussion

3.1. *Anogeissus leiocarpus* - Micro-anatomy

The transverse section of the leaf revealed a very thick upper cuticle measuring $16.00 \pm 0.42 \mu\text{m}$; uniseriate upper epidermis of mainly rectangular or slightly oval cells with slightly undulating periclinal walls and a mean length of $22.00 \pm 0.96 \mu\text{m}$. Palisade mesophyll is one-layered, cylindrical, compact and occasionally in slanting rows. Mean length of palisade mesophyll cell was $62.50 \pm 0.69 \mu\text{m}$ (**Table 2**). Hence, studies by Okeke et al. (2015) reported uniseriate epidermis and one to three layers of palisade cells in the transverse sections of leaf in the genus *Stachyterpheta*, and opined that these features could not proffer any taxonomic relevance to the delimitation of the species.

Meanwhile, Akinsulire et al. (2020) have used leaf and petiole micro-anatomical parameters in the identification of the members of the genus *Combretum* (Combretaceae) and their significance explained. Spongy mesophyll layer is fairly parenchymatous; the cells are polygonal or irregular with intercellular airspaces. Lower epidermal cells are uniseriate and rectangular in shape with undulating periclinal wall while the mean length was $22.64 \pm 0.84 \mu\text{m}$. Akinsulire et al. (2018b) reported similar features in the leaf lamina of some members in Combretaceae. Similarly, the lower cuticle of this species is thick and measured $14.80 \pm 0.28 \mu\text{m}$ (**Fig. 1A**).

One taxonomic character worthy of note is the possession of simple and slender unicellular trichome on the epidermal region of the lamina (**Fig. 1A**). However, Akinsulire et al. (2018b) had reported simple unicellular trichomes in some species of *Terminalia* (Magnoliopsida: Combretaceae), stating its usefulness in plant identification. The midrib of the leaf shows a thick cuticle that is generally darkly stained with a uniseriate row of epidermal cells, followed by 3 to 5 layers of parenchyma. The vascular bundle in the midrib in this species is collateral. Adenegan-Alakinde and Jayeola (2015) had earlier reported collateral vascular bundles in the lamina midrib of some members

of the genus *Rhizophora* Linn. in Nigeria and its usefulness in plants identification. The shape of the vascular bundle in the midrib region is arched or crescentiform while short and slender simple unicellular trichomes are also present on the epidermis.

In the transverse section of the petiole (median), a very thick and darkly stained cuticle (**Fig. 1C**) and a uniseriate or biseriate row of epidermis and hypodermis can be used to characterize this monotypic genus. The cells are also round or polygonal in shape. Types and thickness of cuticle, epidermal cell row and nature of hypodermis have been employed by Priya and Hari (2018) in the identification of *Garcinia indica*. The collateral vascular bundle in the petiole of this species, which resolved into a prominent central arc or semi-ovoid vascular strand, capped on the outside by one to three layers of sclerenchyma is a useful tool for characterization in this plant group. Similar petiole anatomical features have previously been employed by different researchers (Akinsulire et al., 2018b; Priya and Hari, 2018) in the taxonomy of several plant groups. The three-winged petiole outline in this species is a spot character, diagnostic for this taxon (**Fig. 1C**).

Table 1. Sites of collection and coordinates of the studied monotypic genera of Combretaceae

Genus	Species/ accession	Location	Geographical coordinate
<i>Anogeissus</i>	<i>A. leiocarpus</i>	University of Ibadan, Ibadan, Oyo State, Nigeria.	N07°23.47', E003°55.00'
<i>Quisqualis</i>	<i>Q. indica</i>	Department of Food Science & Technology, Obafemi Awolowo University, Ile-Ife (OAU), Nigeria.	N07°31.191'E004°31.634'
	<i>Q. indica</i>	Adjacent Alumni Hall, Obafemi Awolowo University, Ile-Ife, Nigeria.	N07°31.278'E004°30.978'
	<i>Q. indica</i>	Moremi Hall, Obafemi Awolowo University, Ile-Ife (OAU), Nigeria.	N07°31.172'E004°31.286'

Short, slender simple unicellular non-glandular trichomes were observed on the epidermis of the petiole. The taxonomic importance of trichomes has been highlighted by some researchers which include Akinsulire et al. (2018b) on the genus *Terminalia* as well as

Adedeji et al. (2007) on some members of the family Solanaceae. Starch grains were also present between the vascular area and the hypodermis of the petiole (**Fig. 1D**).

Table 2. Qualitative and quantitative characteristics of cells and tissues of two monotypic genera of Combretaceae. Quantitative values are expressed as mean \pm standard error (n = 40)

Characters	<i>A. leiocarpus</i>	<i>Q. indica</i>
Thickness of upper cuticle (μm)	16.00 \pm 0.42	12.48 \pm 0.16
Nature of upper and lower epidermis	Uniseriate	Uniseriate
Shapes of upper epidermal cells	Rectangular/oval	Rectangular/squared/polygonal/ oval
Periclinal walls on upper epidermis	Slightly undulating	Straight/undulating
Thickness of upper epidermis (μm)	22.00 \pm 0.96	36.52 \pm 0.86
Layer of palisade cells	One	One
Thickness of palisade mesophyll (μm)	62.50 \pm 0.69	68.14 \pm 1.90
Shape of lower epidermal cells	Rectangular	Rectangular/oval/squared
Periclinal walls on lower epidermis	Undulating	Undulating
Thickness of lower epidermis (μm)	22.64 \pm 0.84	34.48 \pm 0.65
Thickness of lower cuticle (μm)	14.80 \pm 0.28 μm	12.06 \pm 0.08
Type of trichome on the epidermis (lamina, midrib and petiole)	Slender simple unicellular	Short, slender simple unicellular
Type of vascular bundle (midrib)	Collateral	Collateral
Shape of vascular bundle (midrib)	Arched or crescentiform	arc-shaped
Starch grains in the pith (midrib)	Absent	Present
Petiole outline	Three-winged	Arched and furrowed
Petiole epidermis and hypodermis	Uniseriate/biseriate	Uniseriate
Type of trichome on petiole epidermis	Short, slender simple unicellular	Short, slender simple unicellular

3.2. *Quisqualis indica* - Micro-anatomy

The transverse section of the leaves is characterized by a thinner upper and lower cuticle with dimensions 12.48 \pm 0.16 μm and 12.06 \pm 0.08 μm respectively. The upper epidermis composed of uniseriate row of large epidermal cells that are rectangular, squared or polygonal, occasionally oval with straight to undulating periclinal wall; upper epidermal cells are uniseriate measuring 36.52 \pm 0.86 μm while the lower cells are rectangular, oval or squared with a mean length of 34.48 \pm 0.65 μm (**Fig. 2A**). Palisade mesophyll is 1-layered and cylindrical, compact and highly pigmented with a mean length of 68.14 \pm 1.90 μm . Spongy mesophyll cells are irregular, parenchymatous

and fairly compact with moderate intercellular airspaces. The transverse section of the midrib of this species is characterized by a thick and darkly stained cuticle and a uniseriate row of epidermis, followed by a mass of 5 to 7 layers of thin walled parenchyma (**Fig. 2B**).

The vascular bundle is collateral and arc-shaped. Similar feature was reported by Akinsulire et al. (2018b) in some *Terminalia* species in Combretaceae to which *Quisqualis indica* belongs. Another defining characteristic in *Q. indica* is the parenchymatous pith which shows the presence of starch grains as simple short unicellular trichomes were also observed in the midrib epidermal region.

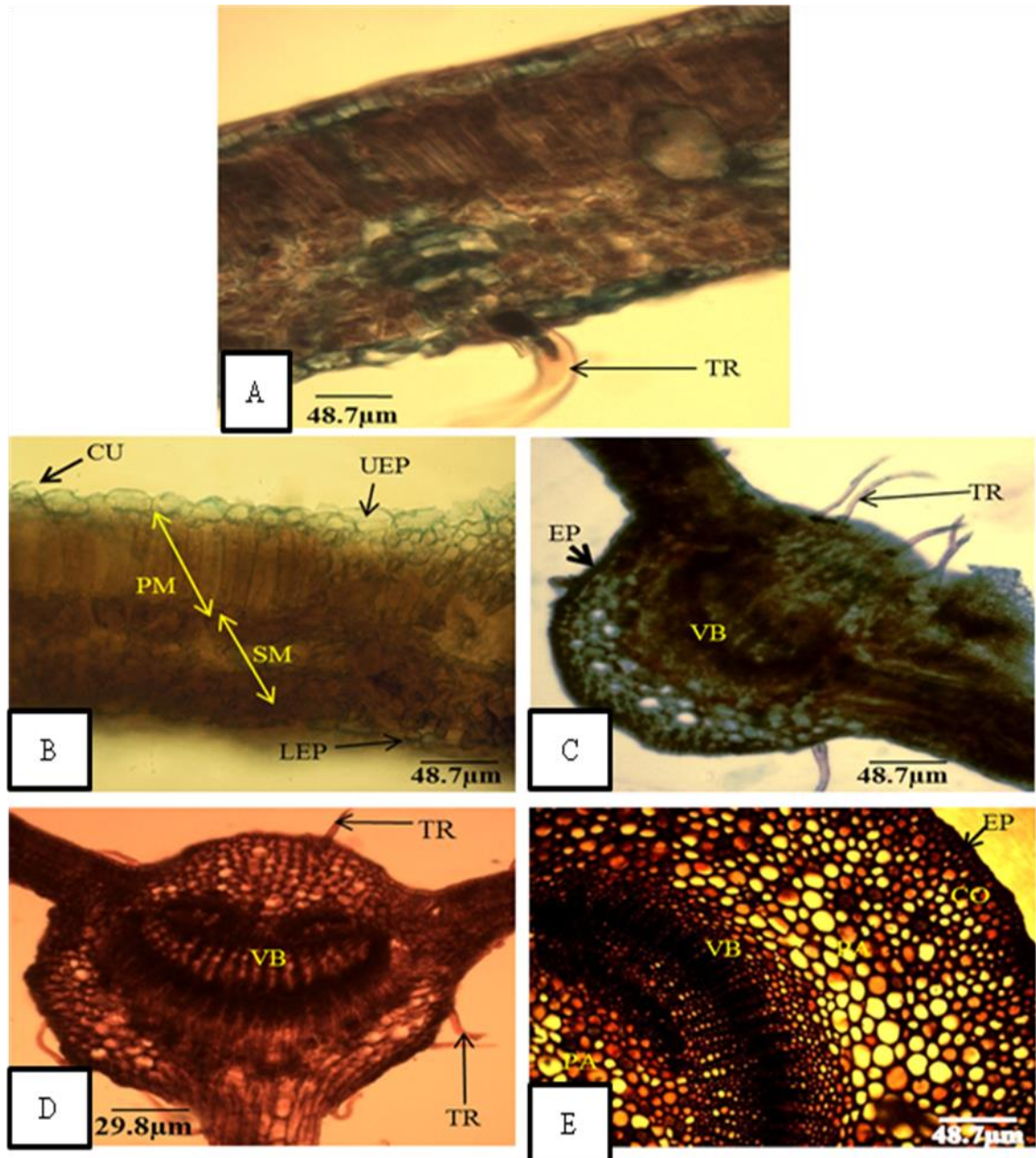


Fig. 1. Micro-anatomy of the transverse sections of the leaf and petiole of *Anogeissus leiocarpus*

A and B = Leaf (Lamina), C = Leaf (Midrib), D = Petiole, E = Petiole (Transect)

Abbreviations: CU = Cuticle, UEP = Upper Epidermis, LEP = Lower Epidermis, CO = Collenchyma, PA = Parenchyma, SM = Spongy Mesophyll, TR = Trichome, PM = Palisade Mesophyll, PH = Phloem, µm = Micrometre, VB = Vascular Bundle

The adaxial outline of the petiole (median) is arched and furrowed (**Fig. 2C**). The epidermis of the petiole is thick with uniseriate row of cells while the hypodermis is also uniseriate. The vascular bundle in the petiole is collateral (**Fig. 2C**) while the vascular architecture is lunar-shaped as reported in some

other members in Combretaceae (Akinsulire et al., 2018b). Outside to the vascular area were thin-walled 6 to 7-layered parenchyma cells which houses sparsely distributed starch grains (**Fig. 2D**) while 2 to 3 layers of angular collenchyma cells were also observed below the hypodermis.

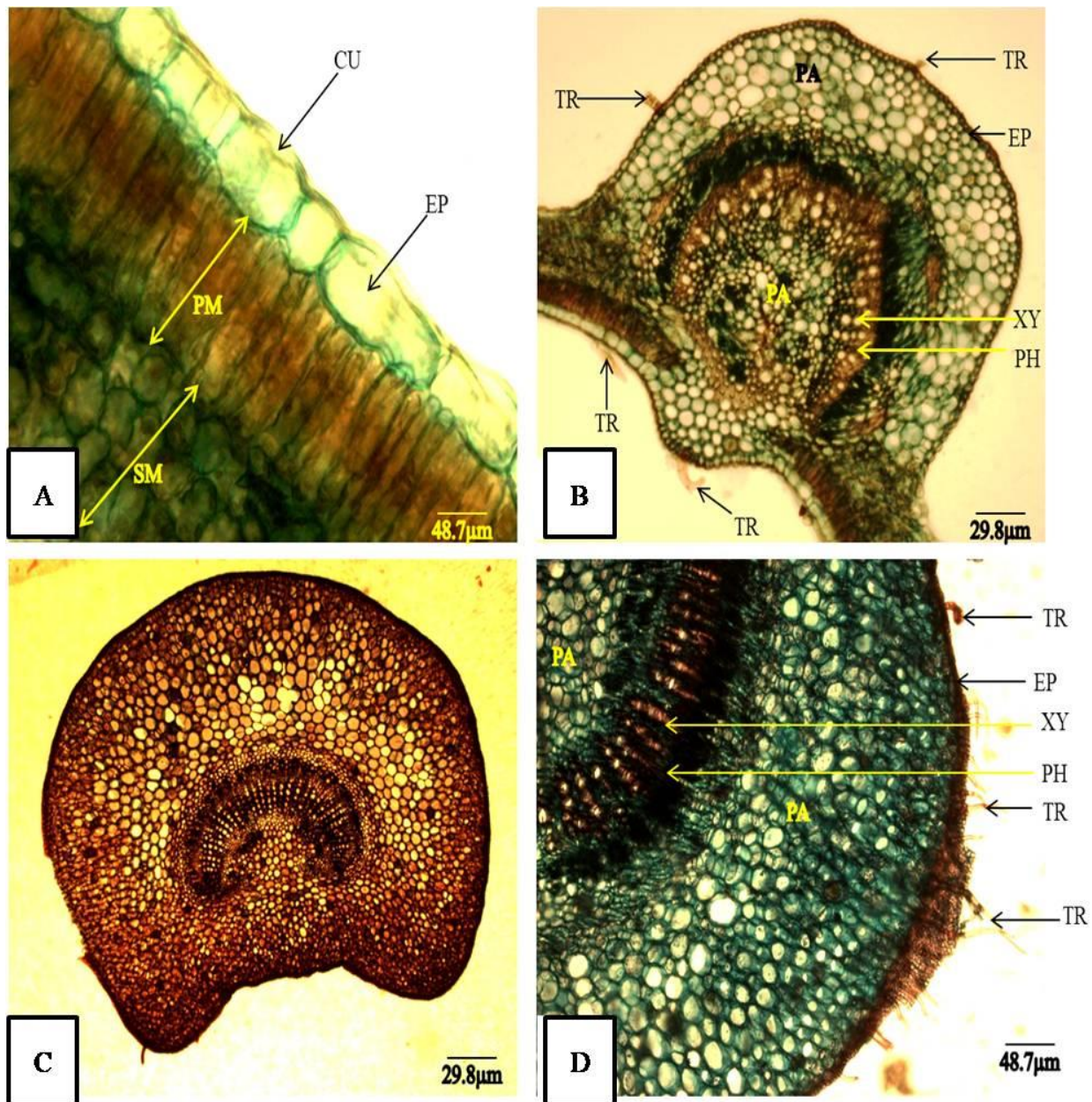


Fig. 2. Micro-anatomy of the transverse sections of the leaf and petiole of *Quisqualis indica*

A = Leaf (Lamina), B = Leaf (Midrib), C = Petiole, E = Petiole (Transect)

Abbreviations: CU = Cuticle, EP = Epidermis, PA = Parenchyma, SM = Spongy Mesophyll, TR = Trichome, PM = Palisade Mesophyll, XY = Xylem, PH = Phloem, µm = Micrometre

4. Conclusions

This study has provided information on the micro-anatomy of the transverse sections of the leaf and petiole of the two monotypic genera thereby enhancing their identification. It is however recommended that molecular investigation into the family Combretaceae

generally be conducted to enhance the taxonomy of the family.

Acknowledgement

We acknowledge Mr. B.E Omomoh of the Department of Forestry and Wood Technology, Federal University of Technology, Akure (FUTA) for the assistance rendered regarding

collection of fresh plant samples; Dr. A. J Akinloye and Mr. Abiodun Omole both in Department of Botany, Obafemi Awolowo University, Ile-Ife (OAU) for the technical assistance rendered as regards slide preparation and photomicrography. Thanks to The Obafemi Awolowo University, Ile-Ife, for providing required facilities and equipment to carry out this research. Anonymous reviewers are also greatly appreciated for the comments and constructive criticism.

Conflict of interest

The authors have declared that there is no conflict of interest.

References

- Adedeji OA, Ajuwon OY, Babawale O (2007) Foliar epidermal studies, organographic distribution and taxonomic importance of trichomes in the family Solanaceae. *International Journal of Botany* 3(3):276–282.
- Adenegan-Alakinde TA, Jayeola AA (2015) Leaf and petiole anatomical studies of the genus *Rhizophora* Linn. in Nigeria. *International Journal of Current Science* 18: E, 125–135.
- Akinsulire OP, Oladipo OT, Illoh HC, Mudasiru OM (2018a) Vegetative and reproductive morphological study of some species in the family Combretaceae in Nigeria. *Ife Journal of Science* 20(2):371–389.
- Akinsulire OP, Oladipo OT, Illoh HC, Akinloye AJ (2018b) Structure, distribution and taxonomic significance of leaf and petiole anatomical characters in five species of *Terminalia* (L.) (Combretaceae: Magnoliopsida). *Brazilian Journal of Biological Sciences* 5(10):515–528.
- Akinsulire OP, Oladipo OT, Akinkunmi OC, Oladipo OE, Adelalu KF (2020) Leaf and petiole micro-anatomical diversities in some selected species of *Combretum* Loefl.: The significance in species identification at vegetative state. *Acta Biologica Marisiensis* 3(1):15–29.
- Andary C, Doumbia B, Sauvan N, Olivier M, Garcia M (2005) *Anogeissus leiocarpa* (DC.) Guill. & Perr. Record from Protabase. Jansen PCM & Cardon D (eds). PROTA (Plant Resources of Tropical Africa / Ressources végétales de l'Afrique tropicale), Wageningen, Netherlands.
- Brandis D (1898) Combretaceae. In: Engler A and KAE Prantyl eds. *Die naturlichen Pflanzen Familien III*. Leipzig: W Engelmann, 7:106–130.
- Fall Touré S (1991) In vitro digestibility and degradability in situ in the rumen of woody forage available on natural grasslands in Senegal. First results. *Revue D'élevage et de Médecine Vétérinaire des Pays Tropicaux* 44:345–354.
- Heuze V, Tran G, Renaudeau D, Bastianelli D (2016) African Birch (*Anogeissus leiocarpa*). Feedipedia, a programme by INRA, CIRAD, AFZ and FAO. <http://www.feedipedia.org/node/701>. Accessed on 17/06/2019.
- Hooker JD (1867) Combretaceae. In: Bentham G and JD Hooker (eds.) *Genera Plantarum I*. London: L Reeve and Co, 782.
- Hutchinson J, Dalziel JM (1958) *Flora of West Tropical Africa*. Crown Agents for Overseas Government and Administration, Nill Bank London, Vol. 1.
- Jainab SI, Kensa MV (2018) Morpho-anatomical studies on *Vitex negundo* L. *International Journal of Botany Studies* 3(2):1–7.
- Jansen PCM, Cardon D (2005) Dyes and tannins. PROTA (Plant Resources of Tropical Africa/ Ressources végétales de l'Afrique tropicale), Wageningen, Netherlands.

14. Jordaan M, Van Wyk AE, Maurin O (2011) Generic status of *Quisqualis* (Combretaceae), with notes on the taxonomy and distribution of *Q. parviflora*. *Bothalia* 41(1):161–169.
15. Lawson MA (1871) Combretaceae. In: Oliver D (ed.) *Flora Tropical Africa*. Vol. 2. London: L Reeve and co, 413–436.
16. Linnaeus C (1762) *Species Plantarum*, edn. 2, 1. Salvius, Stockolm.
17. Mann A, Amupitan JO, Oyewale AO, Okogun J, Ibraheem K (2009) Chemistry of secondary metabolites and their antimicrobial activity in the drug development process: A review of the genus *Anogeissus*. *Medicinal Plants-International Journal of Phytomedicines and Related Industries* 1(2):55. doi:10.5958/j.0975-4261.1.2.010.
18. Maurin O, Mark WC, Marie J, Michelle van der Bank (2010) Phylogenetic relationships of Combretaceae inferred from nuclear and plastid DNA sequence data: implications for generic classification. *Botanical Journal of the Linnean Society* 162(3):453–476.
19. Okeke CU, Iroka CF, Izundu AI, Okereke NC, Onwuazoeze IC, Nyananyo LB (2015) Comparative systematic studies of the genus *Stachytarpheta* found in Awka. *Journal of medicinal plant studies* 3(4):82–84.
20. Oladipo OT, Akinsulire OP, Illoh HC (2016) Comparative systematic wood anatomical study of eleven species in four Genera of the family Combretaceae in Nigeria. *Nigerian Journal of Botany* 29(1):43–57.
21. Priya C, Hari N (2018) A study on leaf and petiole anatomy of endemic and vulnerable species of *Garcinia*. *Journal of Emerging Technology & Innovative Research* 5(12):509–512.
22. Sahu J, Patel P, Dubey B (2012) *Quisqualis indica* Linn: A review of its medicinal properties. *International Journal of Pharmaceutical and Phytopharmacological Research* 1(1):313–321.
23. Sonibare MA, Oke TA, Soladoye MO (2014) A pharmacobotanical study of two medicinal species of Fabaceae. *Asian Pacific Journal of Tropical Biomedicine* 4(2):131–136.
24. USDA (2010) GRIN-Germplasm Resources Information Network. National Germplasm Resources Laboratory, Beltsville, Maryland.
25. Yahaya MS, Takahashi J, Matsuoka S, Kibon A, Dibal DB (2000) Evaluation of Arid Region Browse Species from North eastern Nigeria Using Pen Fed Goats. *Small Ruminants Research* 38:83–86.

INVESTIGATION OF HRP2 GENE DELETION IN *PLASMODIUM FALCIPARUM* IN NORTHWESTERN NIGERIA

Dayyabu SHEHU^{1*}, Farida Muhammad AMINU², Shehu DANLAMI³, Jamila Ahmed MASHI¹

^{*1}Department of Biochemistry, College of Health Sciences, Bayero University, Kano, PMB 3011, Kano Nigeria

²Sokoto State Ministry of Health, Nigeria

³Department of Nursing, College of Medicine, Kaduna State University, Kaduna, Nigeria

*Correspondence:

Dayyabu SHEHU

dshehu.bch@buk.edu.ng

Received: 05 May 2021; **Accepted:** 24 May 2021; **Published:** 30 June 2021

Abstract: Malaria Rapid Diagnostic Tests (RDTs) plays an important role in malaria management and control. The Pf HRP2 based RDT kit is the most widely used RDT for malaria diagnosis in Nigeria but is affected by the deletion of HRP2 gene in *Plasmodium falciparum* parasites. Therefore, identifying the prevalence and distribution of *Plasmodium falciparum* parasites with deleted Pf HRP2 is important for malaria control. Pf HRP2 gene deletion was assessed in this study by first carrying out Giemsa stained thick blood film microscopy and Pf HRP2 RDT strip test. The samples were further analyzed for molecular examination by PCR assay for multiple single-copy genes (Pf Cox3, Pf HRP2, Pf HRP3 and Pf Beta tubulin). This study found the existence of eight (8) *Plasmodium falciparum* isolates lacking the HRP2 gene in the samples analyzed, this necessitates the need to develop a unique RDT Kit targeting other housekeeping genes unique for *Plasmodium falciparum* with far greater sensitivity than the current ones as to reduce the chances of false negative RDT result as well as developing unique RDT Kits targeting both PfHRP2 and PfHRP3 genes concomitantly in order to reduce the chances of having a false positive RDT results.

Keywords: Malaria, *Plasmodium falciparum*, Gene deletion, RDT.

1. Introduction

Malaria is one of the major causes of mortality and morbidity in the tropics and subtropics particularly in Africa (Skeet, 2005). Early diagnosis is very important for disease management and effective treatment of malaria. Diagnosis of malaria using microscopic examination of thin and thick blood smears is still the gold standard (Siahaan, 2018). However, The World Health Organization recently recommended the adoption of malaria rapid diagnostic tests (RDTs) as a universal

testing to confirm the presence of malaria parasites in regions where microscopic examination cannot be performed (Gillet et al., 2011).

Malaria RDTs are immuno-chromatographic tests that detect proteins released from parasitized red blood cells. It has been designed to detect either *Plasmodium falciparum* specifically, or *P. falciparum* in addition to another human malaria parasite or detect all human malaria parasites

(Cunningham et al., 2019). Malaria RDT kits mainly detects antigens *P. falciparum* Histidine Rich Protein 2, parasite Lactate Dehydrogenase (pLDH), and parasite Aldolase (pALD), although pALD and pLDH appear to be highly conserved (Lee et al., 2006; Maltha et al., 2010). The specific antigen remains in the circulation for up to 4 weeks after the malaria parasites clearance due to its high abundance and heat stability (Iqbal et al., 2004).

A structural homologue of PfHRP-2, PfHRP-3, has been found to have cross reactivity with some monoclonal antibodies directed against PfHRP-2 (Lee et al., 2012). Thus, although PfHRP-2 based RDT kits have the highest sensitivities, they also have high false positive rates (Baiden et al., 2012). Therefore, accurate diagnosis of malaria by PfHRP-2 RDT kits can be affected by the pfhrp2 and or pfhrp3 genotype of the parasite, the concentration of PfHRP-2 antigen produced by the parasite and also the prolonged existence of PfHRP-2 antigen after parasite clear (Wurtz et al., 2013).

Diagnosis of malaria by RDT without additional confirmation of parasitaemia nowadays become a major problem due to false positive test results, which leads to the unnecessary administration of anti-malarial drugs when no malaria parasites are actually present in the patient (Gerstl *et al.*, 2010). False positive RDT test results are frequently obtained immediately following an anti-malarial drug regimen, when parasites are cleared or densities very low, but the antigen remains in circulation weeks later (Adu-Gyasi et al., 2012; Gerstl et al., 2010). Additionally, there is failure to produce the HRP2 target molecule for HRP2-based RDTs by the *Plasmodium falciparum* parasites without the “central repeat region of the HRP2 gene” which may cause false-negative RDTs (Dorado et al., 2016; Gamboa et al., 2010; Koita et al., 2012). This could be due to gene deletion,

frame shift mutation or alteration in protein, which may have also contributed to the variable performance of RDT test (Dorado et al., 2016).

Nowadays, concerns have been raised about the diagnostic threat and malaria control posed by parasites without hrp2 such as the effectiveness of PfHRP2-based RDTs in affected regions (Fontecha et al., 2018; Maltha et al., 2012). In response, the World Health Organization has prioritized efforts to address parasites with deletions of the pfhrp2 and/or pfhrp3 genes, for this reason, there is a little amount of data on the frequency of those parasites and the factors responsible for their selection. Recently, deletion of these genes was reported in population-based studies from Peru, Mali, Asia-Pacific region, India, Madagascar, in a clinical case in Uganda and as case report from Brazil (Baker et al., 2005; Maltha et al., 2012; Parr et al., 2017). However, such data is not available in Nigeria. This research sought to analyze the possibility of Pfhrp2 gene deletion in clinical isolates from northwestern Nigeria.

2. Materials and methods

2.1. Materials

2.1.1. Study Area

The study was conducted at Muhammadu Abdullahi Wase Specialist Hospital and Murtala Muhammad General Hospital situated within Kano metropolis, North West geopolitical zone of Nigeria. The area is located in Kano city and has a coordination of latitude 11.96°N and longitude 8.55°E.

2.1.2. Ethical Approval and Consent

The ethical approval was obtained from the Research and Ethical Committees of the Kano State Ministry of Health (MOH/Off/797/T.I/872). Informed verbal consent was obtained from patients or their

parents prior to blood collection with standard questionnaire.

2.1.3. Study population

Patients irrespective of age or sex, with clinical presentation of malaria through consultation and are referred for diagnostic evaluation of *P. falciparum* in vitro.

2.1.4. Inclusion and Exclusion Criteria for Sample

All samples with both positive malaria smear and RDT were excluded, as well as all samples with both negative malaria smear and RDT were also excluded. Whereas all samples with either a positive malaria smear and a negative RDT or samples with negative malaria smear and positive RDT were included.

2.2. Methods

2.2.1. Determination of sample size

The sample size was determined from standard formula for calculation of minimum sample size. Sample size 'n' was given by the formula, where $n = 138.29$ as a minimum number of samples for the study with 2% (3) of these subjects were added to the research for attrition, making a total of approximately 141 subjects (Draugalis & Plaza , 2009).

2.2.2. Sample Collection

Blood samples were collected via venopuncture into Ethylene diamine tetra acetic acid (EDTA) containers and were taken to the laboratory for examination.

2.2.3. Microscopy

Thick blood smears were made, then stained using 3% Giemsa stain and examined 100 fields by oil immersion magnification in which the parasite density was estimated as described by (Wongsrichanalai *et al.*, 2007).

2.2.4. Rapid Diagnostic Test (RDT)

The HRP2-based RDT (CareStart™ Malaria HRP2 Pf) was performed according to the manufacturer's instructions.

2.2.5. DNA Extraction

The EDTA anti-coagulated blood sample that was stored at -4°C was allowed to thaw and vortexed, and then the DNA was extracted using D1800 Blood Genomic DNA Extraction kit (solarbio life science), according to the manufacturers protocol.

2.2.6. Polymerase Chain Reaction (PCR) Amplification

All the PCR reactions were performed by preparing a 20ul reaction mix containing 3ul of DNA template, 0.5ul of each forward and reverse primer, 10ul of high fidelity polymerase (Thermo fisher Scientific) and 6ul of nuclease free water. PCR reaction was set using 3-step PCR set up: 1) One (1) cycle of initial denaturation at 95°C for 3 minutes. 2) Thirty five cycles (35) cycles of denaturation at 94°C for 30 seconds and extension at 72°C for 30 seconds. However, other parameter for the annealing temperature varies depending on the primer used. (3) One (1) cycle of final extension at 72°C for 5 minutes.

PCR was performed using the following set of primers:

- **PF COX3 GENE:** Forward: (5' AGCGGTAAACCTTTCTTTTCCTTAC G 3') and Reverse (5' AGTGCATCATGTATGACAGCATGTTT ACA 3').
 - Annealing temperature used was 58°C for 30 seconds.
- **PF HRP2 GENE:** Forward: ATTCCGCATTTAATAATAACTTGTGT AGC and Reverse: ATGGCGTAGGCAATGTGTGG.
 - Annealing temperature used was 58.5°C for 30 seconds.
- **PF HRP3 GENE:** 5' TATCCGCTGCCGTTTTTGCTTCC 3' and Reverse: 5' TGCATGATGGGCATC ACCTG 3'.
 - Annealing temperature used was 58°C for 30 seconds.

- **PF BETA TUBULIN GENE:** Forward: (5' AATAAATCATAATGATGT GCGCAAGTGATCC 3') and Reverse: (5' AATAAATCATAATCCTTTGTGGACAT TCTTCCTC 3').
 - Annealing temperature used was 58°C for 30 seconds.

Agarose gel electrophoresis was performed on the PCR products. The electrophoresis was performed at 80V for 1 hour 30 minutes using 5 µl of gel ready DNA marker pipetted into the adjacent well. The PCR products were visualized using Alpha Imager Mini after staining with ethidium bromide.

3. Results and discussion

3.1. Results

Seventy (70) samples from patients attending Murtala Muhammad Specialist Hospital (MMSH) were analyzed for microscopy and RDT. Fifty five (55) samples appeared to be positive and fifteen (15) samples were negative for microscopy, while forty six (46) samples appeared to be positive and twenty four (24) samples were negative for RDT (**Table 1**). Seventy (70) samples were also collected from Abdullahi Wase specialist Hospital (AWSH) and analyzed for microscopy and RDT. Forty seven (47) samples appeared to be positive and twenty three (23) samples were negative for microscopy, while twenty three (23) samples appeared to be positive and forty seven (47) samples were negative for RDT (**Table 1**).

Based on the method of Parr et al. (2018), only those samples that appeared RDT-Positive/Microscopy negative and RDT-negative/Microscopy positive are eligible for further screening of Hrp2 gene deletion. Therefore the samples were subjected to a combination of rapid diagnostic and microscopy. Thirty eight (38) samples from MMSH were found to be both positive for

microscopy and RDT while seven (7) samples were found to be both RDT and microscopy negative. Nine (9) samples were RDT positive/microscopy negative, while 16 sample were RDT negative/ microscopy positive (**Table 1**). Twenty two (22) samples from AWSH were found to be both microscopy and RDT positive, twenty three (23) sample were both microscopy and RDT negative, one (1) sample was RDT positive/microscopy negative, while twenty four (24) samples were RDT negative/microscopy positive (**Table 2**).

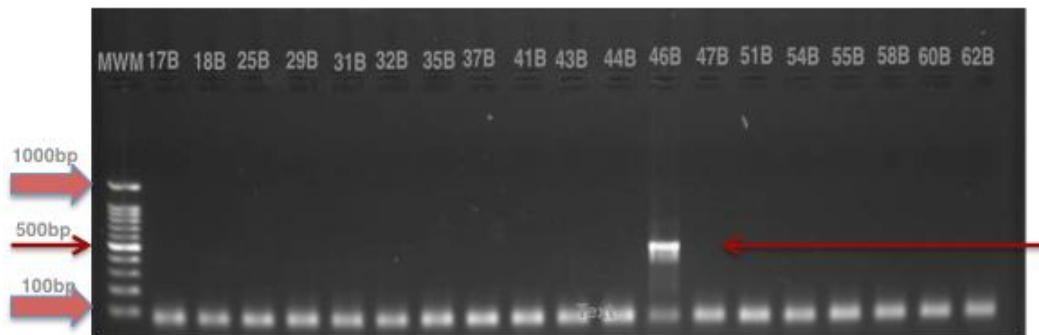
A total of fifty (50) samples from both hospitals were found to be microcopy positive/RDT negative and microscopy negative/RDT positive and were further analyzed for molecular examination in order to assess the possibility of PfHRP2 gene deletion in those samples. However, molecular genotyping was first performed for species identification of the malarial parasite. The samples were analyzed for Pf Cox 3 gene (*Plasmodium falciparum* genotyping) out of which only sixteen (16) samples appeared positive with the expected band size (508bp), while thirty four (34) samples were negative, possibly due to different specie of the malaria parasite (**Fig. 1, 2, 3**). Having confirmed the species of the malarial parasite, the sixteen (16) Cox3-gene positive samples were further analyzed for Pf HRP2 gene out of which five (5) samples appeared to be positive with expected band size (800bp, 900bp) and eleven (11) samples were negative possibly due to absence of the gene (**Fig. 4**). The eleven (11) Pf HRP2 gene negative samples were further amplified for Pf HRP3 gene were ten (10) samples were positive with expected band size (300bp, 400bp, 800bp) and one (1) sample was negative (**Fig. 5**). More so, Pf *Beta tubulin* final confirmation was performed on the one (1) Pf HRP3 gene negative sample which appeared to be negative either due to no or low limit of detection (**Fig. 6**).

Table 1. Microscopy And RDT Results of Samples Analyzed from Murtala Muhammad Specialist Hospital and Abdullahi Wase specialist Hospital

Hospital Name	Microscopy			Hrp2 RDT		
	Microscopy positive	Microscopy negative	Total	RDT positive	RDT negative	Total
MMSH	55	15	70	46	24	70
AWSH	47	23	70	23	47	70
Total sample size			140			140

Table 2. Combination of Microscopy And RDT Results Of Samples Analyzed from Murtala Muhammad Specialist Hospital and Abdullahi Wase Specialist Hospital

Hospital Name	Hrp2 RDT /microscopy positive n=	Hrp2 RDT /microscopy negative n=	Hrp RDT positive/microscopy negative n=(molecular investigation)	Hrp RDT negative/microscopy positive n= (molecular investigation)	Total
MMSH	38	7	9	16	70
AWSH	22	23	1	24	70
Total sample size = n	60	30	10	40	140

**Fig. 1.** Pf cox3 gene PCR (*P. falciparum* genotyping) amplification**Fig. 2.** Pf cox3 gene PCR (*P. falciparum* genotyping) amplification

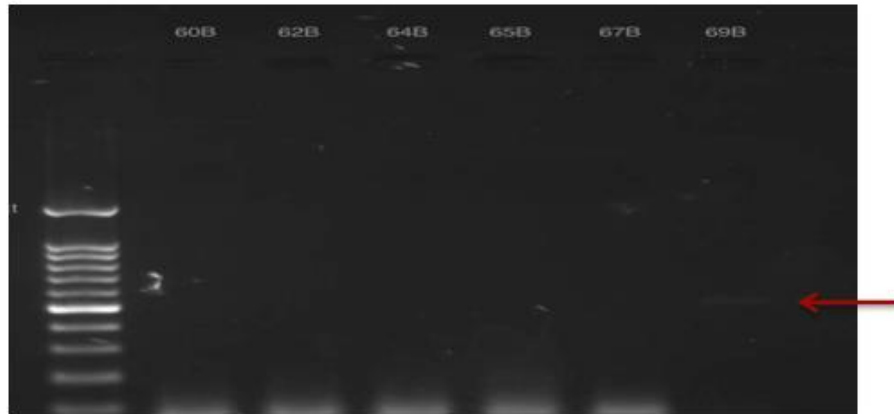


Fig. 3. Fig. 1, 2, 3. Pf cox3 gene PCR (*P. falciparum* genotyping) amplification. MWM is the molecular weight marker while the arrows indicated the 508bp of the 16 successfully amplified Pf cox3 genes

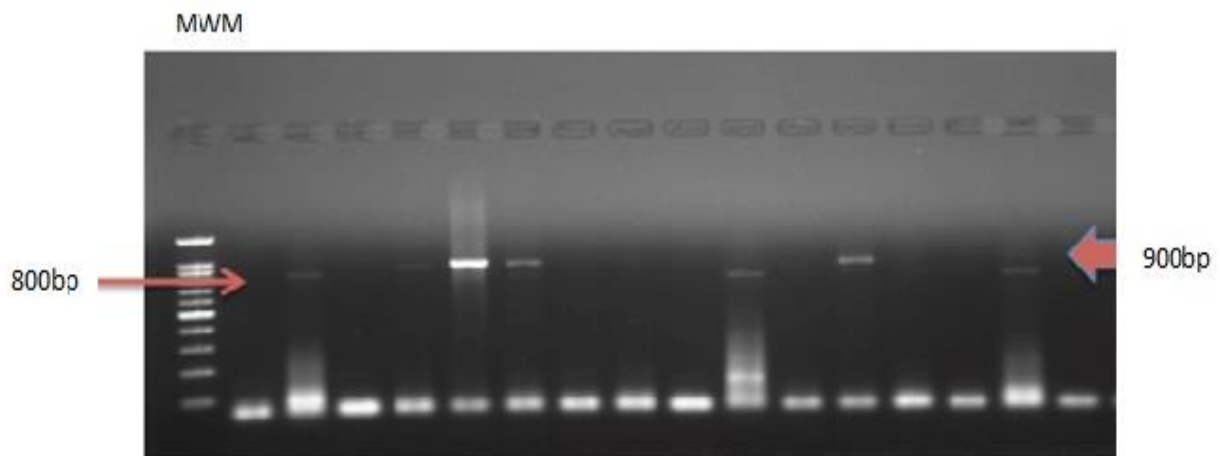


Fig. 4. Pf HRP2 gene amplification. Five (5) samples out of 16 were positive for Pf HRP2 gene with the expected band sizes of 800bp and 900bp

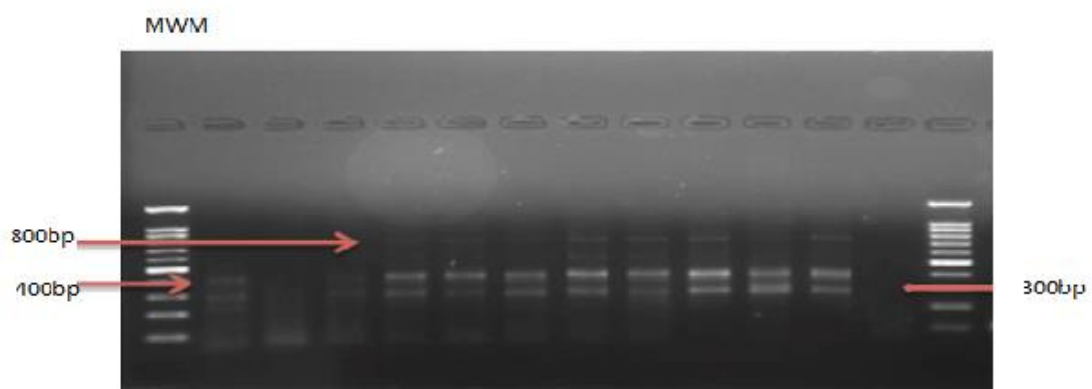


Fig. 5. Pf HRP3 gene amplification. Ten (10) samples out of 11 were positive for Pf HRP3 gene with the expected band sizes of 300bp, 400bp and 900bp

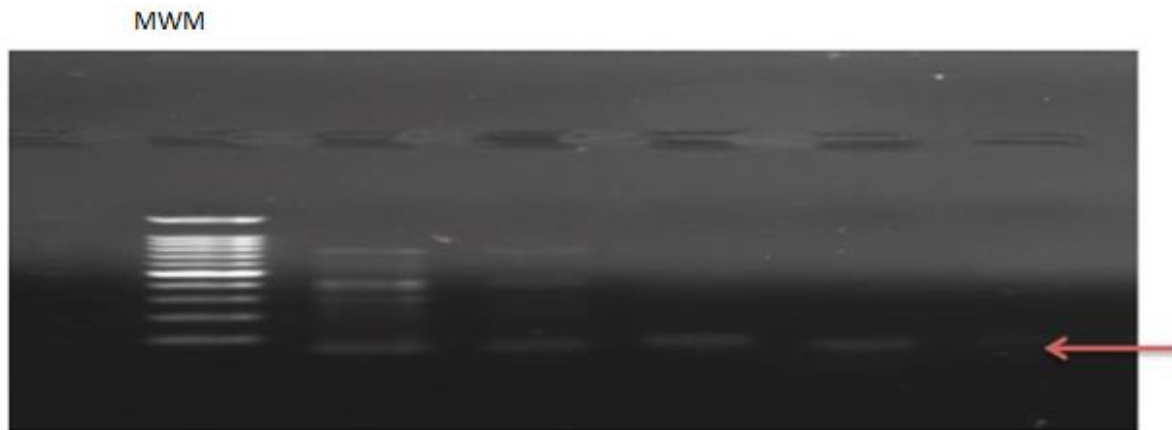


Fig. 6. Pf *Beta tubulin* gene amplification. No amplification was observed

3.2. Discussion

In sub-Saharan Africa, Pf HRP2 RDTs are the tests most commonly used and best recommended for parasitological confirmation of malaria in regions where microscopic examination cannot be performed before treatment. However, several reports have noted significant declines in the sensitivity of Pf HRP2 RDTs after declines in the intensity of transmission (Kumar et al., 2013; Shakely et al., 2013). Thus, in this study Pf HRP2 RDT performance was examined in relation to microscopy, which is considered the gold standard (Zimmerman and Howes, 2015).

By employing the improved approach of testing algorithm for PCR-based detection of PfHRP2/3-negative *P. falciparum*, the identification of PfHRP2-negative parasites must be coupled with verification of *P. falciparum* parasitaemia and confirmation that parasite DNA is present (Kumar et al., 2019; Parr et al., 2017). The presence of amplifiable DNA in PfHRP2-deleted samples were confirmed by PCR assay for multiple single copy genes (Pf Cox3, Pf HRP3 and Pf *Beta tubulin*). In the first stage, i.e. genotyping of *P. falciparum*, PCR amplification of Pf Cox3 gene showed 16 samples that appeared to be positive with an expected band size of about 508bp out of the 50 samples analyzed. The negative

samples may likely not be from *P. falciparum* strain as Cox3-gene is solely used for genotyping *Plasmodium falciparum* (Echeverry et al., 2016).

Having confirmed the specie of the malarial parasite, the second stage is to confirm if there is Pf HRP2 gene deletion. From the sixteen (16) Pf cox3 positive samples, five (5) samples were amplified giving the expected band sizes of 800bp and 900bp in accordance with (Koita et al., 2012) and eleven (11) samples were with no amplification. The eleven samples which showed negative PfHRP2 gene amplification indicated the possibility of having PfHRP2 gene deletion or cross reactivity between the PfHRP2 and PfHRP3 gene products. Therefore in the third stage, the eleven (11) samples were set for amplification of Pf HRP3. After the amplification of Pf HRP3-gene, ten (10) samples appeared positive with expected band sizes of 800bp, 400bp and 300bp in accordance with (Parr et al., 2018) and only one (1) sample was negative. This indicated a possibility for cross reactivity of Pf HRP2 for/with Pf HRP 3 which was found to be positive and/ or negative on the Pf HRP 2 RDT strip. According to (Parr et al., 2017), PfHRP3 antigen triggers a positive PfHRP2- based RDT because some Pf HRP2 antigens shares similar epitopes to Pf

HRP3 antigens resulting to Pf HRP2-deleted parasites with an intact Pf HRP3 gene.

The final confirmatory PCR was carried out on the one (1) PfHRP3 negative sample for the amplification of Pf *Beta tubulin* in which no amplification was recorded, this could be as result of low limit of detection (LOD) or even absence of the amplicon (Parr et al., 2018).

The failure of a parasite to express its antigen on the PfHRP2-based RDT could be as a result of some possible factors; either due to genetic deletions as in deletion of PfHRP2 and PfHRP3 genes (Gamboa et al., 2010), frame shift mutations or alterations in protein expression (Wellems and Howard, 1986), storage and transport conditions of RDT, variability within the parasite antigen technique used to perform test, interpretation of test results or parasite density (Baker et al., 2010; Baker et al., 2005; Maltha et al., 2012).

This study found the existence of *P. falciparum* isolates lacking the HRP2 gene in the samples analyzed. Detection of Pf HRP3 gene in some of the samples, which appeared positive RDT, and negative Pf HRP2 gene confirmed the possibility of cross reactivity of Pf HRP2 and Pf HRP3 gene products on RDT. Also false-negative PfHRP2 RDTs with detection of Pf HRP3 gene in some of the samples has provided new information on the performance of Pf HRP2 RDTs in Nigeria which supports the previously raised concerns that the sensitivity of Pf HRP2 RDTs may decline as malaria control improves. More so, the current situation of Pf HRP2 RDTs has certainly compromised malaria diagnosis and treatment.

4. Conclusions

The existence of *P. falciparum* isolates lacking the HRP2 gene was confirmed in this study so also cross reactivity of Pf HRP2 and Pf HRP3 gene products. The study has

confirmed the already raised fear of PfHRP2 gene deletion which will severely compromise malaria diagnosis and treatment. Based on this finding, there is a need to develop a unique RDT Kit targeting both PfHRP2 and PfHRP3 genes concomitantly in order to reduce the chances of having a false positive result. Furthermore, other house-keeping genes unique for *Plasmodium falciparum* can be considered for developing a kit with far greater sensitivity than the current ones.

Acknowledgement

The authors wish to acknowledge the Sokoto State Ministry of Health for the financial support throughout the study.

Conflict of interest

The authors declare no conflict of interest.

References

1. Adu-Gyasi D, Adams M, Amoako S, Mahama E, Nsoh M, Amenga-Etego S, Owusu-Agyei S et al. (2012) Estimating malaria parasite density: assumed white blood cell count of 10,000/ μ l of blood is appropriate measure in Central Ghana. *Malaria journal*, 11(1), 1-6. <https://doi.org/10.1186/1475-2875-11-238>.
2. Baiden F, Webster J, Tivura M, Delimini R, Berko Y, Amenga-Etego S, Owusu-Agyei S et al. (2012). Accuracy of rapid tests for malaria and treatment outcomes for malaria and non-malaria cases among under-five children in rural Ghana. *PLoS One*, 7(4), e34073. <https://doi.org/10.1371/journal.pone.0034073>.
3. Baker J, Ho M-F, Pelecanos A, Gatton M, Chen N, Abdullah S, Bell D et al. (2010) Global sequence variation in the histidine-rich proteins 2 and 3 of *Plasmodium*

- falciparum: implications for the performance of malaria rapid diagnostic tests. *Malaria journal*, 9(1), 1-12. <https://doi.org/10.1186/1475-2875-9-129>.
4. Baker J, McCarthy J, Gatton M, Kyle DE, Belizario V, Luchavez J, Cheng Q (2005) Genetic diversity of *Plasmodium falciparum* histidine-rich protein 2 (PfHRP2) and its effect on the performance of PfHRP2-based rapid diagnostic tests. *The Journal of infectious diseases*, 192(5), 870-877. <https://doi.org/10.1086/432010>.
 5. Cunningham J, Jones S, Gatton ML, Barnwell JW, Cheng Q, Chiodini PL, Luchavez J et al. (2019) A review of the WHO malaria rapid diagnostic test product testing programme (2008–2018): performance, procurement and policy. *Malaria journal*, 18(1), 1-15. <https://doi.org/10.1186/s12936-019-3028-z>.
 6. Dorado EJ, Okoth SA, Montenegro LM, Diaz G, Barnwell JW, Udhayakumar V & Murillo Solano C (2016) Genetic characterisation of *Plasmodium falciparum* isolates with deletion of the pfhrp2 and/or pfhrp3 genes in Colombia: the Amazon region, a challenge for malaria diagnosis and control. *PLoS One*, 11(9), e0163137. <https://doi.org/10.1371/journal.pone.0163137>.
 7. Draugalis JR, Plaza CM (2009) Best practices for survey research reports revisited: implications of target population, probability sampling, and response rate. *American Journal of Pharmaceutical Education*, 73 (8), 142. DOI: <https://doi.org/10.5688/aj7308142>
 8. Echeverry DF, Deason NA, Davidson J, Makuru V, Xiao H, Niedbalski J, Collins FH et al. (2016) Human malaria diagnosis using a single-step direct-PCR based on the *Plasmodium* cytochrome oxidase III gene. *Malaria journal*, 15(1), 1-12. <https://doi.org/10.1186/s12936-016-1185-x>.
 9. Fontecha G, Mejía RE, Banegas E, Ade MP, Mendoza L, Ortiz B, Pinto A et al. (2018) Deletions of pfhrp2 and pfhrp3 genes of *Plasmodium falciparum* from Honduras, Guatemala and Nicaragua. *Malaria journal*, 17(1), 1-10. <https://doi.org/10.1186/s12936-018-2470-7>.
 10. Gamboa D, Ho M-F, Bendezu J, Torres K, Chiodini PL, Barnwell JW, McCarthy J et al. (2010) A large proportion of *P. falciparum* isolates in the Amazon region of Peru lack pfhrp2 and pfhrp3: implications for malaria rapid diagnostic tests. *PLoS One*, 5(1), e8091. <https://doi.org/10.1371/journal.pone.0008091>.
 11. Gerstl S, Dunkley S, Mukhtar A, De Smet M, Baker S, Maikere J (2010) Assessment of two malaria rapid diagnostic tests in children under five years of age, with follow-up of false-positive pLDH test results, in a hyperendemic falciparum malaria area, Sierra Leone. *Malaria journal*, 9(1), 1-10. <https://doi.org/10.1186/1475-2875-9-28>.
 12. Gillet P, Scheirlinck A, Stokx J et al. (2011) Prozone in malaria rapid diagnostics tests: how many cases are missed? *Malaria journal*, 10, 166. <https://doi.org/10.1186/1475-2875-10-166>
 13. Iqbal J, Siddique A, Jameel M, Hira PR (2004) Persistent histidine-rich protein 2, parasite lactate dehydrogenase, and panmalarial antigen reactivity after clearance of *Plasmodium falciparum* mono-infection. *Journal of clinical microbiology*, 42(9), 4237-4241. [10.1128/JCM.42.9.4237-4241.2004](https://doi.org/10.1128/JCM.42.9.4237-4241.2004).
 14. Koita OA, Doumbo OK, Ouattara A, Tall LK, Konaré A, Diakité M, Doumbo SN et al. (2012) False-negative rapid diagnostic tests for malaria and deletion of the histidine-rich repeat region of the hrp2

- gene. *The American journal of tropical medicine and hygiene*, 86(2), 194-198. <https://doi.org/10.4269/ajtmh.2012.10-0665>.
15. Kumar A, Singh SP, Bhatt R, Singh V (2019) Genetic profiling of the *Plasmodium falciparum* parasite population in uncomplicated malaria from India. *Malaria journal*, 18(1), 1-11. <https://doi.org/10.1186/s12936-019-3022-5>.
 16. Kumar N, Pande V, Bhatt R, Shah NK, Mishra N, Srivastava B, Anvikar AR et al. (2013) Genetic deletion of HRP2 and HRP3 in Indian *Plasmodium falciparum* population and false negative malaria rapid diagnostic test. *Acta tropica*, 125(1), 119-121. <https://doi.org/10.1016/j.actatropica.2012.09.015>.
 17. Lee N, Baker J, Andrews KT, Gatton ML, Bell D, Cheng Q, McCarthy J (2006) Effect of sequence variation in *Plasmodium falciparum* histidine-rich protein 2 on binding of specific monoclonal antibodies: implications for rapid diagnostic tests for malaria. *Journal of clinical microbiology*, 44(8), 2773-2778. [10.1128/JCM.02557-05](https://doi.org/10.1128/JCM.02557-05).
 18. Lee N, Gatton ML, Pelecanos A, Bubb M, Gonzalez I, Bell D, McCarthy JS et al. (2012) Identification of optimal epitopes for *Plasmodium falciparum* rapid diagnostic tests that target histidine-rich proteins 2 and 3. *Journal of clinical microbiology*, 50(4), 1397-1405. [10.1128/JCM.06533-11](https://doi.org/10.1128/JCM.06533-11).
 19. Maltha J, Gamboa D, Bendezu J, Sanchez L, Cnops L, Gillet P, Jacobs J (2012) Rapid diagnostic tests for malaria diagnosis in the Peruvian Amazon: impact of pfhrp2 gene deletions and cross-reactions. *PLoS One*, 7(8), e43094. <https://doi.org/10.1371/journal.pone.0043094>.
 20. Maltha J, Gillet P, Bottieau E, Cnops L, van Esbroeck M, Jacobs J (2010) Evaluation of a rapid diagnostic test (CareStart™ Malaria HRP-2/pLDH (Pf/pan) Combo Test) for the diagnosis of malaria in a reference setting. *Malaria journal*, 9(1), 1-13. <https://doi.org/10.1186/1475-2875-9-171>.
 21. Nakasi R, Mwebaze E, Zawedde A et al. (2020) A new approach for microscopic diagnosis of malaria parasites in thick blood smears using pre-trained deep learning models. *SN Appl. Sci.* 2, 1255. <https://doi.org/10.1007/s42452-020-3000-0>.
 22. Parr JB, Anderson O, Juliano JJ, Meshnick SR (2018) Streamlined, PCR-based testing for pfhrp2-and pfhrp3-negative *Plasmodium falciparum*. *Malaria journal*, 17(1), 1-8. <https://doi.org/10.1186/s12936-018-2287-4>.
 23. Parr JB, Verity R, Doctor SM, Janko M, Carey-Ewend K, Turman BJ, Mwandagalirwa K et al. (2017) Pfhrp2-deleted *Plasmodium falciparum* parasites in the Democratic Republic of the Congo: a national cross-sectional survey. *The Journal of infectious diseases*, 216(1), 36-44. <https://doi.org/10.1093/infdis/jiw538>.
 24. Shakely D, Elfving K, Aydin-Schmidt B, Msellem MI, Morris U, Omar R, Baltzell KA et al. (2013) The usefulness of rapid diagnostic tests in the new context of low malaria transmission in Zanzibar. *PLoS One*, 8(9), e72912. <https://doi.org/10.1371/journal.pone.0072912>.
 25. Skeet J (2005) Malaria: its causes, treatment and methods of prevention. *Nursing times*, 101(20), 43-45. PMID: 15918463 .
 26. Welles TE, Howard RJ (1986) Homologous genes encode two distinct histidine-rich proteins in a cloned isolate of *Plasmodium falciparum*. *Proceedings of the*

- National Academy of Sciences, 83(16), 6065-6069.
<https://doi.org/10.1073/pnas.83.16.6065>.
27. Wongsrichanalai C, Barcus MJ, Muth S, Sutamihardja A, Wernsdorfer WH (2007) A review of malaria diagnostic tools: microscopy and rapid diagnostic test (RDT). *The American journal of tropical medicine and hygiene*, 77(6_Suppl), 119-127. PMID: 18165483.
 28. Wurtz N, Fall B, Bui K, Pascual A, Fall M, Camara C, Diémé Y et al. (2013) Pfhrrp2 and pfhrrp3 polymorphisms in *Plasmodium falciparum* isolates from Dakar, Senegal: impact on rapid malaria diagnostic tests. *Malaria journal*, 12(1), 1-8.
<https://doi.org/10.1186/1475-2875-12-34>.
 29. Zimmerman PA, Howes RE (2015) Malaria diagnosis for malaria elimination. *Current opinion in infectious diseases*, 28(5), 446-454. 10.1097/QCO.0000000000000191.

EFFECT OF LIGHT-EMITTING DIODES (LEDs) ON SOME PHYSICAL AND BIOACTIVE COMPOUNDS OF 'ICEBERG' LETTUCE (*LACTUCA SATIVA* L.)

Asmaa Sayed AHMED¹, Arshad Abdulkhalq YASEEN^{1,2*}, Triska Dlashad BAKR^{1,3}

¹Department of Horticulture, College of Agricultural Engineering Sciences, Salahaddin University-Erbil, 44002 Kurdistan Region, Iraq

²Institute of Horticultural Sciences, Faculty of the Agricultural and Food Sciences and Environmental Management, University of Debrecen, H-4032 Debrecen, Böszörményi Street 138

³Khabat Technical Institute, Department of Horticulture Erbil Polytechnic University, Erbil, Kurdistan Region, Iraq

*Correspondence:

Arshad Abdulkhalq YASEEN
arshadabdulkhalq@gmail.com

Received: 15 May 2021; **Accepted:** 26 May 2021; **Published:** 30 June 2021

Abstract: The use of light-emitting diodes (LEDs) is a recent concerned application in the indoor crop system of the modern plant production. In our research, we evaluated the influence of four monochromatic LED lights including 100% White (W), Yellow (Y), Red (R) and Blue (B) in comparison to solar lightening condition (GR) as a control. In this regard, some morphological characteristics and biochemical content of the common outdoor 'Iceberg' lettuce (*Lactuca sativa* L.) was measured. The results show that leaf length, leaf area and total head weight were significantly greater in the plants grown under B LED, while all the other physical parameters were significantly higher in the plants grown under GR environmental conditions. On the other hand, chlorophyll (Chl), carotenoids (Car), and nitrate content were also influenced by different light treatments. Plants grown under LED light treatment resulted in significantly higher chlorophyll content compared to the control. However, significantly greater carotenoid content was in the plants grown under GR condition. The highest total chlorophyll content was recorded under B and R LED, whereas the lowest was in the GR condition. The lowest nitrate content in the blade and petiole was recorded in the plants grown under Y LED, while the highest nitrate content was recorded in the GR. Based on our result, it is possible to grow and improve some quality parameters of common outdoor 'iceberg' lettuce under LED where the solar light is limited or unavailable. Thus, plants performed better under GR light conditions than monochromatic LEDs; however, some LED lights could improve some quality parameters and biochemical contents in the 'iceberg' lettuce variety.

Keywords: LED light, morphological parameters, bioactive contents, common outdoor 'iceberg' lettuce (*Lactuca sativa* L.), nitrate content.

1. Introduction

The Light spectrum determines most of the morphological formation and biochemical content in leafy vegetables through photosynthetic apparatus, which gives the vigor power to the plant (Walters, 2005; Matsuda et

al., 2007). Improvement of vegetable quality and year-round cultivation with a minimum cost, safe to the environment and lower energy consumption is the current interest among crop growers (Pinho et al., 2012). Scientists have

shown the photoreceptors like phytochrome, cryptochrome and phototropin, which have the main role of photosynthetic efficiency in plants, are affected by light quality and this leads to gene expressions through initiating the signaling cascade (Lillo and Appenroth, 2001; Giliberto et al., 2005).

In recent years, the new inventions in lightening as the use of LEDs in horticulture crop production that has a tremendous revolution in high-tech greenhouses and this has inspired continuous development in plant growth and development (Massa et al., 2008). Plants require specific light (short and long) wavelengths depending on the growing cycle, blue light is needed for the stomatal opening and chloroplast development (Cosgrove and Green, 1981; Akoyunoglou and Anni, 1984; Schwartz and Zeiger, 1984; Takemiya et al., 2007), CO₂ exchange, stem elongation and phototropism (Blaauw and Blaauw-Jansen, 1970; Cosgrove and Green, 1981). Meanwhile R light is for seed germination and photosynthesis apparatus (McAllister, 1937; Balegh and Biddulph, 1970; Sæbø et al., 1995), flowering stimulation (Deitzer et al 1979), and internode elongation (Morgan and Smith, 1979). Many studies have shown a positive influence of the combination of B and R LED on lettuce growth and development (Yanagi et al., 1996; Lee et al., 2007; Chen et al., 2014; Amoozgar et al., 2017; Naznin et al., 2019), while very limited research on a monochromic LED light in comparison to the normal light spectrum has been conducted. The first suggested research on the combination of R and B lights on lettuce growth was by Bula et al. (1991), thereby they found lettuce seedlings faced etiolation under the influence of the monochromic R LED. Subsequently, Hoenecke et al. (1992) mentioned that it is necessary to mix some blue light with R to get adequate plant growth in lettuce seedling production. This is because plants naturally grow under

artificial light mixtures or normal sunlight (Kim et al., 2004; Matsuda et al., 2007). Although, it is confirmed that R and B lights are the most important lights in the improvement of photosynthesis, produce greater biomass, lower nitrate content in lettuce plant (Lin et al., 2013). Other monochromatic lights which are in between 400 nm and 700 nm PAR spectral region such as violet, white, green, yellow, orange and even invisible light spectrums under 400 as UV and above 700 nm as infrared has to be tested on the plants too, since they might have a similar or even greater result on the plant performance. UV light may have the same influence as blue light (Senger, 1984), since phytochrome is influenced by a small amount of far-red radiation (Yorio et al., 2001). On the other hand, W LED incorporates R and B lights, so that plants can survive under W light (Chen et al., 2016), where W LED is also typically used for general illumination and cultivation of plants (Lin et al., 2013).

‘Iceberg’ lettuce variety is a common outdoor cultivated lettuce in the USA and the Middle East, besides there is no or very limited research on the plant influences by LED (Amoozgar et al., 2017). The nature of the plant reactions for specific light has to be addressed in the use of modern technology for plant growth and development. Thus, this research aimed to investigate the response of a common outdoor Crisphead lettuce variety ‘Iceberg’ to different LED lightning in comparison to the GR (control) light condition.

2. Materials and methods

2.1. Experimental set-up and growth conditions

Seeds of ‘iceberg’ lettuce were sown in a tray with 80 cells containing peat-moss only. Twenty-five days after the seed sowing, the seedlings were transplanted under the custom-made lighting equipment. The homogenized

seedlings were transplanted in four plastic pots with 25 cm in height and 25 cm in diameter in the top and 15 cm at the base. Four growth cabinets with a size of 80 cm height 60 cm length were prepared in a complete dark laboratory room to the (four light treatments) or light-emitting diodes (LEDs). The boxes were covered with aluminum foil to avoid light absorption. The light treatments were installed in four separate cabinets. The LED lamps generate included 100% White (W) (430 nm and 582 nm), Yellow (Y) (570 nm), Red (R) (660 nm), Blue (B) (460 nm). Four pots were placed under each light treatment and one seedling was grown in each pot. All the pots were filled with the same substrate (peat-moss) under the same environmental condition except for the control (GR) treatment. Similar to the LED treatments, four pot seedlings were also grown with the same size and substrate, but under the optimal condition in a greenhouse (GR) as the control. The seedlings under LED light treatments were supplied the light treatment of 16/8 (day/night), RH of $65\% \pm 5$, and the temperature of 18-20 °C for 22 days, while plants under control condition rely on the sunlight 10/14 day/night light duration with the same temperature 18-20 °C.

2.2. Measurements of plant growth and morphology

To measure the morphological characters such as head weight, leaf number, leaf width, leaf length and leaf area, three plants were considered on the day of 22 from transplanting as the replication per light treatment. All the parameters were directly measured from fresh leaves on the harvesting day. The millimeter graph paper method was performed to measure the lettuce leaf area (cm²) as described by Pandey and Singh (2011) based on the following equation:

$$\text{Leaf area (cm}^2\text{)} = x/y$$

x: is the weight (g) of the area covered by the leaf outline on a millimeter graph paper

y: is the weight of one cm² of the same graph paper

2.3. Determination of nitrate

A simple method and portable apparatus were performed a quick measure of nitrate level in fresh lettuce leaf blade (mg kg⁻¹) and petiole (mg kg⁻¹) using Green test eco with margin error of about 10% as it is done by Klemo and Biti (2018).

2.4. Pigment measurement

Fresh lettuce leaf (0.5) g was grounded in a mortar and pestle. The grounded leaf was submerged in 10 ml of 80% acetone till the leaf color turned to white. The homogenized extracted juice was then centrifuged in 80-2 tabletop low speed centrifuge 4000 rpm for 15 min at 4 °C. The solution mixture was analyzed for chlorophyll a (Chl a), chlorophyll b (Chl b), total chlorophyll (Chl a+ Chl b) and carotenoids (Car) content in UV/Visible spectrophotometer at A_{663nm} Chl a, A_{646nm} Chl b, and A_{470nm} Car. Then the achieved data was calculated based on the following equations by Sumanta et al. (2014) (**Table 1**):

$$\text{Chl a} = 12.25A_{663} - 2.79A_{646}$$

$$\text{Chl b} = 21.5A_{646} - 5.1A_{663}$$

$$\text{Total Chl (a+ b)} = 7.15(A_{663}) + 18.71(A_{646})$$

$$\text{Car} = (1000A_{470} - 1.82 \text{ Chl a} - 85.02 \text{ Chl b})/198$$

2.5. Statistical analysis

The data were analyzed using one-way analysis of variance (ANOVA), combined with Duncan's multiple range tests at the confidence levels of $p < 0.05$ using SPSS statistical analysis software version 25.0. The mean value and standard errors were expressed in Excel software.

Table 1. Spectrophotometric determination of absorbance for Chlorophyll a, Chlorophyll b and Carotenoids using 80% acetone as a solvent

Light treatment	Chl a (A _{663nm})	Chl b (A _{646nm})	Car (A _{470nm})
GR	0.229	0.161	1.367
W LED	0.532	0.298	1.184
Y LED	0.878	0.599	1.144
R LED	0.594	0.433	1.144
B LED	1.209	0.535	1.150

Note: Ch a = Chlorophyll a, Ch b = Chlorophyll b, Car = Carotenoids

3. Results

3.1. Plant morphology and growth characteristics

The morphological characteristics of lettuce were statistically influenced by the light spectra treatments. Based on the data from (Table 2), plants grown in the GR condition responded greater than under the artificial light (LEDs) condition. Leaf number, for example, was significantly higher in the plants grown under the GR (13.25) than under LEDs. Plants also reacted positively under different LED treatments themselves, for example, plants under 430, 582 nm (W LED) formed significantly more leaves (10.63), while the least leaf number was under the longest wavelength 660 nm R LED (7.62). The greatest

positive influence of 460 nm Blue light was found on the leaf expansion (leaf length) and leaf area at 17.03 (cm) and 74.84 (cm²) respectively, while the lowest result was for the plants grown under W LED at 14.50 (cm) and 24.96 (cm²) respectively. Significant greater leaf width was for the plants under GR light condition followed by W, B, Y and R LED light treatments. Significantly greater head weight was recorded in the plants grown under GR and B LED at 8.19 and 8.18 (g), while the lowest head weight was in the plants grown under W, R and Y LED at 4.56, 5.17 and 5.63 (g) respectively. Significantly bigger fresh head weight was under GR growth condition rather than LED light treatments (Table 2).

Table 2. Influence of light quality on leaf number, leaf length, leaf width, leaf area, and head fresh weight of Iceberg lettuce 22 days after transplanting

Light treatment	Peak wavelength (nm)	Parameters				
		Leaf number	Leaf length (cm)	Leaf width (cm)	Leaf area (cm ²)	Head weight (g)
GR		13.25 ± 1.28 ^a	12.93 ± 1.21 ^c	7.58 ± 1.25 ^a	51.65 ± 3.09 ^b	8.19 ± 0.73 ^a
W LED	(430, 582)	10.63 ± 1.92 ^b	14.50 ± 2.38 ^{bc}	5.34 ± 0.88 ^b	24.96 ± 3.05 ^c	4.56 ± 0.42 ^b
Y LED	580	8.63 ± 1.30 ^c	14.53 ± 1.95 ^{bc}	4.38 ± 0.92 ^{bc}	44.84 ± 5.67 ^{3b}	5.63 ± 0.34 ^b
R LED	660	7.62 ± 1.60 ^c	15.00 ± 1.16 ^b	3.43 ± 0.76 ^c	49.43 ± 1.82 ^b	5.17 ± 0.70 ^b
B LED	460	8.50 ± 1.85 ^c	17.03 ± 2.26 ^a	4.61 ± 0.99 ^b	74.84 ± 7.72 ^a	8.18 ± 1.16 ^a

Note: Mean values ± SD with same letter are not significantly different at $p \geq 0.05$ with Duncan multiple range test; Values in each column are mean ± SD (n=8). GR is the control (Greenhouse), W LED is WHITE light, Y LED is YELLOW light, R LED is RED light, B LED is BLUE light

3.2. Chlorophyll and carotenoid contents

In general, pigment accumulation in the plant grown under light-emitting diodes (LEDs) resulted in significantly higher than under greenhouse conditions (**Fig. 1 and 2**). **Figure 1** demonstrates that chlorophyll concentration had a distinct response to different LED light treatments, too. The Chl a content in the lettuce leaves is higher than Chl b in all the light treatments including the GR. Plants under 460 nm B LED produced significantly higher Chl a content, while the control treatment was the lowest Chl a. However, the main significant difference of the Chl b was in the plants grown under 580 nm Y LED and the lowest was under GR treatment. Total chlorophyll was significantly higher

under 460 nm B LED followed by 570 nm Y LED at 18.85 and 17.48 (mg. mL^{-1}) respectively (**Fig. 1**). **Figure 2** indicates that lettuce leaves grown under GR light condition recorded a significantly greater carotenoid content at 5.89 (mg. mL^{-1}) compare to the LED lighting conditions.

Different LED colors have also impacted the carotenoid pigment content. 430, 582 nm W and 460 nm B LED recorded the highest carotenoid content 4.081 and 3.395 (mg. mL^{-1}) respectively, whereas 580 nm Y LED was the most influenced light treatment on the leaf carotene content by recording the lowest content followed by 660 nm R LED at 2.09 and 3.02 (mg. mL^{-1}) respectively.

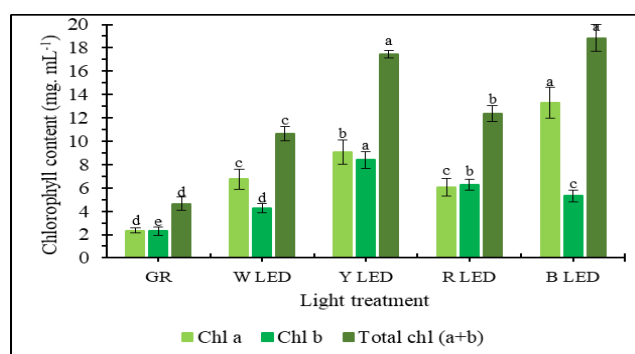


Fig. 1. Chlorophyll content under the influence of various light treatments. Error bars indicate standard deviation (SD); Similar letters are not significantly different at Duncan multiple range test $p \geq 0.05$; GR is the control (Greenhouse), W LED is WHITE light, Y LED is YELLOW light, R LED is RED light, B LED is BLUE light

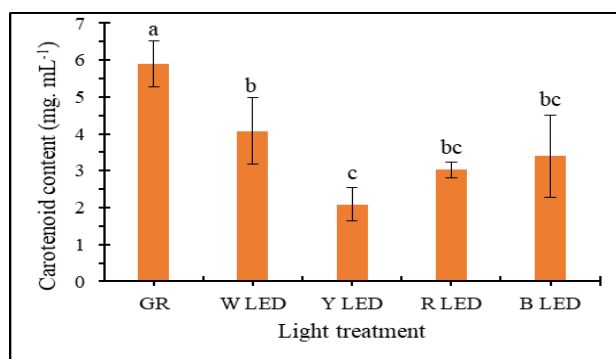


Fig. 2. Carotenoids content under the influence of various light treatments. Error bars indicate standard deviation; Similar letters are not significantly different at Duncan multiple range test $p \geq 0.05$ GR is the control (Greenhouse), W LED is WHITE light, Y LED is YELLOW light, R LED is RED light, B LED is BLUE light

The GR treatment was adverse to chlorophyll pigment accumulation, while it is more appropriate to carotenoids.

3.3. Nitrate content in lettuce leaves (mg. kg⁻¹)

Nitrate concentration in lettuce leaf blade and petiole was different between the plant growth conditions (GR and LEDs). Statistically, the lowest nitrate accumulation in leaf blade was in the 580 nm Y LED at 112.43 (mg. kg⁻¹), whereas, there were similar and

non-significantly different among other treatments. Also, the lowest nitrate content in leaf petiole was recorded in 580 nm Y LED and GR (control) at 63.33 and 115.00 (mg. kg⁻¹) respectively, while the highest nitrate content was recorded in the plants grown under B LED followed by W and R LED at 496.67, 316.67 and 298.67 (mg. kg⁻¹) respectively. In general, nitrate concentration was far much higher in the leaf petiole than in the blade (**Fig. 3A and B**).

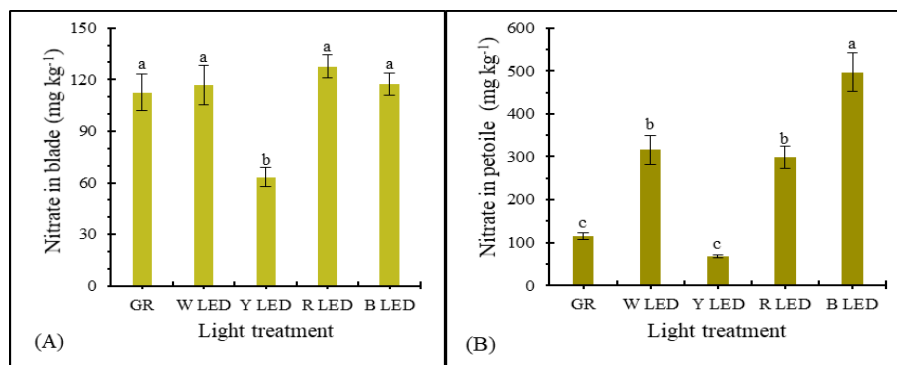


Fig. 3. Nitrate level in lettuce leaf blade (A) and petiole (B) under the influence of various light treatments. Error bars indicate standard deviation; Similar letters are not significantly different at Duncan multiple range test $p \geq 0.5$; GR is the control (Greenhouse), W LED is WHITE light, Y LED is YELLOW light, R LED is RED light, B LED is BLUE light

4. Discussion

The majority of morphological parameters (leaf number, leaf width, head fresh weight) were significantly greater in the 'Iceberg' lettuce grown under GR light condition. On the contrary, higher biochemical contents (pigments) were obtained in the lettuce leaves grown under light emitting diodes (LEDs). This results agree to the result observed by Fan et al., (2013) where they found the best pigment accumulation in Chinese cabbage grown under mixture R/B LED and Dysprosium lamp rather than monochromic LED lights. Among the LED light treatments, the greatest chlorophyll pigments were observed in the seedlings grown under B and Y LED, whereas carotenoid pigment under W and B LED. Researchers

agree that blue light is more beneficial to the pigment accumulation in plants (Kurilčik et al., 2008; Poudel et al., 2008) since plants under long term blue light improve the ALA-synthesizing activity (Kamiya et al., 1981). Plants cultured under GR produced significantly more leaves than under monochromic LEDs. Only leaf length and leaf area were significantly higher under the B LED. A similar result was recorded by Hogewoning et al. (2010) where they found that *Cucumis* leaf was significantly increased under blue light irradiation compare to R LED. Solar light contains all the light spectrums so that plants having more than a single light can perform better in improving pigment content,

biomass and morphological characteristics (Chen et al., 2014). Lettuce seedlings responded differently among the LEDs, too. Some LED lights influenced negatively on some physical quality parameters, whereas positive impacts were found for some chemical contents as nitrate level.

In general, the lowest morphological parameters (leaf and head biomass) were in the plants grown under R LED. Brown et al. (1995) demonstrated that pepper grown under R LED produced significantly lower biomass in comparison to those cultured under B LED and broad spectrum metal halide (MH) lamps.

Lower nitrate accumulation is considered as a better quality in leafy vegetables (Santamaria, 2006) since it influences human health while converted to nitrite. Among the LED light treatments, we observed that lettuce under Y LED accumulated significantly lower nitrate content in both leaf blade and petiole, whereas the highest nitrate was found in the plants grown under the B LED ($496.67 \text{ mg.kg}^{-1}$) in the leaf petiole, this might be because of changes in some regulatory mechanism in the plant (Chen et al., 2014) or the nitrate reductase genes of messenger RNA in the plant cells (Lillo, 1994). Matsuda et al. (2007) have also found that nitrogen level increased per unit leaf area in Spinach (*Spinacia oleracea* L.) with increasing blue-light PFD up to $100 \mu\text{mol m}^{-2} \text{ s}^{-1}$.

In our research, leaf morphological abnormality was found in the 'iceberg' lettuce cultured under red light, while some chemical contents respond positively with red light such as total chlorophyll and carotenoids. Y LED, for example, resulted in the lowest nitrate content in the lettuce blade and petiole however, lower fresh biomass was performed in comparison to other lights including GR (control). The higher chlorophyll content in the plants grown under B LED light might be due to the stomatal opening which B LED is known

for controlling stomal opening in plant leaves (Sharkey and Raschke, 1981; Zeiger, 1984). The greater chlorophyll content and leaf area were found in the cultures irradiated with B LED. Similar results were recorded by Sæbø et al. (1995) working on *in vitro* culture of *Betula pendula* Roth under red and blue light. Naznin et al., (2019) have discovered that pigments (Chl a, Chl b, and total Chl) in lettuce and basil increased with the increase of B LED lightening percentage to R LED. Other research studies have proven the greater chlorophyll (Chl) a/b ratio in the plants grown under B light (Leong and Anderson, 1984; Lopez-Juez and Hughes, 1995).

In this research, we found significantly higher carotenoid content in the GR, while the lowest was recorded in the monochromic Y LED. Chen et al. (2014) have found significantly greater chlorophyll and carotenoids in the plants grown under fluorescent light compare to the other monochromic LED lights.

5. Conclusions

This research shows the potential irradiation source for indoor lettuce production. It also demonstrates that not only B and R LED are important for the modern lettuce production technics, but other LEDs like Y and W can positively influence some lettuce quality parameters and they might be more suitable in proper combination with other wavelengths of light. Strategically, light emitting diodes might be the most appropriate alternative to solar light. However, monochromic lights are unprofitable for the morphological parameters of outdoor lettuce. It is also important to determine other tests on the influence of LED on the common outdoor lettuce variety 'Iceberg'.

Conflict of interest

The authors have declared that there is no conflict of interest.

References

1. Akoyunoglou G, Anni H (1984) Blue light effect on chloroplast development in higher plants. In *Blue light effects in biological systems*. Springer, Berlin, Heidelberg.
2. Amoozgar A, Mohammadi A, Sabzalian MR (2017) Impact of light-emitting diode irradiation on photosynthesis, phytochemical composition and mineral element content of lettuce cv. Grizzly. *Photosynthetica* 55:85–95. doi: 10.1007/s11099-016-0216-8
3. Balegh S, Biddulph O (1970) The Photosynthetic Action Spectrum of the Bean Plant. *Plant Physiol* 46:1–5.
4. Blaauw OH, Blaauw-Jansen G (1970) The phototropic responses of *Avena coleoptiles*. *Acta Botanica Neerlandica* 19:755–763.
5. Brown C s., Schuerger AC, Sager JC (1995) Growth and photomorphogenesis of pepper plants under red light-emitting diodes with supplemental blue or far-red lighting. *Journal of the American Society for Horticultural Science* 120:808–813. doi: 10.1016/j.envexpbot.2009.06.011
6. Bula RJ, Morrow RC, Tibbitts TW, et al (1991) Light-emitting Diodes as a Radiation Source for Plants. *HortScience* 26:203–205. doi: 10.1007/s004420050624
7. Chen X li, Guo W zhong, Xue X zhang, et al (2014) Growth and quality responses of “Green Oak Leaf” lettuce as affected by monochromic or mixed radiation provided by fluorescent lamp (FL) and light-emitting diode (LED). *Scientia Horticulturae* 172:168–175. doi: 10.1016/j.scienta.2014.04.009
8. Chen X li, Xue X zhang, Guo W zhong, et al (2016) Growth and nutritional properties of lettuce affected by mixed irradiation of white and supplemental light provided by light-emitting diode. *Scientia Horticulturae* 200:111–118. doi: 10.1016/j.scienta.2016.01.007
9. Cosgrove DJ, Green PB (1981) Rapid Suppression of Growth by Blue Light. *Plant Physiology* 67:584–590. doi: 10.1104/pp.68.6.1447
10. Deitzer GF, Hayes R, Jabben M (1979) Kinetics and Time Dependence of the Effect of Far Red Light on the Photoperiodic Induction of Flowering in Wintex Barley. *Plant Physiology* 64:1015–1021. doi: 10.1104/pp.64.6.1015
11. Fan X, Zang J, Xu Z, et al (2013) Effects of different light quality on growth , chlorophyll concentration and chlorophyll biosynthesis precursors of non-heading Chinese cabbage Effects of different light quality on growth, chlorophyll concentration and chlorophyll biosynthesis precursor. *Acta physiologiae plantarum* 35:2721–2726. doi: 10.1007/s11738-013-1304-z
12. Giliberto L, Perrotta G, Pallara P, et al (2005) Manipulation of the blue light photoreceptor cryptochrome 2 in tomato affects vegetative development, flowering time, and fruit antioxidant content. *Plant Physiology* 137:199–208. doi: 10.1104/pp.104.051987
13. Hoenecke ME, Bula RJ, Tibbitts TW (1992) Importance of “blue” photon levels for lettuce seedlings grown under red-light-emitting diodes. *HortScience* 27:427–430. doi: 10.21273/hortsci.27.5.427
14. Hogewoning SW, Trouwborst G, Maljaars H, et al (2010) Blue light dose-responses of leaf photosynthesis, morphology, and chemical composition of *Cucumis sativus* grown under different combinations of red

- and blue light. *Journal of experimental botany* 61:3107–3117.
doi: 10.1093/jxb/erq132
15. Kamiya A, Ikegami I, Hase E (1981) Effects of Light on Chlorophyll Formation in Cultured Tobacco Cells I. Chlorophyll Accumulation and Phototransformation of Protochlorophyll (ide) in Callus Cells under Blue and Red light. *Plant and cell physiology* 22:1385–1396.
 16. Kim HH, Goins GD, Wheeler RM, Sager JC (2004) Green-light supplementation for enhanced lettuce growth under red-and blue-light-emitting diodes. *HortScience* 39:1617–1622.
doi: 10.21273/hortsci.39.7.1617
 17. Klemo M, Biti B (2018) Nitrate Concentration in Plant Products of Albanian Market. *Knowledge International Journal* 28:1289–1294.
doi: 10.35120/kij28041289m
 18. Kurilčik A, Miklušytė-čanová R, Dapkūnienė S, et al (2008) In vitro culture of Chrysanthemum plantlets using light-emitting diodes. *Central European Journal of Biology* 3:161–167.
doi: 10.2478/s11535-008-0006-9
 19. Lee SH, Tewari RK, Hahn EJ, Paek KY (2007) Photon flux density and light quality induce changes in growth, stomatal development, photosynthesis and transpiration of *Withania Somnifera* (L.) Dunal. plantlets. *Plant Cell, Tissue and Organ Culture* 90:141–151.
doi: 10.1007/s11240-006-9191-2
 20. Leong TY, Anderson JM (1984) Adaptation of the thylakoid membranes of pea chloroplasts to light intensities. I. Study on the distribution of chlorophyll-protein complexes. *Photosynthesis research* 5:105–115.
 21. Lillo C (1994) Light regulation of nitrate reductase in green leaves of higher plants. *Physiologia Plantarum* 90:616–620. doi: 10.1111/j.1399-3054.1994.tb08822.x
 22. Lillo C, Appenroth KJ (2001) Light regulation of nitrate reductase in higher plants: Which photoreceptors are involved? *Plant Biology* 3:455–465. doi: 10.1055/s-2001-17732
 23. Lin KH, Huang MY, Huang WD, et al (2013) The effects of red, blue, and white light-emitting diodes on the growth, development, and edible quality of hydroponically grown lettuce (*Lactuca sativa* L. var. capitata). *Scientia Horticulturae* 150:86–91.
doi:https://doi.org/10.1016/j.scienta.2012.10.002
 24. Lopez-Juez E, Hughes MJ (1995) Effect of blue light and red light on the control of chloroplast acclimation of lightgrown pea leaves to increased fluence rates. *Photochemistry and photobiology*. 61:106–111.
 25. Massa GD, Kim HH, Wheeler RM, Mitchell CA (2008) Plant productivity in response to LED lighting. *HortScience* 43:1951–1956.
doi: 10.21273/hortsci.43.7.1951
 26. Matsuda R, Ohashi-Kaneko K, Fujiwara K, Kurata K (2007) Analysis of the relationship between blue-light photon flux density and the photosynthetic properties of spinach (*Spinacia oleracea* L.) leaves with regard to the acclimation of photosynthesis to growth irradiance. *Soil Science and Plant Nutrition* 53:459–465. doi: 10.1111/j.1747-0765.2007.00150.x
 27. McAllister F and (1937) Wavelengths of radiation in the visible spectrum promoting the germination of lightsensitive lettuce seed. *Smithsonian Inst. Publs., Misc. Collections* 96:1–8.
 28. Morgan DC, Smith H (1979) A systematic relationship between phytochrome-controlled development and species habitat,

- for plants grown in simulated natural radiation. *Planta* 145:253–258.
29. Naznin MT, Lefsrud M, Gravel V, Azad MOK (2019) Blue light added with red LEDs enhance growth characteristics, pigments content, and antioxidant capacity in lettuce, Spinach, Kale, Basil, and sweet pepper in a controlled environment. *Plants*. doi: 10.3390/plants8040093
30. Pandey SK, Singh H (2011) A Simple, Cost-Effective Method for Leaf Area Estimation. *Journal of Botany* 2011:1–6. doi: 10.1155/2011/658240
31. Pinho P, Jokinen K, Halonen L (2012) Horticultural lighting - Present and future challenges. *Lighting Research and Technology* 44:427–437. doi: 10.1177/1477153511424986
32. Poudel PR, Kataoka I, Ryosuke M (2008) Effect of red- and blue-light-emitting diodes on growth and morphogenesis of grapes. *Plant cell, tissue and organ culture* 92:147–153. doi: 10.1007/s11240-007-9317-1
33. Sæbø A, Krekling T, Appelgren M (1995) Light quality affects photosynthesis and leaf anatomy of birch plantlets in vitro. *Plant Cell, Tissue and Organ Culture* 41:177–185.
34. Santamaria P (2006) Nitrate in vegetables: Toxicity, content, intake and EC regulation. *Journal of the Science of Food and Agriculture* 86:10–17. doi: 10.1002/jsfa.2351
35. Schwartz A, Zeiger E (1984) Metabolic energy for stomatal opening: Roles of photophosphorylation and oxidative phosphorylation. *Planta* 161:129–136. doi: <https://doi.org/10.1007/BF00395472>
36. Senger H (1984) Blue light effects in biological systems. Springer-Verlag, Berlin
37. Sharkey TD, Raschke K (1981) Effect of Light Quality on Stomatal Opening in Leaves of *Xanthium strumarium* L. . *Plant Physiology* 68:1170–1174. doi: 10.1104/pp.68.5.1170
38. Sumanta N, Haque CI, Nishika J, Suprakash R (2014) Spectrophotometric Analysis of Chlorophylls and Carotenoids from Commonly Grown Fern Species by Using Various Extracting Solvents. *Research Journal of Chemical Sciences Res. J. Chem. Sci* 4:63–69.
39. Takemiya A, Takahashi Y, Shimazaki K (2007) Leaf temperature reduction by blue light-dependent stomatal opening. *Cryobiology and Cryotechnology* 53:1–5.
40. Walters RG (2005) Towards an understanding of photosynthetic acclimation. *Journal of Experimental Botany* 56:435–447. doi: 10.1093/jxb/eri060
41. Yanagi T, Okamoto K, Takita S (1996) Effects of blue, red, and blue/red lights of two different PPF levels on growth and morphogenesis of lettuce plants. *Acta Horticulturae* 440:117–122. doi: 10.17660/ActaHortic.1996.440.21
42. Yorio NC, Goins GD, Kagie HR, et al (2001) Improving Spinach, Radish, and peak height), which closely matches a peak absorbance of chlorophyll (McCree, 1972). Lettuce Growth under Red Light- Although red LEDs have great potential for use as a light source to drive photosynthe- emitting Diodes (LED. *HortScience* 36:380–383.
43. Zeiger E (1984) Blue light and stomatal function. In *Blue light effects in biological systems*. Springer, Berlin, Heidelberg.

HOMAGE TO GEORGE E. PALADE CELL PROTEIN SECRETION IN VASCULAR BIOLOGY: OVERVIEW AND UPDATES

George N. CHALDAKOV^{1*}, Luigi ALOE², Anna KÁDÁR³, Peter GHENEV⁴, Marco FIORE⁵,
Rouzha Z. PANCHEVA⁶, Plamen PANAYOTOV⁷

^{*1}Department of Anatomy and Cell Biology, and Department of Translational Stem Cell Biology,
Research Institute, Medical University, Varna, Bulgaria

²Fondazione Iret Tecnopolo R. Levi-Montalcini, Rome, Italy

³Department of Pathology, Faculty of Medicine, Semmelweis University, Budapest, Hungary

⁴Department of Pathology, Medical University, Varna, Bulgaria,

⁵Institute of Biochemistry and Cell Biology, Section of Neurobiology, National Research Council
(CNR), Rome, Italy

⁶Department of Hygiene and Epidemiology, Faculty of Public Health, Medical University, Varna,
Bulgaria

⁷Department of Cardiac Surgery, St Marina University Hospital, Varna, Bulgaria

*Correspondence:

George N. CHALDAKOV
chaldakov@yahoo.com

Received: 15 May 2021; **Accepted:** 1 June 2021; **Published:** 30 June 2021

Abstract: This short overview and updates expresses our brain-and-heart homage to George Emil Palade, "the most influential cell biologist ever". In his 1971 paper Palade wrote for Albert Claude, the founder of biological electron microscopic method: "Seldom has a field owed so much to a single man". Herein, we articulate the same words for George Palade, the Teacher of many generations in cell biology research and education. Accordingly, we focus on two paradigm shifts in the cell biology, namely (i) the transition from light to transmission electron microscopy in studying cell protein secretion made by George Palade, and (ii) the transition from contractile to secretory phenotype of vascular smooth muscle cells made by Maria Daria Haust followed and developed by our research group. Altogether, we argue that one of the present challenges in vascular biology is to cultivate secreto-centric thinking and thus further focusing on how we could make the vascular muscle's secretory pathways work for the benefit of human's cardiovascular health.

Keywords: George Palade, proteins, secretory pathways, rough endoplasmic reticulum, Golgi complex, microtubules, colchicine, therapy, cardiovascular diseases.

Introduction

Some people are so much known that it is sufficient to mention their initials only to recognize them:

L - Carl Linnaeus

N - Napoleon Bonaparte

FDR - Franklin Delano Roosevelt

JFK - John Fitzgerald Kennedy

RLM - Rita Levi-Montalcini

GEP - George Emil Palade



George Emil Palade (November 19, 1912 – October 7, 2008) was a Romanian-American cell biologist graduated in 1940 from the Carol Davila School of Medicine in Bucharest.

In his 1971 paper George Palade wrote for Albert Claude, the founder of biological electron microscopic method: “Seldom has a field owed so much to a single man” (Palade 1971). Herein, we, most respectfully, articulate the same words for him, the Teacher of many generations in cell biology research and education (Singer, 2003; Farquhar, 2012; Chaldakov, 2016). We, particularly one of us (GNC), learned a lot of his concept of cell protein secretion in exocrine pancreatic cells and applied (1972-1992) it to his transmission electron microscopy (TEM) studies on the secretion in vascular smooth muscle cells (VSMC).

George Palade’s Eureka

- Ribosomes and polyribosomes (polysomes) – free in the cytoplasm or attached on the surface of endoplasmic reticulum’s cisterns.
- Endoplasmic reticulum – smooth (without attached polysomes) or rough (with attached polysomes (**Fig. 1**).

- Mitochondria
- Golgi complex and Golgi-derived secretion vacuoles (granules)
- Specific granules in heart’s atrial cardiomyocytes
- Plasmalemmal vesicles (caveolae) (**Fig. 2**)
- Weibel-Palade bodies, the structural signature of vascular endothelial cells
- The concept of cell protein secretion (Palade, 1975)

In the present brief overview and updates, we focus on two paradigm shifts in the cell biology, namely (i) the transition from light microscopy to TEM in studying cell protein secretion made by George Palade, “the most influential cell biologist ever”, and (ii) the transition from contractile to secretory phenotype of VSMC made by the centurial approaching Maria Daria Haust (Haust et al., 1960), the Great Lady of atherosclerosis research, followed and developed by our research group (Chaldakov and Nikolov, 1975; Chaldakov et al., 1977; Chaldakov and Kádár, 1978; reviewed in Chaldakov and Vankov, 1986a, b).

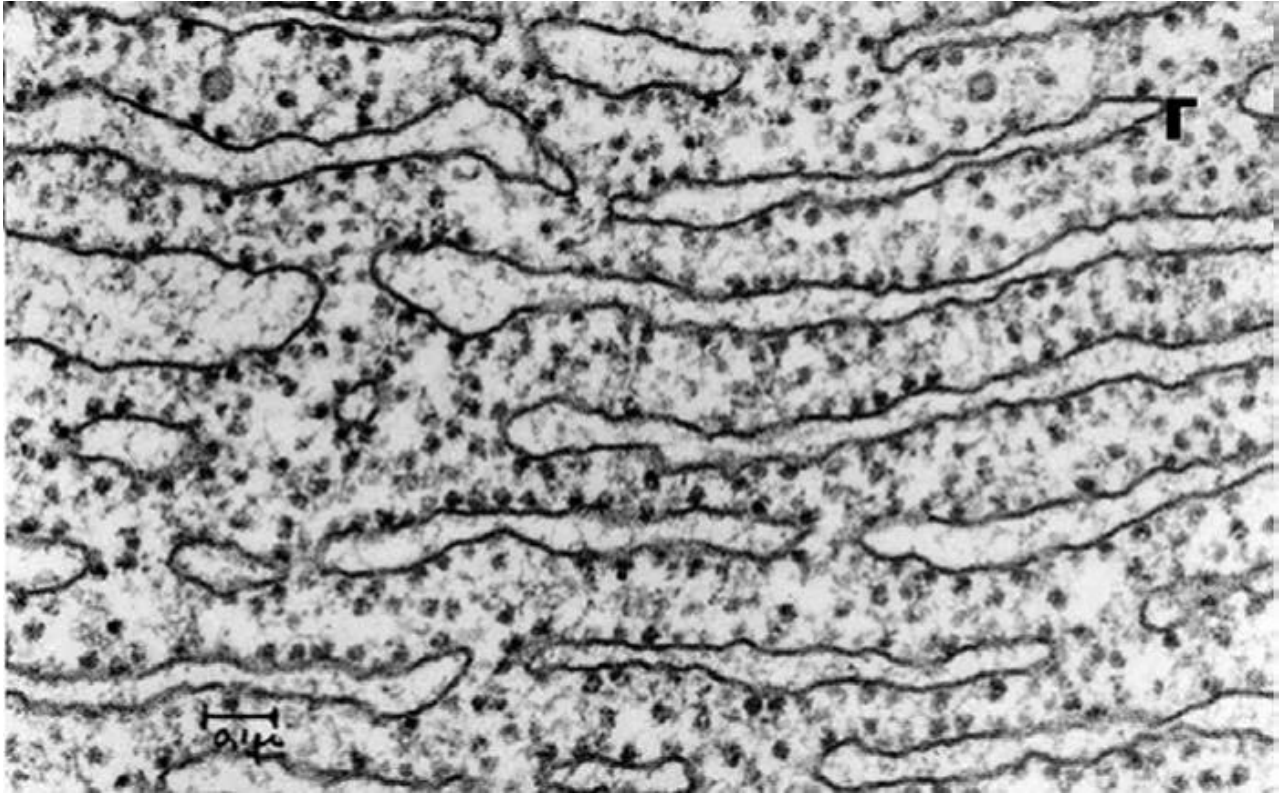


Fig. 1. TEM image of rough endoplasmic reticulum from the George E. Palade EM Collection

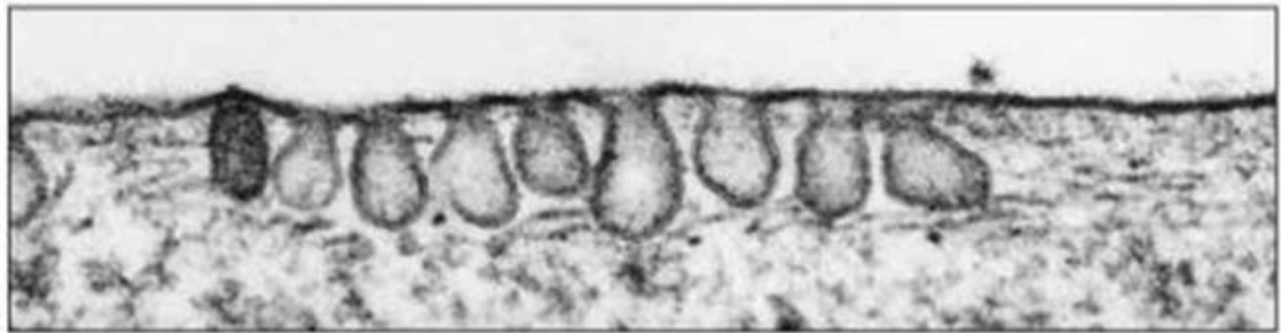


Fig. 2. TEM micrograph of plasmalemma-derived pinocytotic vesicles (Greek *pino* – drink, and *kytos* – cell) which are 50–100 nm plasmalemmal invaginations found in many cell types. Nowadays, these vesicles are called caveolae (Latin, “little caves”) coated with caveolin protein, hence, caveolin-coated vesicles. The biological importance of caveolae was enriched by recent studies using caveolin knockout mice that show severe abnormalities in the cardiovascular and other systems. Image from the George E. Palade EM Collection.

Contextual background

The secretion (synthesis, sorting, targeting, storage, and release) is a fundamental biological process in (almost) all cell types. In 1898, Camillo Golgi reported his discovery of

internal reticular apparatus, a novel intracellular organelle observed in nerve cells using his silver nitrate impregnation method (**Fig. 3**) (reviewed in Mazzarello et al., 2009).

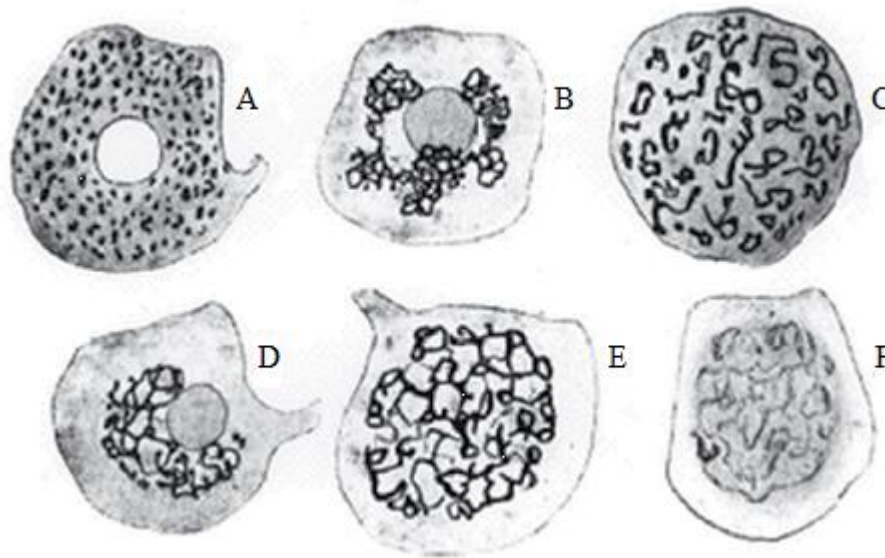


Fig. 3. Drawings of Camilo Golgi illustrating *internal reticular apparatus* presented in his lecture on 19 April 1898 at the University of Pavia, Pavia, Italy. This organelle was visualized by the procedure initially named by Golgi *la reazione nera* (Italian, “the black reaction”), later known as Golgi method of impregnation with silver salts. In the first years of 20th century *internal reticular apparatus* was named Golgi apparatus, latter Golgi complex – a discovery with of high scientific value in cell biology. *Internal reticular apparatus*’ perinuclear location (**A, B, D**) observed at different levels of cross-sections is shown (**A–F**).

However, the real existence of this organelle was seriously questioned until it was finally identified by TEM in the mid-1950s,

mainly due to the excellent work of George Palade (Palade 1971; Farquhar and Palade, 1998; Farquhar, 2012) (**Fig. 4**).

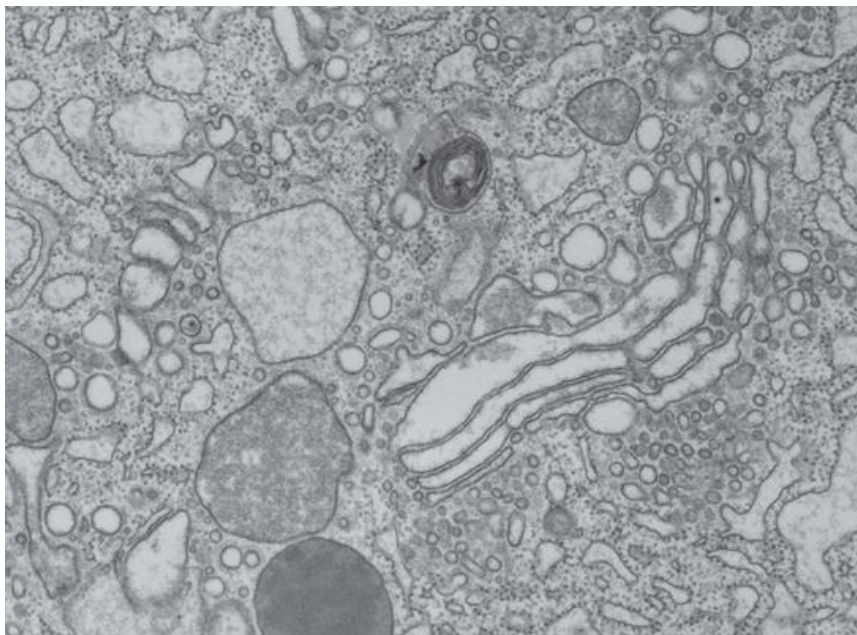


Fig. 4. TEM micrograph of the Golgi complex in a pancreatic exocrine cell. x25 000. Image from the George E. Palade EM Collection

According to Palade's concept (Palade, 1975) and to Günter Blobel's signal hypothesis (Blobel, 2000), the protein secretory pathway constitutes of several intracellular steps: synthesis, sorting, targeting, storage (in case of

regulated *versus* constitutive secretion), translocation and, finally, exocytosis (**Fig. 5-7**) including porocytosis (Silver and Pappas, 2005) mediated by porosomes (Jena, 2010).

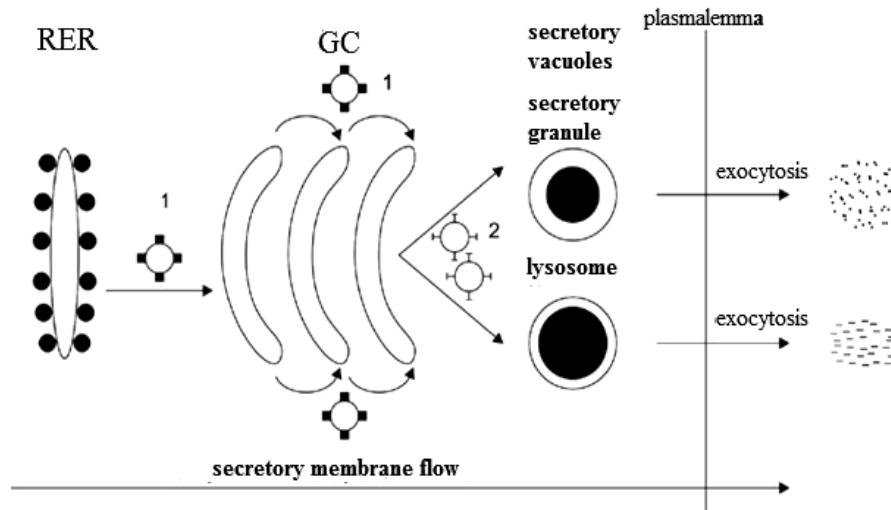


Fig. 5. Schematic representation of rough endoplasmic reticulum (RER)-Golgi pathway (secretory membrane flow). **1.** COated Protein (COP II) vesicles originate from RER and translocated to Golgi complex (GC) through membrane fission-fusion way. **2.** GC-derived clathrin- and adaptin-coated vesicles. Note, GC delivers both secretory vacuoles (granules) and lysosomes; their content, as exportable proteins, is discharged *via* exocytosis. COP I vesicles (not shown) transport proteins from *cis* Golgi complex back to RER, also between Golgi subcompartments, a transport termed *retrograde transport*, in contrast to the *anterograde transport* associated with COP II vesicles, which transport proteins from RER to GC. From (Chaldakov 2021)

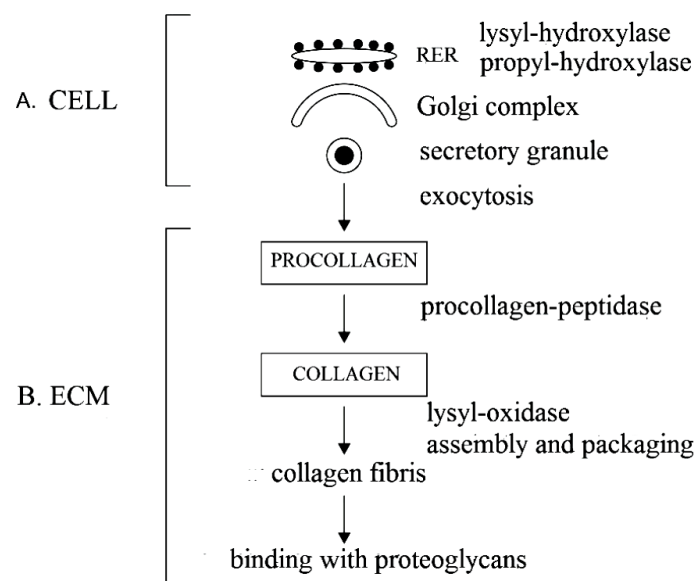


Fig. 6. Schematic representation of intra- and extracellular secretory pathways of procollagen to collagen biosynthesis. RER, rough endoplasmic reticulum; ECM, extracellular matrix. From (Chaldakov, 2021)

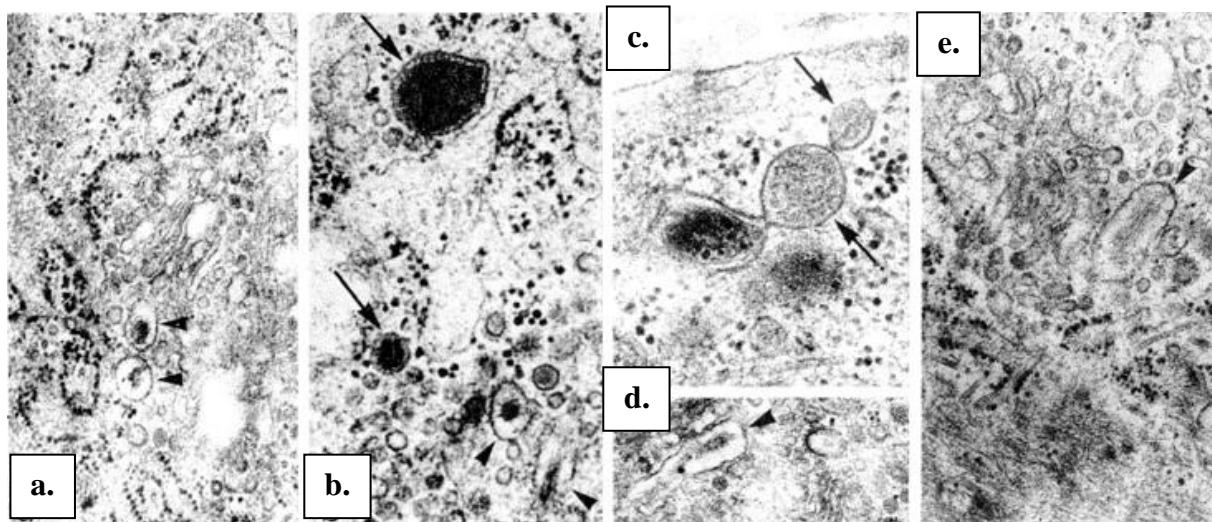


Fig. 7. TEM micrographs of secretory-state (secretory phenotype) aortic smooth muscle cells of the rabbit. **a-e.** Spherical-shaped (arrows) and elongated-shaped (arrowheads) secretion granules.

a-e, x20 000. From (Chaldakov and Vankov, 1986a)

In 1974, the Nobel Prize in Physiology or Medicine was awarded to Albert Claude, George Palade, and Christian de Duve “for their discoveries concerning the structural and functional organization of the cell”. Then, the Chairman of the Nobel committee remarked: “The trio was largely responsible for the creation of modern cell biology”. Indeed, it has been discovering a novel world of the cell, revealing membrane-bound organelles (mitochondria, caveolae, endoplasmic reticulum, Golgi complex, endosomes, lysosomes, etc) and non-membrane-bound organelles (polyribosomes, cytoskeletal filaments and microtubules, spliceosomes, proteasomes, etc). When received the Nobel prize, George Palade said: “Cell biology finally makes possible a century-old dream: that of analysis of diseases at the cellular level, the first step toward their control.” This statement might be envisaged as an ideogenetic beginning of the translational research.

All cells secrete proteins

The human body could be viewed as composed of multiple types of secretory cells delivering a vast number of (neuro)peptides,

cellular proteins (cytokines, chemokines, cell growth factors, adipokines, myokines, adipomyokines, osteokines, gastrokines, etc), extracellular matrix proteins, glycoproteins and proteoglycans (collagen, elastin, fibrillin, aggrecan, laminin, fibronectin, etc), also steroids and other signaling and structural molecules, which control many biological processes and functions in health and disease (Palade, 1975; Blobel, 2000; Chaldakov et al., 2003; Töre et al., 2007; Chaldakov and Fiore, 2010; Frohlich et al., 2021).

The secretory proteins are two major classes: imported and exported proteins. Accordingly, they are targeted to five loci: cytosol, organelles, nucleus, plasmalemma, and outside the cell. A large number of exported proteins are processed by the RER-Golgi complex-TGN (trans-Golgi network) route including targeting processes using signal recognition particle (SRP)-polyribosome-signal peptide (SP) receptor-mediated interactions; these latter represent the Blobel’s topology concept of cell protein secretion (Blobel, 2000).

However, such a SRP-SP dependent protein secretion cannot explain the processing of SP-lacking proteins which are also exported

such as cell growth factors and cytokines. These proteins gain access to the cell exterior *via* an unconventional secretory pathway, which does not use Golgi complex (Nickel, 2010). Intriguing examples of such a secretion are extracellular vesicles (also dubbed nanosomes): (i) exosomes, 30-100 nm vesicles derived from multivesicular bodies (Lai and Breakefield, 2012; Zar et al., 2020), and (ii) ectosomes (microparticles), 100-900 nm vesicles shed from plasma membrane (Sadallah et al., 2011). Both exosomes and ectosomes carrying important bioactive molecules, e.g. DNA, mRNA, microRNA, cytokines and immunoglobulins, to communicate among cells *via* endo- and paracrine way, hence, collectively designated singnalosomes (Chaldakov, 2021).

Two membrane flows operate inside the cell:

- i. Protein secretory membrane flow (secretory pathway) starting on free polyribosomes, followed by RER,

posttranslational modification in Golgi complex, Golgi-derived vacuoles, the motor protein kinesin [a microtubule (MT)-based anterograde (+) motor] and, finally, plasmalemma, where the release of vacuole-stored proteins occurred (see Fig. 5-7). There are two different secretory pathways: regulated and constitutive (**Fig. 8**).

- ii. endocytotic membrane flow (endocytic pathway) starting from plasmalemma and moves in the following order: coated pits, coated vesicles, caveolae, caveolosomes, early endosomes, late endosomes, MVB and lysosomes in collaboration with dynein [MT-based retrograde (-) motor protein]. It is the way of internalization of molecules (pinocytosis, potocytosis, and trogocytosis) and microbes (phagocytosis) from outside into inside of the cell.

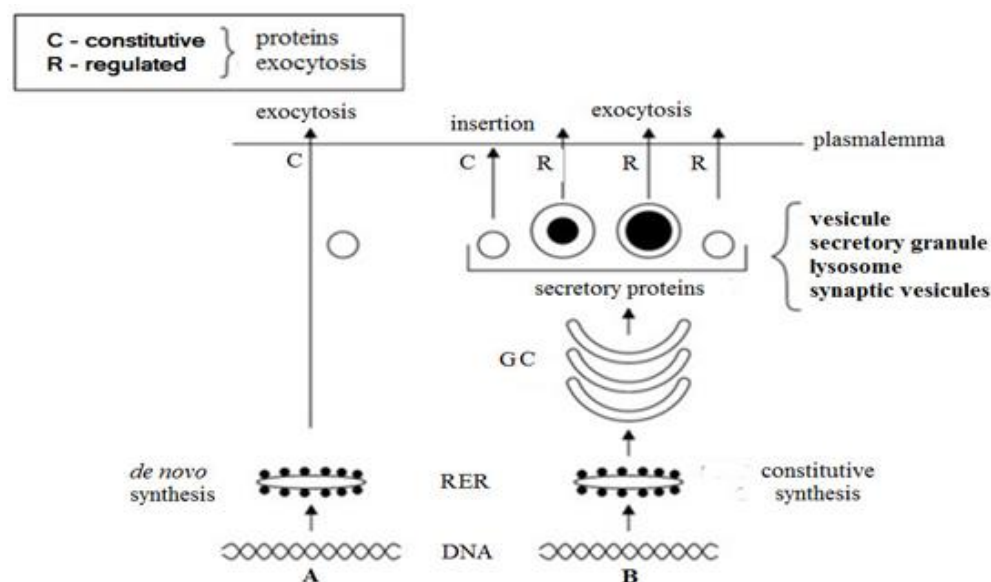


Fig. 8. Schematic illustration of constitutive (C) and regulated (R) secretory pathways. In the C pathway, secretory vacuoles continuously translocate proteins synthesized in (i) rough endoplasmic reticulum (RER) to the plasmalemma for exocytosis (A), and (ii) RER-Golgi complex (GC) for the insertion within the plasmalemma (B). In the R pathway, RER-GC synthesized proteins are stored within various types of secretory granules or vesicles until they released in response to specific signals (B). From (Chaldakov, 2021)

Table 1 presents a summing view of “Palade dixit” about cell protein secretion.

Table 1. The intracellular protein secretory pathway

PALADE DIXT

The protein secretory pathway

• Synthesis	Ribosomes, RER
• Post-translational modification	Golgi complex
• Sorting	Günter Blobel's signaling amino acid sequence
• Storage	Golgi complex, Secretory vacuoles
• Transport	Microtubules, Kinesin, COP I, COP II Actin filaments, Myosin II
• Exocytosis	Plasmalemma/Porosomes

Abbreviations: RER, rough endoplasmic reticulum; COP, coat protein, COP I and COP II vesicles, respectively.

Vascular biology: secretory phenotype smooth muscle cells

In 1960 Maria Daria Haust and colleagues (Haust et al., 1960) published their seminal article suggesting the fibrogenic potential of VSMC as related to extracellular matrix production. Since then VSMC secretion, proliferation and migration have been increasingly studied as key cellular phenomena in the initiation and development of atherosclerosis. This concept was further developed (Ross, 1999; Libby, 2021). Of note, in the last 10-15 years a new paradigm shift in the process of atherogenesis has been emerging addressing the pivotal role of the atherosclerotic plaque's fibrous cap (Ghenev et al., 2017; Chaldakov et al., 2020).

In 1973 in Heidelberg, Germany, a Symposium on *The Smooth Muscle of the Artery* was held. There, one of us (GNC) presented a lecture on their own TEM findings on the significance of (i) Golgi-derived secretion granules and clathrin-coated vesicles, and (ii) cytoplasmic MT in the secretory pathway of VSMC (Chaldakov and Nikolov, 1975) (**Fig. 9**). Based on these and related own results (cited herein), the term “secretion” was

for the first time linked to VSMC functions, and it was appreciated by the vascular biology community, thus replacing the terms “modified SMC” and “synthetic SMC”, which were not conceptually correct in sense of Palade's understanding of the cell protein secretion. Here is placed the great significance to find the Teacher, and to creatively follow Him.

Microtubules are essential for the secretion in vascular smooth muscle cells

It is well known that the major architectural components of cytoskeletal MT are α - and β -tubulins, MT-associated proteins (MAP 1-4 and tau protein) being tightly involved in the microtubulogenesis. Microtubules are essential for a variety of cellular functions, including the translocation of RER- and Golgi-derived vesicles and vacuoles during the secretory process. There are chemical substances which can disassemble already formed MT and inhibit *de novo* MT formation *via* their tubulin-binding properties, hence these agents are termed antitubulins or MT-disassembling agents, colchicine being the classical example of them (reviewed in Yanev et al., 2016; Chaldakov, 2018).

Our colchicine study for the first time aimed at testing the possible role of MT for VSMC secretory process. The experimental rabbits were treated with a sub-antimitotic dose of colchicine aimed at the disassembly of cytoplasmic, not mitotic, MT. The VSMC of untreated rabbits showed well-developed RER and Golgi complex, and MT associated with Golgi-derived secretion granules and with cisternae of RER. Colchicine treatment affected

(i) MT in a monotypic way (all VSMC contained no MT after colchicine), and (ii) Golgi complexes and RER in a dual way, resulting in two structural subpopulations of VSMC. One subpopulation displayed a significant accumulation of Golgi-derived secretion granules (**Fig. 10a**), whereas another showed a vacuolar dilation of RER cisternae (**Fig. 10b**).

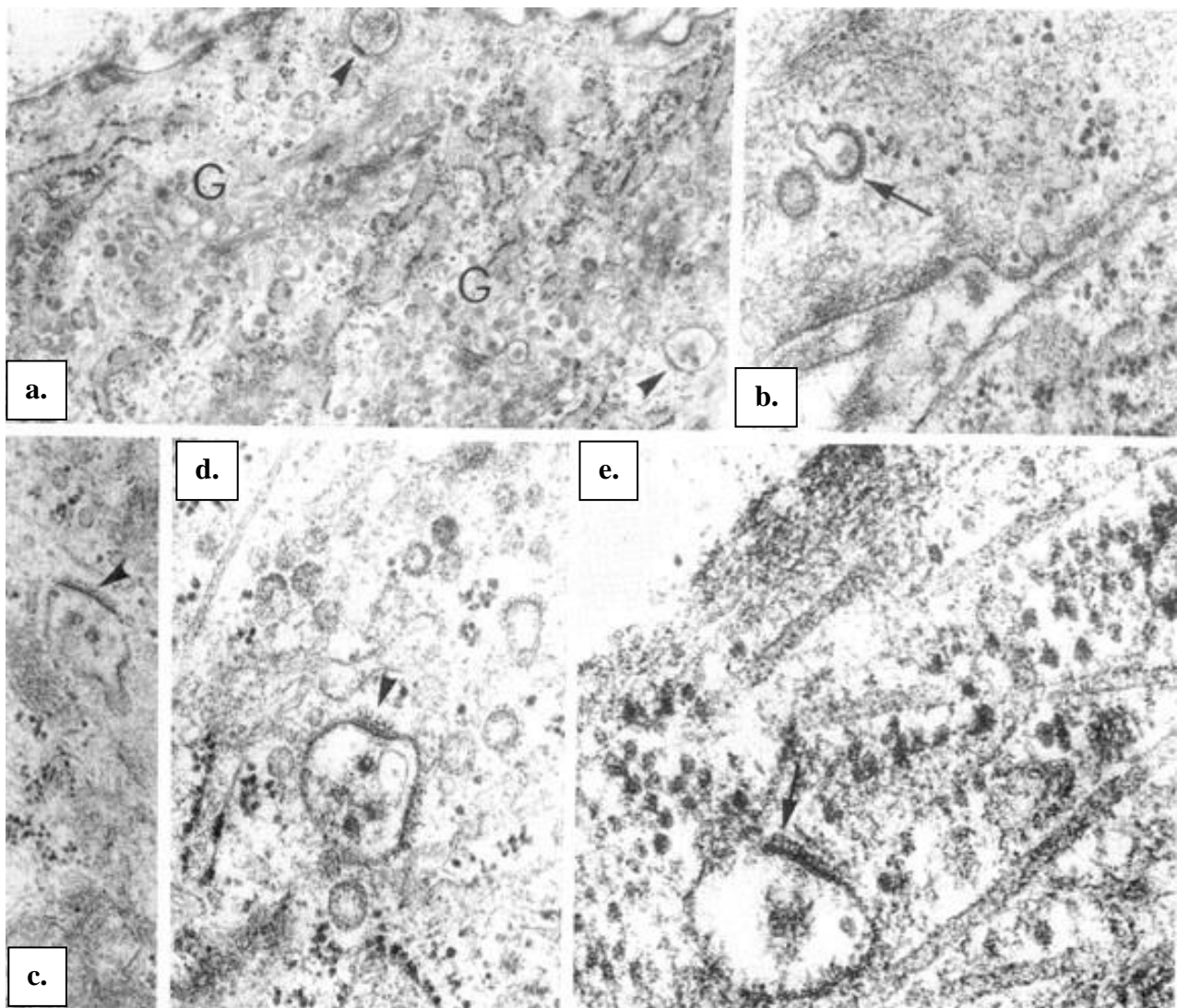


Fig. 9. Electron micrographs of secretory-state (secretory phenotype) aortic smooth muscle cells of the rabbit. **a.** Well developed Golgi complex (G). **b-e.** Vacuoles with a fuzzy (probably not clathrin) coat (arrowheads and arrows). **e.** Vacuole-associated microtubules. **a.** x11 000; **b.** x30 000; **c.** x20 000; **d.** x45 000; **e.** x80 000. From (Chaldakov and Vankov, 1986)

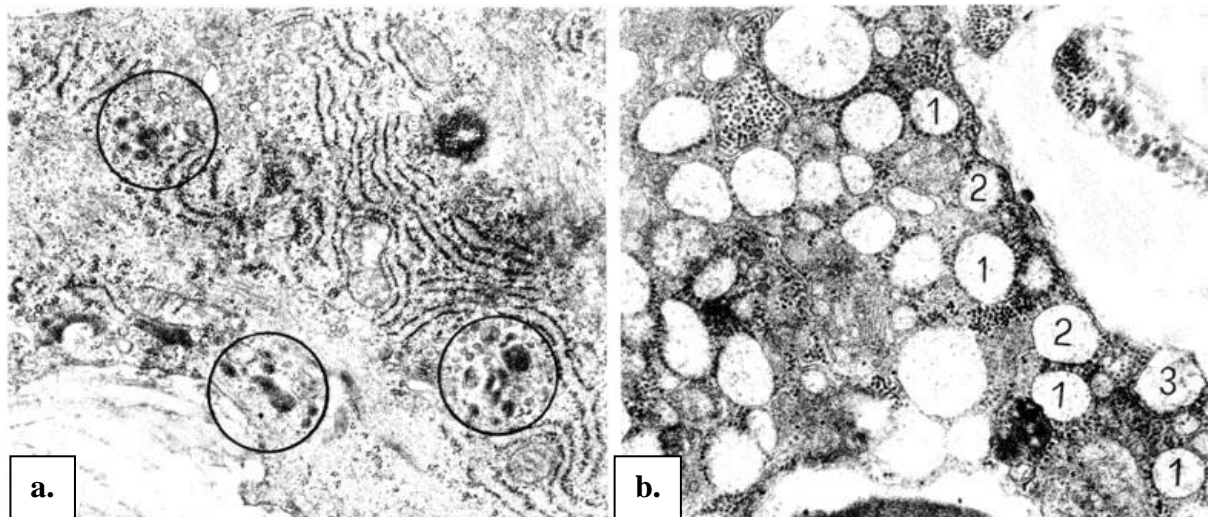


Fig. 10. Electron micrographs of secretory-state (secretory phenotype) aortic smooth muscle cells of the rabbit treated with a sub-antimitotic dose of colchicine. The cells responded to the treatment by **(a)** an accumulation of secretion granules (circles), or **(b)** vacuolar type dilation of rough endoplasmic reticulum (RER) cisternae, some of them approaching the cell periphery (1, 2, 3), suggesting of a direct RER, not dependent on MT, way of exocytosis. **a, b**, x10 000. From (Chaldakov, 2018)

Colchicine and cardiovascular diseases: Bench-to-bedside data

Atherosclerotic cardiovascular disease and its complications (erosion and rupture of the plaque fibrous cap) lead to acute coronary syndromes, myocardial infarction or stroke. Accordingly, VSMC of the innermost media undergo phenotypic modulation towards a secretory state involved in matrix proteins production (see Fig. 6). The risk of plaque rupture is inversely correlated with the presence of secretory phenotype VSMC and collagen fibrils within the fibrous cap (Shankman et al., 2015; Ghenev et al., 2017; Wirka et al., 2019; Chaldakov et al., 2020).

Bench-to-bedside (B2B) investigations are the process of translating basic science discoveries into clinical applications. The B2B model begins with experiments in the laboratory and ends with success or failure in clinical trials.

For instance, the therapeutic use of colchicine has extended from its classical application in gouty arthritis to familial

Mediterranean fever, Behcet's disease, liver fibrosis, osteoarthritis, pericarditis, and a variety of disorders associated with the cardiovascular disease (e.g., acute coronary syndromes, myocardial infarction, atrial fibrillation, and hypertrophic cardiomyopathy – it is known that the accumulation of MT in hypertrophied cardiomyocytes impedes their contraction, whereas MT disassembly by colchicine causes striking improvement in contractile function) (reviewed in Chaldakov and Vankov, 1986b).

Recently, our abovementioned colchicine results (also see Cecconi et al., 2021) gained a therapeutic appreciation in cardiovascular diseases using 0.5 mg/day, low-dose colchicine (LoDoCo) therapy (Nidorf et al., 2013; Lee et al., 2016; Vaidya et al., 2017; Tardif et al., 2019).

Whatsoever, a more effective approach would be a “bench-to-bedside-to-bench” (B2B2B) as some colleagues proposed.

Conclusions

We argue that one of the present challenges in vascular biology is to cultivate secreto-centric thinking applied to further focusing on how we could make VSMC phenotypic modulation and secretory pathways work for the benefit of human's cardiovascular health, including in thoracic aortic aneurysms related to Marfan syndrome (Xiong et al., 2008; Mullen et al., 2019).

Acknowledgement

We appreciate the valuable and stimulating discussions with our brain-and-heart friends (BHF) Maria Daria Haust, Zanka B. Jurukova, Michael S. Davidoff, Gheorghe Benga, Yukio Yamori, Takashi Fujiwara, Stanislav Yanev, Maria D. Zhelyazkova-Savova, Wale A.R. Sulaiman, Anton B. Tonchev, and Alexander K. Stoychev. Partial republishing with the agreement of the journals *Biomedical Reviews* and *Adipobiology*.

Conflict of interest

The authors have declared that there is no conflict of interest.

References

1. Blobel G (2000) Protein targeting. *Biosci Rep* 20:303-344. doi: 10.1023/a:1010318832604
2. Cecconi A, Vilchez-Tschischke JP, Mateo J, Sanchez Gonzalez J, España S, *et al.* (2021) Effects of colchicine on atherosclerotic plaque stabilization: a multimodality imaging study in an animal model. *J Cardiovasc Transl Res* 14(1):150-160. doi:10.1007/s12265-020-09974-7
3. Chaldakov GN and Nikolov SD (1975) Ultrastructure of the arterial smooth muscle cell. In: Wolf S, Werthessen NT, editors. *The Smooth Muscle of the Artery*. New York City, NY: Plenum Press. *Adv Exp Med Biol* 57:14-20.
4. Chaldakov GN, Nikolov S, Vancov V (1977) Fine morphological aspects of the secretory process in arterial smooth muscle cells. II. Role of microtubules. *Acta Morphol Acad Sci Hung* 25:167-174.
5. Chaldakov GN and Kádár A (1978) Microtubules in arterial smooth muscle cells in vivo and in tissue culture. An electron microscope study. In: W. Hauss, R. Wissler, R. Lehman, editors. *State of Prevention and Therapy of Human Arteriosclerosis and in Animal Models*. Rheinisch-Westfälische Akad. Der Wissenschaften, p. 211-231.
6. Chaldakov G (2016) GEORGE E. PALADE LECTURE. Human body as a multicrine system, with special reference to cell protein secretion: from vascular smooth muscles to adipose tissue. *Adipobiology* 8:6-18. doi: 10.14748/adipo.v8.2089
7. Chaldakov G, Stankulov I, Hristova M, Ghenev P (2003) Adipobiology of disease: Adipokines and adipokine-targeted pharmacology. *Curr Pharm Des* 9: 1023-1031. doi: 10.2174/1381612033455152
8. Chaldakov GN (1982) Antitubulins - a new therapeutic approach for atherosclerosis? *Atherosclerosis* 44:385-390. doi: 10.1016/0021-9150(82)90013-2
9. Chaldakov GN (2018) Colchicine, a microtubule-disassembling drug, in the therapy of cardiovascular diseases. *Cell Biol Int* 42:1079-1084. doi: 10.1002/cbin.10988
10. Chaldakov GN, Beltowsky J, Ghenev PI, Fiore M, Panayotov P, Rančić G, Aloe L (2012) Adipoparacrinology - vascular periadventitial adipose tissue (tunica adiposa) as an example. *Cell Biol Int* 36:327-330. doi: 10.1042/cbi20110422

11. Chaldakov GN and Fiore M (2010) Human body as a multicrine gland. *Adipobiology* 2: 73-75. doi: 10.14748/adipo.v2.263
12. Chaldakov GN and Vankov VN (1986a) Morphological aspects of secretion in the arterial smooth muscle cell, with special reference to the golgi complex and microtubular cytoskeleton. *Atherosclerosis* 61: 175-192. doi: 10.1016/0021-9150(86)90137-1
13. Chaldakov GN and Vankov VN (1986b) Antifibrotic approach in the therapy of arterial occlusive diseases: new considerations. In: G. Trubestein, editor. *Conservative Therapy of Arterial Occlusive Disease*. Stuttgart, New York, Georg Thieme Verlag, p. 224-226
14. Chaldakov GN, Zhelyazkova-Savova MD, Panayotova D, Fiore M, Yanev S (2020) Phenotypic modulation of smooth muscle cells and matrix metalloproteinases as targets for atherosclerotic plaque stabilization. *Biomed Rev* 31: 49-60. doi: 10.14748/bmr.v31.7704
15. Chaldakov GN (2021) *Principles of Cell and Tissue Biology* (in press).
16. Farquhar MG (2012) A Man for all seasons: Reflections on the life and legacy of George Palade. *Ann Rev Cell Dev Biol* 28: 1-28. doi: 10.1146/annurev-cellbio-101011-155813
17. Farquhar MG and Palade GE (1998) The Golgi apparatus: 100 years of progress and controversy. *Trends Cell Biol* 8:2-10. doi: 10.1016/S0962-8924(97)01187-2
18. Frohlich J, Chaldakov GN, Vinciguerra M (2021) Cardio- and neurometabolic adipobiology: Consequences and implications for therapy. *Int J Mol Sci* 22: 4137. doi: 10.3390/ijms22084137
19. Ghenev PI, Aloe L, Kisheva AR, Singh M, Panayotov P, Fiore M, et al. (2017) QUO VADIS, ATHEROGENESIS? Part 1. Smooth muscle cell secretion – how foe becomes friend in the fight against the atherosclerotic plaque. *Biomed Rev* 28:134-138.
20. Haust MD, More RH, Movat HZ (1960) The role of smooth muscle cells in the fibrogenesis of arteriosclerosis. *Am J Pathol* 37:377-389.
21. Jena BP (2010) Porosome: the universal secretory portal in cells. *Biomed Rev* 21: 1-15. doi: 10.14748/bmr.v21.42
22. Lai CP and Breakefield XO (2012) Role of exosomes/microvesicles in the nervous system and use in emerging therapies. *Front Physiol* 3: 228. doi: 10.3389/fphys.2012.00228
23. Lee JZ, Singh N, Howe CL, Low S-W, Huang JJ, Ortega G, et al. (2016) Colchicine for prevention of post-operative atrial fibrillation. A meta-analysis. *J Am Coll Cardiol Clin Electrophysiol* 2(1): 78-85. doi: <https://doi.org/10.1016/j.jacep.2015.09.016>
24. Libby P (2021) Inflammation in atherosclerosis - No longer a theory. *Clin Chem* 67:131-142. doi:10.1093/clinchem/hvaa275
25. Mazzearello P, Garbarino C, Calligaro A (2009) How Camillo Golgi became "the Golgi". *FEBS Lett* 583: 3732-3737. doi: 10.1016/j.febslet.2009.10.018
26. Mullen M, Jin XY, Child A, Stuart AG, Dodd M, Aragon-Martin JA, et al. (2019) Irbesartan in Marfan syndrome (AIMS): a double-blind, placebo-controlled randomised trial. *Lancet* 394: 2263–2270. doi: 10.1016/S0140-6736(19)32518-8
27. Nickel W (2010) Pathways of unconventional protein secretion. *Curr Opin Biotechnol* 21: 621-626. doi: 10.1016/j.copbio.2010.06.004
28. Nidorf SM, Eikelboom JW, Budgeon CA, Thompson PL (2013) Low-dose colchicine for secondary prevention of cardiovascular

- disease. *J Am Coll Cardiol* 61(4):404-410. doi: 10.1016/j.jacc.2012.10.02
29. Palade G (1975) Intracellular aspects of the process of protein synthesis. *Science* 189: 347-358. doi: 10.1126/science.1096303
30. Palade GE (1971) Albert Claude and the beginnings of biological electron microscopy. *J Cell Biol* 50: 5d-19d. doi: 10.1083/jcb.50.1.5d
31. Ross R (1999) Atherosclerosis - An inflammatory disease. *N Engl J Med* 340: 115-126. doi: 10.1056/nejm199901143400207
32. Sadallah S, Eken C, Martin PJ, Schifferli JA (2011) Microparticles (ectosomes) shed by stored human platelets downregulate macrophages and modify the development of dendritic cells. *J Immunol* 186: 6543-6552. doi: 10.4049/jimmunol.1002788
33. Shankman LS, Gomez D, Cherepanova OA, Salmon M, Alencar GF, Haskins RM, et al. (2015) KLF4-dependent phenotypic modulation of smooth muscle cells has a key role in atherosclerotic plaque pathogenesis. *Nat Med* 21(6): 628-637. doi: 10.1038/nm.3866
34. Silver R and Pappas G (2005) Secretion without membrane fusion: Porocytosis. *Anat Rec B New Anat* 282: 18-37. doi: 10.1002/ar.b.20050
35. Singer MV (2003) Legacy of a distinguished scientist: George E. Palade. *Pancreatology* 3:518-519. doi: 10.1159/000076328
36. Tardif J-C, Kouz S, Waters DD, Bertrand OF, Diaz R, Maggioni AP, et al. (2019) Efficacy and safety of low-dose colchicine after myocardial infarction. *N Engl J Med* 381(26):2497-2505. doi: 10.1056/NEJMoa1912388
37. Töre F, Tonchev A, Fiore M, Tunçel N, Atanassova P, Aloe L, et al. (2007) From adipose tissue protein secretion to adipopharmacology of disease. *Immun Endoc Metab Agents Med Chem* 7: 149-155. doi: 10.2174/187152207780363712
38. Vaidya K, Arnott C, Martínez GJ, Ng B, McCormack S, Sullivan DR, et al. (2017) Colchicine therapy and plaque stabilization in patients with acute coronary syndrome. *J Am Coll Cardiol Img.* doi: <https://doi.org/10.1016/j.jcmg.2017.08.013>
39. Wirka RC, Wagh DA, Paik DT, et al. (2019) Atheroprotective roles of smooth muscle cell phenotypic modulation and the TCF21 disease gene as revealed by single-cell analysis. *Nat Med* 25(8): doi:10.1038/s41591-019-0512-5
40. Xiong W, Knispel RA, Dietz HC, Ramirez F, Baxter BT (2008) Doxycycline delays aneurysm rupture in a mouse model of Marfan syndrome. *J Vasc Surg* 47(1): 166-172. doi:10.1016/j.jvs.2007.09.016
41. Yanev S, Fiore M, Hinev A, Ghenev PI, Hristova MG, Panayotov P, et al. (2016) From antitubulins to trackins. *Biomed Rev* 27:59-67.
42. Zar M, Amadio P, Campodonico J, et al. (2020) Exosomes in cardiovascular diseases. *Diagnostics* 10:943. doi:10.3390/diagnostics1011094

PERSPECTIVES ON ANTIVIRAL DRUGS DEVELOPMENT IN THE TREATMENT OF COVID-19

Aura RUSU^{1†}, Eliza-Mihaela ARBĂNAȘI^{1†}, Ioana-Andreea LUNGU^{2*}, Octavia-Laura MOLDOVAN³

¹Department F2, Discipline of Pharmaceutical and Therapeutical Chemistry, “George Emil Palade” University of Medicine, Pharmacy, Science, and Technology of Târgu Mureș

²Department F2, Discipline of Pharmacology and Clinical Pharmacy, “George Emil Palade” University of Medicine, Pharmacy, Science, and Technology of Târgu Mureș

³Department F1, Discipline of Organic Chemistry, “George Emil Palade” University of Medicine, Pharmacy, Science, and Technology of Târgu Mureș

*Correspondence:

Ioana-Andreea LUNGU

ioana-andreea.lungu@umfst.ro

†These authors share the first authorship.

Received: 1 June 2021; **Accepted:** 11 June 2021; **Published:** 30 June 2021

Abstract: The main objective of this review is to highlight the urgent development of new antiviral drugs against SARS-CoV-2 in the context of the coronavirus pandemic. Antiviral medication against SARS-CoV-2 comprises only remdesivir as an approved drug. Scientists are making considerable efforts to identify other effective antivirals. Investments into the *de novo* design of new drugs against the SARS-CoV-2 virus are few. Molnupiravir proved to be effective against the SARS-CoV-2 virus and is very close to approval. Pfizer's two new compounds (PF-07321332, oral administration and PF-07304814, systemic administration) are in the early stages of development. Two types of methods are preferred to discover new antivirals in a short period. Repositioning of approved drugs for antiviral effect conducted to some clinical results for favipiravir, lopinavir/ritonavir, danoprevir/ritonavir, umifenovir, hydroxychloroquine, camostat and nafamostat. Virtual screening of known molecules' libraries indicated several compounds that were tested or are being tested in clinical trials. In conclusion, only a few innovative antiviral molecules are in various stages of development. However, the repositioning of many known compounds is being studied, including using virtual screening. The pharmaceutical industry is adapting and reinventing itself so that humanity can face a new pandemic in the future.

Keywords: COVID-19, antivirals, remdesivir, molnupiravir, hydroxychloroquine, azithromycin, ivermectin, camostat.

Introduction

Although most patients with COVID-19 have a mild or moderate course, up to 5-10% may have a severe, life-threatening course, and there is an urgent need for effective medication. Thus, more than 300 clinical trials are ongoing (Şimşek Yavuz and Ünal, 2020). Among the best known is the „Solidarity” clinical trial for

COVID-19 treatments to further evaluate remdesivir, hydroxychloroquine/chloroquine and lopinavir-ritonavir with and without interferon beta, launched by World Health Organization (WHO) (Şimşek Yavuz and Ünal, 2020; “Solidarity clinical trial for COVID-19 treatments,” n.d.).

Unfortunately, there is only one antiviral approved for treatment, namely remdesivir. Remdesivir is an antiviral that has been developed and produced by Gilead Sciences & U.S. Centers for Disease Control Prevention (CDC) & U.S. Army Medical Research Institute of Infectious Diseases (USAMRIID) (Eastman et al., 2020). This drug was initially used in clinical trials for the treatment of Ebola virus and Marburg virus infections (Şimşek Yavuz and Ünal, 2020), SARS-CoV, and MERS-CoV (Kouznetsov, 2020). Remdesivir has been approved as an emergency measure by the U.S. Food and Drug Administration (FDA) on 1 May 2020 to treat severe cases of COVID-19 (FDA, 2020). This antiviral molecule is an adenosine nucleotide analogue, a prodrug; the mechanism of action consists of the inhibition of viral RNA-dependent RNA-polymerase (RdRp). It is administered on the first day, 200 mg intravenously, and then on days 2 to 5 (or to 10), only 100 mg per day (Şimşek Yavuz and Ünal, 2020). Based on clinical trials, remdesivir was considered beneficial in treating COVID-19 due to a shorter recovery time in hospitalized adults, mainly by reducing the percentage of patients receiving invasive mechanical ventilation or Extracorporeal Membrane Oxygenation Therapy (ECMO) (Kaka et al., 2021). Treatment for a short duration of 5 days may be sufficient to treat patients with moderate or severe COVID-19 (Lai et al., 2021).

Five large randomized trials highlighted that remdesivir has many disadvantages due to a lack of decreasing the mortality rate of COVID-19 and the fact that it needs administration in a hospital. Remdesivir was more effective when it was administered at the disease's first symptoms. Thus, the clinical efficacy of the 5-day remdesivir regimen was not assessed in critical COVID-19 patients who received mechanical ventilation or ECMO; time to recovery was not improved for those

cases (Srinivas et al., 2020; Kaka et al., 2021). Therefore, the Surviving Sepsis Campaign Guidelines (SSCG) only suggest using remdesivir in non-ventilated patients with moderate to severe COVID-19. Also, SSCG are against using remdesivir in patients with critical COVID-19 outside the clinical trials (Lai et al., 2021; "SCCM | COVID-19 Guidelines," 2021).

Remdesivir treatment also involves side effects. The most common side effects of remdesivir are constipation, hypoalbuminemia, hypokalemia, anemia, thrombocytopenia and increased total bilirubin (Benloch et al., 2020; Marcolino et al., 2020). The use of remdesivir for five days or until hospitalization is the only recommendation for patients who do not require oxygen therapy. In adult patients, remdesivir did not reduce or reduced the mortality very little, but improved the percentage of recovered patients, reduced severe damages and may lead to a decreased number of patients who become ventilated ("Antiviral Therapy," 2021; Kaka et al., 2021). However, the results of the WHO "Solidarity" study on the efficacy of remdesivir were discouraging. No drug included in the study brought significant benefits to patients hospitalized with COVID-19 ("Repurposed Antiviral Drugs for Covid-19 — Interim WHO Solidarity Trial Results," 2021). Another recent trial conducted for three months concluded, as well, that using remdesivir brought an improvement in the rehabilitation of patients with COVID-19, but that is the only advantage that the drug has had over a placebo. Even more, being costly, difficult to fabricate, and designated for intravenous use, only in hospitals, remdesivir is a less acceptable alternative (Dolgin, 2021).

The Institute for Clinical and Economic Review has updated its assessment on pricing models for remdesivir and concluded that remdesivir does not meet a critical cost-

effectiveness threshold for a 5-day treatment course. Still, a dry powder formulation for inhalation of remdesivir is investigated. The purpose of this formulation is to increase the absorption of the drug into the lungs (Glaus MJ and Von Ruden S, 2020; Sahakijpijarn et al., 2020; Kaka et al., 2021). The new formulation of remdesivir is a promising alternative for COVID-19 treatment in preclinical studies conducted on Syrian hamsters (Sahakijpijarn et al., 2021).

An unprecedented global effort has been made to obtain the vaccines needed to achieve herd immunity (Adamson et al., 2021). Although several effective anti-COVID-19 vaccines have been approved (FDA, 2021; Pinho, 2021), the exact period of immunity for vaccinated people is yet unknown. A part of the population cannot be vaccinated, for various reasons. An essential alternative to the vaccine is the development of new efficient antivirals. However, investment in the pharmaceutical industry depends mainly on the success of approved vaccines in immunizing the population. So far, significant investments have been channeled into discovering antivirals against persistent or latent viruses, e.g., herpes (*Herpes simplex*), viral hepatitis, Acquired Immunodeficiency Syndrome (AIDS). The approved antiviral drugs are available for only ten viruses, although over 220 viruses are known to infect humans. COVID-19 has shown humanity that it is not prepared for a pandemic of this magnitude (Adamson et al., 2021). The antivirals discovery projects that emerged for persistent or latent viruses have enabled expertise, logistics and technology to identify new molecules efficient against SARS-CoV-2 (Richman, 2020).

It seems that the pharmaceutical industry has had an awakening after the COVID-19 pandemic. Initiatives are already in place to develop therapies against SARS-CoV-2. A program was initiated by the U.S. National

Institutes of Health (NIH) to develop treatments for viral pandemics. The pharmaceutical industry is teaming up to create new compounds to fight influenza viruses and coronaviruses. Molnupiravir is a new antiviral, a cost-effective drug, which is very close to approval in an advanced clinical trial stage (Dolgin, 2021). There are research centers such as Antiviral Drug Discovery and Development Center (of the University of Alabama at Birmingham) that aim to develop effective antiviral drugs in the treatment of COVID-19 (Everts, n.d.). The approval of a new antiviral for the treatment of COVID-19 must meet the so-called democratic conditions. The drug must be cheap, available in pharmacies for a large part of the population, without significant side effects and with some effectiveness (Benlloch et al., 2020).

The main objective of this review is to highlight the need to develop new antiviral drugs and find the most effective molecules in the treatment of COVID-19 in the shortest possible time, in the context of the SARS-CoV-2 pandemic, but also of the future pandemics.

1. The research methodology and literature review

This review is based on relevant articles obtained by using Clarivate Analytics Web of Science and PubMed databases. The selected papers are mainly published between the last two years.

The search methodology used the main keywords and MeSH terms:

"antivirals", "antiviral agents", "COVID-19", "COVID-19 treatment", "SARS-CoV-2", and "drug repurposing". The following key words were used in addition separately: "remdesivir", "favipiravir", "lopinavir", "danoprevir", "molnupiravir", "umifenovir", "hydroxychloroquine", "azithromycin", "ivermectin", and "camostat".

2. Methods of discovery of antiviral drugs against SARS-CoV-2 infection

New drug development methods are time-consuming and require significant investments (funds, logistics, and specialized human resources). Few antiviral drugs are in development, as *de novo* compounds (new chemical entities). To obtain more effective compounds against SARS-CoV-2 faster, repositioning of known drugs and virtual screening are preferred (Fig. 1).

2.1. *De novo* design of antivirals

Molnupiravir is a promising antiviral, prodrug of ribonucleoside analogue β -d-N4-hydroxycytidine (EIDD-1931). It is an orally-bioavailable form developed at Drug Innovations at Emory and licensed by Ridgeback; all funds for the development of molnupiravir have been provided by Wayne and Wendy Holman and Merck (Painter et al., 2021; Reina, 2021; Ridgeback Biotherapeutics, LP, 2021). This new antiviral is in advanced clinical study, in five phase III studies against COVID-19 (Kouznetsov, 2020; Ridgeback Biotherapeutics, LP, 2021). Molnupiravir is easy to synthesize in just three steps with a yield of 69%. This method is environmentally friendly (Halford, 2021).

A new helpful oral antiviral for SARS-CoV-2 has been developed by the Pfizer company from scratch, which acts by inhibiting the infection that causes COVID-19. The new molecule PF-07321332 has shown its potency *in vitro* by inhibiting the viral replication activity of SARS-CoV-2 (inhibitor of SARS-CoV-2's main protease). This new antiviral acts as a reversible covalent inhibitor of the main protease of SARS-CoV-2 through cysteine residues. PF-07321332 is considered a potential treatment for the upcoming coronavirus risks. This oral antiviral drug would be given at the first symptoms, and patients would not need to be hospitalized. The drug is in Phase 1 clinical trial. In addition, the

Pfizer company reported PF-07304814, another compound with intravenous administration for the already hospitalized victims. The development of PF-07304814 began during the severe acute respiratory syndrome (SARS) pandemic severe acute respiratory syndrome in 2002-2003. The drug is currently in Phase 1b multi-dose trial. So, having both would construct a full therapy model. The first trial will show the tolerability and pharmacokinetics of this new oral antiviral ("Pfizer Initiates Phase 1 Study of Novel Oral Antiviral Therapeutic Agent Against SARS-CoV-2 | pfpfizeruscom," 2021; "Pfizer unveils its oral SARS-CoV-2 inhibitor," 2021).

2.2. Repositioning of known drugs

The repositioning of a drug is the strategy to find a new biological effect other than that for which the drug was initially approved. It has many advantages, including the simplification of authorization procedures and the speed of being placed on the market at much lower costs (Jourdan et al., 2020). The most affordable alternative method for discovering the treatment of COVID-19 is the repositioning of existing drugs that are potentially active against SARS-CoV-2 (Akilesh et al., 2021; Bhowmick et al., 2021; Gatti and De Ponti, 2021).

These drugs are supposed to work upon different elements in the disease pathophysiology, and these correspond to two primary therapeutic classifications: drugs that inhibit the viral activity (e.g., favipiravir, remdesivir, azithromycin, lopinavir-ritonavir, hydroxychloroquine) and drugs that modulate the antiviral immune reaction in the host (e.g., corticosteroids, interferons, tocilizumab). Along with these, other agents have been investigated in the management of COVID-19: ivermectin - an antiparasitic agent, and doxycycline - a broad-spectrum tetracycline antibiotic (Bhowmick et al., 2021).

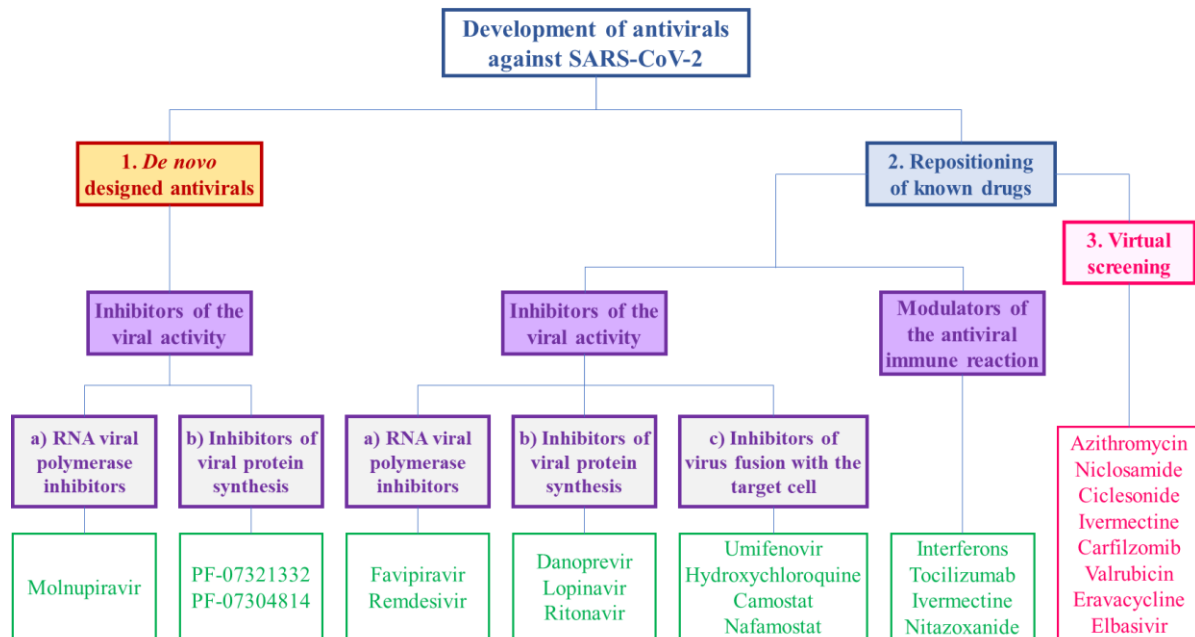


Fig. 1. Strategies for the development of antiviral drugs against SARS-CoV-2 and their classification by mechanism of action.

In a trial reported by the ISRCTN Registry and ClinicalTrials.gov, WHO specialists used four known antiviral drugs that could potentially affect mortality for patients with COVID-19. These four were: lopinavir, hydroxychloroquine, interferon (all three were discontinued), and remdesivir. The regimens used tablets of 200 mg of lopinavir twice a day for 14 days and tablets of 200 mg of hydroxychloroquine sulfate for ten days. Interferon beta-1 was used subcutaneously for six days with three doses of 44 µg each day, and remdesivir was used intravenously with a 200 mg dose on the first day and then just 100 mg for the next nine days. The study does not use any placebo. The study was conducted to test the hospital mortality for the assigned cases, and it concluded that the trial drug versus the control one had no particular benefit. Even more, none of the drugs reduced the mortality nor the hospitalization time or mechanical ventilation requirement. The similitude of all four drugs' insufficient impact proves that none has any solid effect on curing the COVID-19 infected patients. Only an

individual aspect came out, that the recovery time is faster in remdesivir, compared to the other three drugs ("Repurposed Antiviral Drugs for Covid-19 — Interim WHO Solidarity Trial Results," 2021).

Supposedly, the most effective solution for COVID-19 would be an antiviral that has a component that can lower the increase of the viral load. A planned three-phase study is ongoing and focused on drugs that combat other viral diseases (e.g., daclatasvir used for hepatitis C virus and atazanavir used for human immunodeficiency virus (HIV)). This trial will show the changes in the increase of the viral load and measure the number of days without ventilatory support (Hospital do Coracao, 2020). A clinical trial using a combination of lopinavir-ritonavir, interferon beta-1b, and ribavirin suggested an increased rate of viral clearance. Still, the conclusion was difficult to outline because there was no placebo group to compare it to, and more investigations need to be done. The central aspect that came out was that ribavirin had significant side effects and could prove dangerous to use (Lee et al., 2020).

Also, new pharmaceutical formulations containing known drugs (e.g., remdesivir, hydroxychloroquine, heparin, pirfenidone) have been tested. The novel formulations comprise aerosol/nebulized inhalatory formulations, controlled-released formulations, nanoparticles/lipidic carriers, chiral switch. The antiviral effect was observed, alongside with the pharmacokinetic and pharmacologic properties and the safety profile (Gatti and De Ponti, 2021).

2.3. Virtual screening *in silico*

Some antivirals have been found using platforms to test the libraries with approved drugs for the *in vitro* action against SARS-CoV-2 in cell cultures. These platforms simultaneously screen the compounds' toxicity on those cells. Thus, through this type of screening, it was discovered that azithromycin (a new generation antibiotic in the macrolide class) offers a therapeutic window in the treatment of COVID-19 (Benlloch et al., 2020). Azithromycin has been established to have antiviral and immunomodulatory effects, which may be effective in the hyperinflammatory syndrome caused by SARS-CoV-2. Azithromycin has also been clinically effective in respiratory distress syndrome and viral infections. Immunomodulatory activity is present during both the acute and the chronic inflammation phases (Pani et al., 2020; Echeverría-Esnal et al., 2021). Also, niclosamide (an anthelmintic drug) and ciclesonide (a corticosteroid drug) were selected as antivirals against SARS-CoV-2 through computational methods (Benlloch et al., 2020; Xu et al., 2020; Pérez-Moraga et al., 2021; Salvi, 2021).

A virtual screening approach against viral proteins is another method to discover a new antiviral molecule. There are *in silico* studies that highlight the superior efficacy of ivermectin against SARS-CoV-2 versus remdesivir and hydroxychloroquine. The

affinity of ivermectin for different targets has been demonstrated (Azam et al., 2020; Choudhury et al., 2021; Kaur et al., 2021).

Ivermectin (an antiparasitic drug) was identified to interact with viral protein targets using computational methods (Kaur et al., 2021). Thus, it was shown in a clinical study that ivermectin reduced COVID-19 mortality by 40% (however, the study had some limitations) (Benlloch et al., 2020). Several drugs were shown to inhibit the primary protease in SARS-CoV-2 infection in a computational drug repositioning study. Among them are carfilzomib (an approved anticancer drug that acts as a protease inhibitor), valrubicin (a compound used in cancer chemotherapy), eravacycline (a new antibiotic by the tetracycline class used to treat intra-abdominal infections), elbasivir (an antiviral used to treat chronic hepatitis C). *In vitro* and *in vivo* studies are needed in the future to confirm the effectiveness of these drugs (Frediansyah et al., 2020; Wang, 2020).

In silico studies highlight ivermectin's efficacy versus remdesivir. The used computational methods were molecular docking and molecular dynamic simulation. Ivermectin was found to be a blocker of viral protease, replicase, and human TMPRSS2. Also, ivermectin has a sturdy hydrophobic interlinkage to the structure of the viral protease of SARS-CoV-2, and it binds better with the proteins of interest than remdesivir. The great lipophilicity and water-solubility of ivermectin lower the diffusion into the skin. With that, ivermectin is way better than remdesivir when it comes to the interaction with the ruling protease and the viral spike proteins. Even more, the pharmacokinetic characteristics of ivermectin make it a generally safe drug when used against SARS-CoV-2 (Choudhury et al., 2021).

In a study conducted *in silico* fifteen potential COVID-19 targets were used to

underscore ivermectin affinity. The used computational techniques were molecular docking, molecular mechanics, generalized Born surface area analysis, and molecular dynamics simulation studies. The resulted intermolecular interaction profile of ivermectin could complete the experimental studies and designing of new anti-COVID-19 drugs successfully (Azam et al., 2020).

A COVID-19 drug repurposing strategy based on virtual screening was published recently. Molecular docking and transcriptomic analyses were used to discover known drugs targeting viral proteins. A topological data analysis (TDA) compared numerous protein structures. The results obtained included 16 candidates from different pharmacological classes (Pérez-Moraga et al., 2021). In a recent docking-based virtual screening observation, using SARS-CoV-2 M^{pro} enzyme chymotrypsin-like cysteine protease as a target, 15 compounds from an in-house database were selected and two of them confirmed to have an *in vitro* ability to inhibit this protease activity. Presently, computation for these molecules is needed (Amendola et al., 2021).

3. Classification of antiviral drugs currently undergoing studies

The classification of the antiviral drugs currently undergoing studies (*in vitro* studies and clinical trials) (Şimşek Yavuz and Ünal, 2020) comprises:

- RNA viral polymerase inhibitors (inhibition of RNA synthesis)
- Inhibitors of viral protein synthesis (viral protease inhibitors, inhibitors that prevent the maturation of HIV)
- Inhibitors of virus fusion with the target cell (inhibition of viral entry)
- Immunomodulatory agents

The studied molecules with the potential to become efficient antivirals against SARS-CoV-

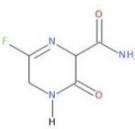
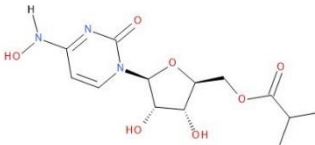
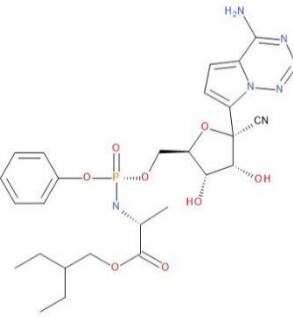
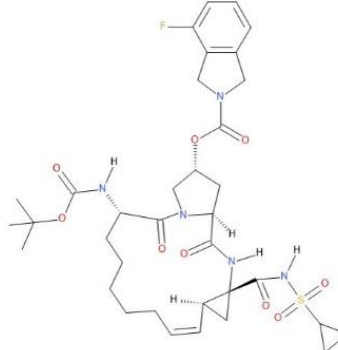
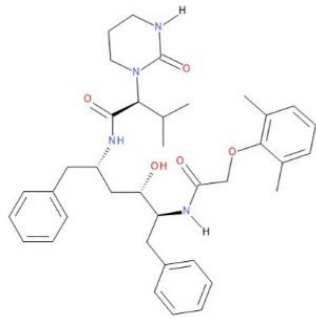
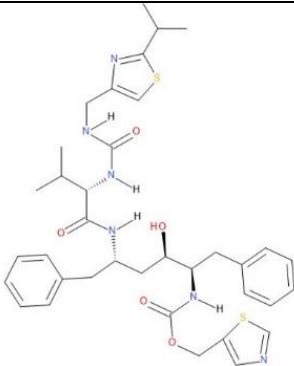
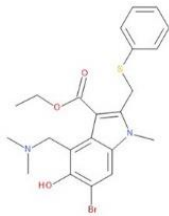
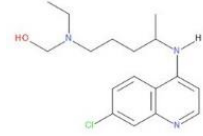
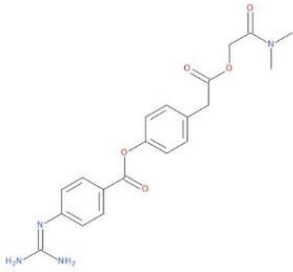
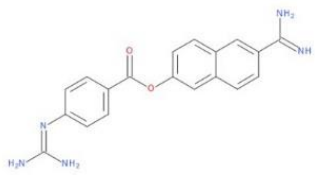
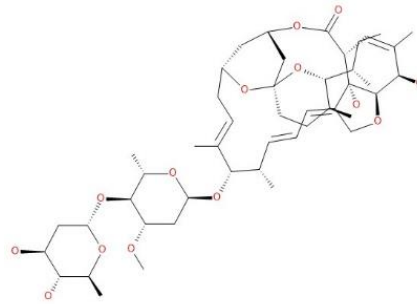
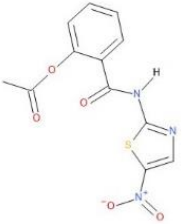
2 are presented below, grouped by their mechanism of action (**Table 1.**).

3.1. RNA viral polymerase inhibitors

Favipiravir is a nucleotide guanosine analogue (*prodrug*) (Şimşek Yavuz and Ünal, 2020) with activity against a wide variety of RNA viruses (Jomah et al., 2020; Kouznetsov, 2020). This antiviral was first approved in Japan for the treatment of influenza infections in 2014 (Agrawal et al., 2020). Favipiravir acts as an RdRp inhibitor (Şimşek Yavuz and Ünal, 2020). This simple molecule demonstrated a better efficacy compared to the lopinavir-ritonavir combination (Şimşek Yavuz and Ünal, 2020), (viral protease inhibitors) used to treat HIV infection (Pani et al., 2020). Also, compared to Umifenovir (Arbidol), an antiviral currently under study, favipiravir significantly improved the symptoms of pyrexia and cough, and the side effects were mild and controllable (Marcolino et al., 2020). The drug is administered orally, 1600 mg (or 2200 mg) on the first day, twice a day (Jomah et al., 2020), and on days 2 to 7 (or 10), 600 mg are given twice a day (Jomah et al., 2020; Şimşek Yavuz and Ünal, 2020).

Overall, favipiravir was well tolerated (in all five completed clinical trials) (Jomah et al., 2020). Adverse reactions such as diarrhea, psychiatric reactions, liver toxicity, hyperuricemia have been reported, but most of them have disappeared until patients were discharged. The safety of favipiravir is currently being investigated (Agrawal et al., 2020; Jomah et al., 2020; Marcolino et al., 2020; Dabbous et al., 2021). Favipiravir presents some valuable advantages, like oral administration and the recommendation to non-hospitalized patients with mild to moderate condition. This antiviral drug could be used relatively safely in the treatment of a large number of patients with COVID-19 (Agrawal et al., 2020).

Table 1. Chemical structures of antivirals with potential against SARS-CoV-2.

RNA viral polymerase inhibitors			Inhibitors of viral protein synthesis		
					
Favipiravir			Danoprevir		
Molnupiravir			Lopinavir		
Remdesivir			Ritonavir		
Inhibitors of virus fusion with the target cell				Immunomodulatory agents	
					
Umifenovir				Ivermectin	
Hydroxychloroquine				Nitazoxanide	
Camostat					
Nafamostat					

Molnupiravir (EIDD-2801) is an antiviral, prodrug of ribonucleoside analogue β -d-N4-hydroxycytidine. This compound has been proven to be active against numerous RNA viruses (Painter et al., 2021; Reina, 2021). The active form blocks RNA polymerase, an essential component of viral replication. Molnupiravir also acts by RNA mutagenesis via the template strand (Gordon et al., 2021). This potential anti-COVID-19 drug is administrated orally. The dosing of this drug is from 50 mg to up to 1600 mg (as a single dose). Still, administering it has proved to be effective to treat pathogenic respiratory RNA viruses and improving the function of the lungs by just giving lower doses of a maximum of 500 mg. Its side effects are relatively low, primarily headaches and diarrhea; when the dose is higher than 800 mg, the substance has to be formulated into an oral solution (Painter et al., 2021). Compared to remdesivir, molnupiravir is given orally and is generally well tolerated (Painter et al., 2021). Therefore, it has a high chance of being approved and administered in the treatment of COVID-19, being in advanced clinical study, in five phase III studies against COVID-19 (Kouznetsov, 2020; Ridgeback Biotherapeutics, LP, 2021).

3.2. Inhibitors of viral protein synthesis

There are antivirals in this group that have been shown to have some potential in the treatment of COVID-19.

Lopinavir/ritonavir is a combination of two inhibitors of viral protein synthesis used in the treatment of HIV infection (Jomah et al., 2020; Kouznetsov, 2020; Şimşek Yavuz and Ünal, 2020) but with limited efficacy against SARS-CoV-2 (Teoh et al., 2020). The combination is administered orally twice a day, in dosages of 400mg/100mg (1-10 or 14 days) (Şimşek Yavuz and Ünal, 2020). It is recommended to avoid higher doses due to severe gastrointestinal side effects (loss of appetite, diarrhea, nausea, vomiting),

hypokalemia, self-limiting rash and increased level of alanyl transferase.

Many side effects and drug interactions occur with lopinavir/ritonavir as a result of strong inhibition of CYP3A4 (Jomah et al., 2020; Teoh et al., 2020; Srinivas et al., 2020). The occurrence of these severe side effects has contributed to the discontinuation of therapy in some studies (Jomah et al., 2020; Teoh et al., 2020).

The WHO tried to reposition lopinavir through the international “Solidarity” clinical trial, but without success. The results indicated lesser effects or lack of effects in COVID-10 treatment (“Repurposed Antiviral Drugs for Covid-19 — Interim WHO Solidarity Trial Results,” 2021). An essential disadvantage of lopinavir/ritonavir is the occurrence of drug interactions (Teoh et al., 2020). Lopinavir/ritonavir is not included in the recommendations of the US National Institutes of Health (NIH) guidelines for the treatment of COVID-19, except for a clinical study (“Antiviral Therapy,” 2021).

Danoprevir/ritonavir is another combination that can be used in the treatment of COVID-19. Danoprevir is known to be a potent hepatitis C virus (HCV) protease inhibitor. Since 2018, it has been approved and marketed in China as a direct-acting antiviral agent (oral administration), potentiated by another viral protease inhibitor, ritonavir, and interferon. Following the therapeutical success of three patients infected with SARS-CoV-2, the hypothesis that this combination may be effective for patients with a moderate form of COVID-19 was issued (Marcolino et al., 2020). Another recent clinical trial enrolled 11 patients who tolerated the combination of danoprevir and ritonavir well, without composite side effects (Chen et al., 2020). In a study conducted on 33 COVID-19 patients danoprevir has been proven to be an appropriate treatment plan due to a shorter

hospitalization period compared to lopinavir/ritonavir (Zhang et al., 2020).

3.3. Inhibitors of virus fusion with the target cell

Umifenovir is an indole derivative (approved in China and Russia for the treatment of influenza A and B virus) with activity against both encapsulated and capsule-free viruses. *In vitro*, Umifenovir has effective antiviral activity against SARS-Cov-2, but is still undergoing study (Frediansyah et al., 2020; Jomah et al., 2020). Its primary therapeutic action is still uncertain. It is not clear if it has a direct antiviral activity, if it stimulates the immune system or has anti-inflammatory action (Kouznetsov, 2020). The main advantage of Umifenovir is the lack of significant side effects, with only mild gastrointestinal side effects reported in some patients (Jomah et al., 2020).

Hydroxychloroquine and chloroquine belong to this category of antivirals. The effects of the two compounds (usually used as antimalarials or to treat autoimmune diseases) are: reduction of pneumonic symptoms, a significant reduction in viral load and a shorter average duration of treatment (Marcolino et al., 2020). The mechanisms of action are multiple, related to viral replication, endosomal pH, glycosylation process, modification of viral proteins, and activity of the immune system (Marcolino et al., 2020; Şimşek Yavuz and Ünal, 2020). The oral administration of drugs has the following treatment schedule: 200 mg twice a day, during 1-5 days for hydroxychloroquine and 500 mg twice a day, during 1-5 (or 10) days for chloroquine (Şimşek Yavuz and Ünal, 2020). According to the World Health Organization (WHO), the efficacy and safety of hydroxychloroquine for the treatment of COVID-19 are debatable ("Targeted Update," 2020). In combination with azithromycin (an antibiotic from a new generation of macrolides), hydroxychloroquine

was significantly more effective (Marcolino et al., 2020). Azithromycin is known to have immunomodulatory and antiviral properties (Pani et al., 2020).

However, the recommendations of the NIH guideline do not include the use of hydroxychloroquine with or without azithromycin for both hospitalized and non-hospitalized patients diagnosed with COVID-19. Also, the NIH guide does not recommend using high doses of chloroquine for the treatment of COVID-19 ("Antiviral Therapy," 2021). Unfortunately, hydroxychloroquine was also found inefficient when used in the regimen of the hospitalized COVID-19 patients by the results of the "Solidarity" clinical trial ("Repurposed Antiviral Drugs for Covid-19 — Interim WHO Solidarity Trial Results," 2021).

Camostat (mesylate) is a serine protease inhibitor (a synthetic proteolytic enzyme inhibitor for trypsin, plasmin, kallikrein, tissue kallikrein and thrombin) (Frediansyah et al., 2020; Marcolino et al., 2020). This drug has been shown to be effective in treating COVID-19, reducing mortality, with a survival rate of 60%. The proper dosage of the compound to control viral spread is not yet known (Marcolino et al., 2020).

Nafamostat (mesylate) is also a serine protease inhibitor approved in Japan to treat acute pancreatitis. Currently, it is being studied for COVID-19 treatment (Frediansyah et al., 2020; Marcolino et al., 2020).

3.4. Immunomodulatory agents

Ivermectin is an antiparasitic agent approved by the FDA that has shown action for the RNA and DNA viruses. Thus, ivermectin has been studied for its antiviral activity against a wide range of viruses *in vitro*. It inhibits HIV replication and limits retrovirus, adenovirus and pseudorabies virus (PRV) infection both *in vitro* and *in vivo*. However, no efficacy of this drug against the Zika virus has been observed. Therefore, ivermectin has been promising for

treating COVID-19 in *in vitro* studies, even proving its effect on inhibiting the replication of the SARS-CoV-2 virus (Marcolino et al., 2020; Bello, 2021). Its binding interaction mediates the potential therapeutic mechanism to the target sites such as importin α/β (IMP α/β)-mediated nuclear transport of HIV-1 integrase, NS5 polymerase, NS3 helicase, nuclear import of UL42, and nuclear localization signal mediated nuclear import of Cap (Caly et al., 2020; Şimşek Yavuz and Ünal, 2020; Taher et al., 2021). However, the NIH guide does not recommend either for or against the use of ivermectin for the treatment of COVID-19, except for a clinical study (“Antiviral Therapy,” 2021).

Nitazoxanide is an antiparasitic drug that has been clinically authorized and commercialized for its antiviral activity. It works by interfering with the route of the type 1 interferons and viral duplication. It has been demonstrated that it represses the replication of many viruses, such as influenza viruses, MERS, hepatitis B and C and other pulmonary viruses (Eastman et al., 2020). Furthermore, it has been shown to inhibit SARS-CoV-2 replication at low micromolar concentrations in Vero CCL81 cells (Kouznetsov, 2020). In addition, nitazoxanide is orally bioavailable and broadly well-tolerated, thus representing a promising alternative for the management of COVID-19 were it to prove effective *in vivo*. In a recent study, patients with mild Covid-19 symptoms and who were given nitazoxanide (500 mg) for five days showed no advantage and no symptom reduction versus the placebo groups. Early nitazoxanide therapy was safe and reduced viral load significantly, and no serious adverse events were observed (Rocco et al., 2020). Even increasing the dose had no adverse events, most patients just reported feeling nauseous, having headaches or diarrhea. The primary outcome is that nitazoxanide reduced the viral load, compared to the

placebo, if given at the early symptoms of SARS-CoV-2 (Mendieta Zerón et al., 2021).

Many other drugs may be repositioned as effective medicines (as immunomodulators) in the treatment of COVID-19, such as tocilizumab, ribavirin, ruxolitinib, ingavirin etc. (Kouznetsov, 2020). Antivirals have little effect on mortality in patients hospitalized with COVID-19, suggest WHO interim trial results (Robinson, 2020). A triple combination of interferon beta-1b with lopinavir-ritonavir and ribavirin was also tested in a clinical study (Hung et al., 2020). The clinical efficacy of this triple combination is challenging to assess due to the absence of a more appropriate control group and the questionable effectiveness of lopinavir-ritonavir and ribavirin against SARS-Cov-2, respectively. However, the results showed accelerated viral clearance in these combinations with interferon beta-1b (Hung et al., 2020; Lee et al., 2020).

Conclusions

The COVID-19 pandemic has restarted the pharmaceutical industry in terms of antiviral therapy. The initial lack of an effective SARS-CoV-2 vaccine has led to numerous studies and trials of many existing drugs, from antiviral and other drug classes. Although several vaccines have been authorized internationally, the need for effective antivirals against SARS-CoV-2 has remained pressing. The range of antivirals available in the pharmaceutical market has been addressed mainly for persistent or latent viruses, such as HIV or hepatitis viruses. Significant investments for the development of new antivirals have been missing in SARS-type viruses, the focus being mainly on producing vaccines. A global effort is needed to develop new effective antiviral drugs, in order to prevent another global pandemic situation. By analyzing the most recently published data, we identified three

strategies for developing new antiviral compounds, useful in the treatment of COVID-19 and other coronavirus pandemics. The first strategy, *de novo* design, is time and resources consuming. Therefore, many resources are channeled towards faster development strategies, such as repositioning already known drugs or the virtual screening of the extensive library of known compounds. The development of new drugs from scratch is less preferred. Repositioning of available drugs is a desirable alternative that will provide effective compounds in the treatment of COVID-19 in a short time. Also, virtual screening (*in silico* methods) is a modern alternative with many advantages, among the most important being the decreasing of costs and the shorter time for identification of lead compounds with potential in the regimens of COVID-19. More extensive randomized controlled trials are needed to identify the best candidates, including anti-COVID-19 therapeutic combinations. Based on the correlated data, we are optimistic that there is an excellent chance that new antiviral drugs effective in the treatment of COVID-19 will be approved in the near future.

Conflict of interest

The authors declare that the research was conducted in the absence of any commercial or financial relationships that could be construed as a potential conflict of interest.

References

1. Adamson CS, Chibale K, Goss RJM, Jaspars M, Newman DJ, Dorrington RA (2021) Antiviral drug discovery: preparing for the next pandemic. *Chem Soc Rev* 50:3647–3655. doi: 10.1039/D0CS01118E
2. Agrawal U, Raju R, Udawadia ZF (2020) Favipiravir: A new and emerging antiviral option in COVID-19. *Med J Armed Forces India* 76:370–376. doi: 10.1016/j.mjafi.2020.08.004
3. Akilesh SM, J R, Palanisamy D, Wadhwani A (2021) Repositioning of Drugs to Counter COVID-19 Pandemic - An Insight. *Curr Pharm Biotechnol* 22:192–199. doi:10.2174/1389201021999200820155927
4. Amendola G, Ettari R, Previti S, Di Chio C, Messere A, Di Maro S, Hammerschmidt SJ, Zimmer C, Zimmermann RA, Schirmeister T, Zappalà M, Cosconati S (2021) Lead Discovery of SARS-CoV-2 Main Protease Inhibitors through Covalent Docking-Based Virtual Screening. *J Chem Inf Model* 61:2062–2073. doi: 10.1021/acs.jcim.1c00184
5. Antiviral Therapy [WWW Document] (Last updated: 11 Feb 2021) COVID-19 Treatment Guidelines. <https://www.covid19treatmentguidelines.nih.gov/antiviral-therapy/> Accessed 20 May 2021
6. Azam F, Taban IM, Eid EEM, Iqbal M, Alam O, Khan S, Mahmood D, Anwar MJ, Khalilullah H, Khan MU (2020) An in-silico analysis of ivermectin interaction with potential SARS-CoV-2 targets and host nuclear importin α . *J Biomol Struct Dyn* 1–14. doi: 10.1080/07391102.2020.1841028
7. Bello M (2021) Elucidation of the inhibitory activity of ivermectin with host nuclear importin α and several SARS-CoV-2 targets. *J Biomol Struct Dyn* 1–9. doi: 10.1080/07391102.2021.1911857
8. Benlloch J-M, Cortés J-C, Martínez-Rodríguez D, Julián R-S, Villanueva R-J (2020) Effect of the early use of antivirals on the COVID-19 pandemic. A computational network modeling approach. *Chaos Soliton Fract* 140:110168. doi: 10.1016/j.chaos.2020.110168
9. Bhowmick S, Dang A, Vallish BN, Dang S (2021) Safety and Efficacy of Ivermectin and Doxycycline Monotherapy and in

- Combination in the Treatment of COVID-19: A Scoping Review. *Drug Saf*. doi: 10.1007/s40264-021-01066-y
10. Caly L, Druce JD, Catton MG, Jans DA, Wagstaff KM (2020) The FDA-approved drug ivermectin inhibits the replication of SARS-CoV-2 *in vitro*. *Antivir Res* 178:104787. doi: 10.1016/j.antiviral.2020.104787
 11. Chen H, Zhang Z, Wang L, Huang Z, Gong F, Li X, Chen Y, Wu JJ (2020) First clinical study using HCV protease inhibitor danoprevir to treat COVID-19 patients. *Medicine (Baltimore)* 99. doi: 10.1097/MD.00000000000023357
 12. Choudhury A, Das NC, Patra R, Bhattacharya M, Ghosh P, Patra BC, Mukherjee S (2021) Exploring the binding efficacy of ivermectin against the key proteins of SARS-CoV-2 pathogenesis: an *in silico* approach. *Future Virol* 16:277–291. doi: 10.2217/fvl-2020-0342
 13. Dabbous HM, El-Sayed MH, El Assal G, Elghazaly H, Ebeid FFS, Sherief AF, Elgaafary M, Fawzy E, Hassany SM, Riad AR, TagelDin MA (2021) Safety and efficacy of favipiravir versus hydroxychloroquine in management of COVID-19: A randomised controlled trial. *Sci Rep-UK* 11:7282. doi: 10.1038/s41598-021-85227-0
 14. Dolgin E (2021) The race for antiviral drugs to beat COVID — and the next pandemic. *Nature* 592:340–343. doi: 10.1038/d41586-021-00958-4
 15. Eastman RT, Roth JS, Brimacombe KR, Simeonov A, Shen M, Patnaik S, Hall MD (2020) Remdesivir: A Review of Its Discovery and Development Leading to Emergency Use Authorization for Treatment of COVID-19. *ACS Cent Sci* 6:672–683. doi: 10.1021/acscentsci.0c00489
 16. Echeverría-Esnal D, Martín-Ontiyuelo C, Navarrete-Rouco ME, Cuscó MD-A, Ferrández O, Horcajada JP, Grau S (2021) Azithromycin in the treatment of COVID-19: a review. *Expert Rev Anti-infe* 19:147–163. doi: 10.1080/14787210.2020.1813024
 17. Everts M, n.d. Antiviral Drug Discovery and Development Center | UAB [WWW Document]. <https://www.uab.edu/medicine/ad3c/> Accessed 20 May 2021
 18. FDA (2020) Coronavirus (COVID-19) Update: FDA Issues Emergency Use Authorization for Potential COVID-19 Treatment [WWW Document]. FDA. <https://www.fda.gov/news-events/press-announcements/coronavirus-covid-19-update-fda-issues-emergency-use-authorization-potential-covid-19-treatment> Accessed 30 Sep 2020
 19. FDA (2021) COVID-19 Vaccines. <https://www.fda.gov/emergency-preparedness-and-response/coronavirus-disease-2019-covid-19/covid-19-vaccines> Accessed 21 May 2021
 20. Frediansyah A, Tiwari R, Sharun K, Dhama K, Harapan H (2021) Antivirals for COVID-19: A critical review. *Clin Epidemiol Glob Health* 9:90–98. doi: 10.1016/j.cegh.2020.07.006
 21. Gatti M, De Ponti F (2021) Drug Repurposing in the COVID-19 Era: Insights from Case Studies Showing Pharmaceutical Peculiarities. *Pharmaceutics* 13. doi: 10.3390/pharmaceutics13030302
 22. Gordon CJ, Tchesnokov EP, Schinazi RF, Götte M (2021) Molnupiravir promotes SARS-CoV-2 mutagenesis via the RNA template. *J Biol Chem*. doi: 10.1016/j.jbc.2021.100770
 23. Glaus MJ, Von Ruden S (2020) Remdesivir and COVID-19. *The Lancet* 396:952.

- doi: 10.1016/S0140-6736(20)32021-3
24. Halford B (2021) PROCESS CHEMISTRY Chemists shorten synthesis of molnupiravir. *Chem. Eng. News* 99, 7–7.
 25. Hospital do Coracao (2020) Antiviral for Adult Patients Hospitalized for SARS-CoV-2 Infection: a Randomized, Phase 2/3, Multicenter, Placebo Controlled, Adaptive, Multi-arm, Multi-stage Clinical Trial - Coalition Brazil COVID-19 IX: REVOLUTiOn (Clinical trial registration No. NCT04468087). clinicaltrials.gov.
 26. Hung IF-N, Lung K-C, Tso EY-K, Liu R, Chung TW-H, Chu M-Y, Ng Y-Y, Lo J, Chan J, Tam AR, Shum H-P, Chan V, Wu AK-L, Sin K-M, Leung W-S, Law W-L, Lung DC, Sin S, Yeung P, Yip CC-Y, Zhang RR, Fung AY-F, Yan EY-W, Leung K-H, Ip JD, Chu AW-H, Chan W-M, Ng AC-K, Lee R, Fung K, Yeung A, Wu T-C, Chan JW-M, Yan W-W, Chan W-M, Chan JF-W, Lie AK-W, Tsang OT-Y, Cheng VC-C, Que T-L, Lau C-S, Chan K-H, To KK-W, Yuen K-Y (2020) Triple combination of interferon beta-1b, lopinavir–ritonavir, and ribavirin in the treatment of patients admitted to hospital with COVID-19: an open-label, randomised, phase 2 trial. *The Lancet* 395:1695–1704. doi: 10.1016/S0140-6736(20)31042-4
 27. Jomah S, Asdaq SMB, Al-Yamani MJ (2020) Clinical efficacy of antivirals against novel coronavirus (COVID-19): A review. *J Infect Public Heal* 13:1187–1195. doi: 10.1016/j.jiph.2020.07.013
 28. Jourdan J-P, Bureau R, Rochais C, Dallemagne P (2020) Drug repositioning: a brief overview. *J Pharm Pharmacol* 72:1145–1151. doi: 10.1111/jphp.13273
 29. Kaka AS, MacDonald R, Greer N, Vela K, Duan-Porter W, Obley A, Wilt TJ (2021) Major Update: Remdesivir for Adults With COVID-19: A Living Systematic Review and Meta-analysis for the American College of Physicians Practice Points. *Ann Intern Med*. doi: 10.7326/M20-8148
 30. Kaur H, Shekhar N, Sharma S, Sarma P, Prakash A, Medhi B (2021) Ivermectin as a potential drug for treatment of COVID-19: an in-syn review with clinical and computational attributes. *Pharmacol Rep*. doi: 10.1007/s43440-020-00195-y
 31. Kouznetsov VV (2020) COVID-19 treatment: Much research and testing, but far, few magic bullets against SARS-CoV-2 coronavirus. *Eur J Med Chem* 203:112647. doi: 10.1016/j.ejmech.2020.112647
 32. Lai C-C, Chen C-H, Wang C-Y, Chen K-H, Wang Y-H, Hsueh P-R (2021) Clinical efficacy and safety of remdesivir in patients with COVID-19: a systematic review and network meta-analysis of randomized controlled trials. *J Antimicrob Chemother*. doi: 10.1093/jac/dkab093
 33. Lee N, Ison M, Dunning J (2020) Early triple antiviral therapy for COVID-19. *The Lancet* 396:1487–1488. doi: 10.1016/S0140-6736(20)32274-1
 34. Marcolino VA, Pimentel TC, Barão CE (2020) What to expect from different drugs used in the treatment of COVID-19: A study on applications and *in vivo* and *in vitro* results. *Eur J Pharmacol* 887:173467. doi: 10.1016/j.ejphar.2020.173467
 35. Mendieta Zerón H, Meneses Calderón J, Paniagua Coria L, Meneses Figueroa J, Vargas Contreras MJ, Vives Aceves HL, Carranza Salazar FM, Californias Hernández D, Miraflores Vidaurri E, Carrillo González A, Anaya Herrera J (2021) Nitazoxanide as an early treatment to reduce the intensity of COVID-19 outbreaks among health personnel. *World Academy of Sciences Journal* 3:1–6. doi: 10.3892/wasj.2021.94

36. Painter WP, Holman W, Bush JA, Almazedi F, Malik H, Eraut NCJE, Morin MJ, Szewczyk LJ, Painter GR (2021) Human Safety, Tolerability, and Pharmacokinetics of Molnupiravir, a Novel Broad-Spectrum Oral Antiviral Agent with Activity Against SARS-CoV-2. *Antimicrob Agents Chemother*. doi: 10.1128/AAC.02428-20
37. Pani A, Lauriola M, Romandini A, Scaglione F (2020) Macrolides and viral infections: focus on azithromycin in COVID-19 pathology. *Int J Antimicrob Ag* 56:106053. doi: 10.1016/j.ijantimicag.2020.106053
38. Pérez-Moraga R, Forés-Martos J, Suay-García B, Duval J-L, Falcó A, Climent J (2021) A COVID-19 Drug Repurposing Strategy through Quantitative Homological Similarities Using a Topological Data Analysis-Based Framework. *Pharmaceutics* 13:488. doi: 10.3390/pharmaceutics13040488
39. Pfizer Initiates Phase 1 Study of Novel Oral Antiviral Therapeutic Agent Against SARS-CoV-2 | pfizer.com [WWW Document] (23 Mar 2021) <https://www.pfizer.com/news/press-release/press-release-detail/pfizer-initiates-phase-1-study-novel-oral-antiviral> Accessed 21 May 2021
40. Pfizer unveils its oral SARS-CoV-2 inhibitor [WWW Document] (07 Apr 2021) *Chemical & Engineering News*. <https://cen.acs.org/acs-news/acs-meeting-news/Pfizer-unveils-oral-SARS-CoV99/i13> Accessed 21 May 2021
41. Pinho AC (2021) COVID-19 vaccines [WWW Document]. *European Medicines Agency*. <https://www.ema.europa.eu/en/human-regulatory/overview/public-health-threats/coronavirus-disease-covid-19/treatments-vaccines/covid-19-vaccines> Accessed 19 May 2021
42. Reina J (2021) [Plitidepsin, an inhibitor of the cell elongation factor eEF1a, and molnupiravir an analogue of the ribonucleoside cytidine, two new chemical compounds with intense activity against SARS-CoV-2]. *Rev Esp Quimioter*. doi: 10.37201/req/042.2021
43. Repurposed Antiviral Drugs for Covid-19 — Interim WHO Solidarity Trial Results (2021) *New Engl J Med* 384:497–511. doi: 10.1056/NEJMoa2023184
44. Richman DD (2020) Antiviral Drug Discovery To Address the COVID-19 Pandemic. *mBio* 11. doi: 10.1128/mBio.02134-20
45. Ridgeback Biotherapeutics, LP (2021) The Safety of EIDD-2801 and Its Effect on Viral Shedding of SARS-CoV-2 (Clinical trial registration No. NCT04405739). clinicaltrials.gov.
46. Robinson J (19 Oct 2020) Antivirals have little effect on mortality in patients hospitalised with COVID-19, suggest WHO trial interim results [WWW Document]. *The Pharmaceutical Journal*. <https://pharmaceutical-journal.com/article/news/antivirals-have-little-effect-on-mortality-in-patients-hospitalised-with-covid-19-suggest-who-trial-interim-results> Accessed 30 Apr 2021
47. Rocco PRM, Silva PL, Cruz FF, Junior MACM, Tierno PFGMM, Moura MA, Oliveira LFGD, Lima CC, Santos EAD, Junior WF, Fernandes APSM, Franchini KG, Magri E, Moraes NF, de Gonçalves JMJ, Carbonieri MN, Santos ISD, Paes NF, Maciel PVM, Rocha RP, Carvalho AF, de Alves PA, Modena JLP, Cordeiro AT, Trivella DBB, Marques RE, Luiz RR, Pelosi P, Silva JRL (2020) Early use of nitazoxanide in mild Covid-19 disease: randomised, placebo-controlled trial. *Eur*

- Respir J. doi: 10.1183/13993003.03725-2020
48. Sahakijpijarn S, Moon C, Koleng JJ, Christensen DJ, Williams RO (2020) Development of Remdesivir as a Dry Powder for Inhalation by Thin Film Freezing. *Pharmaceutics* 12:1002. doi: 10.3390/pharmaceutics12111002
49. Sahakijpijarn S, Moon C, Warnken ZN, Maier EY, DeVore JE, Christensen DJ, Koleng JJ, Williams RO (2021) *In vivo* pharmacokinetic study of remdesivir dry powder for inhalation in hamsters. *International Journal of Pharmaceutics*: X 3:100073. doi: 10.1016/j.ijpx.2021.100073
50. Salvi SS (2021) Is there a role for inhaled ciclesonide in the treatment of COVID-19? *Lung India* 38:1–4. doi: 10.4103/lungindia.lungindia_473_20
51. SCCM | COVID-19 Guidelines [WWW Document] (29 Jan 2021) Society of Critical Care Medicine (SCCM). <https://sccm.org/SurvivingSepsisCampaign/Guidelines/COVID-19> Accessed 12 May 2021
52. Şimşek Yavuz S, Ünal S (2020) Antiviral treatment of COVID-19. *Turk J Med Sci* 50:611–619. doi: 10.3906/sag-2004-145
53. Solidarity clinical trial for COVID-19 treatments [WWW Document], n.d. <https://www.who.int/emergencies/diseases/novel-coronavirus-2019/global-research-on-novel-coronavirus-2019-ncov/solidarity-clinical-trial-for-covid-19-treatments> Accessed 12 Dec 2020
54. Srinivas P, Sacha G, Koval C (2020) Antivirals for COVID-19. *Clev Clin J Med*. doi: 10.3949/ccjm.87a.ccc030
55. Taher M, Tik N, Susanti D (2021) Drugs intervention study in COVID-19 management. *Drug Metab Pers Ther*. doi: 10.1515/dmdi-2020-0173
56. Targeted Update: Safety and efficacy of hydroxychloroquine or chloroquine for treatment of COVID-19 [WWW Document] (17 Jun 2020) <https://www.who.int/publications/m/item/targeted-update-safety-and-efficacy-of-hydroxychloroquine-or-chloroquine-for-treatment-of-covid-19> Accessed 13 Oct 2020
57. Teoh SL, Lim YH, Lai NM, Lee SWH (2020) Directly Acting Antivirals for COVID-19: Where Do We Stand? *Front Microbiol* 11. doi: 10.3389/fmicb.2020.01857
58. Wang J (2020) Fast Identification of Possible Drug Treatment of Coronavirus Disease -19 (COVID-19) Through Computational Drug Repurposing Study. doi: 10.26434/chemrxiv.11875446.v1
59. Xu J, Shi P-Y, Li H, Zhou J (2020) Broad Spectrum Antiviral Agent Niclosamide and Its Therapeutic Potential. *ACS Infect Dis*. doi: 10.1021/acsinfecdis.0c00052
60. Zhang Z, Wang S, Tu X, Peng X, Huang Y, Wang L, Ju W, Rao J, Li X, Zhu D, Sun H, Chen H (2020) A comparative study on the time to achieve negative nucleic acid testing and hospital stays between danoprevir and lopinavir/ritonavir in the treatment of patients with COVID-19. *J Med Virol* 92:2631–2636. doi: 10.1002/jmv.26141

ECOSYSTEM SERVICES OF HOSPITAL GARDENS - BASED ON MICROCLIMATE ANALYSES OF GREEN AND BLUE GARDEN ELEMENTS

Vera TAKÁCSNÉ ZAJACZ^{1*}, prof. Kinga M SZILÁGYI²

¹Institute of Landscape Architecture, Urban Planning and Garden Art, Hungarian University of Agriculture and Life Sciences, Budapest, Hungary

²Doctoral School of Landscape Architecture and Landscape Ecology, Hungarian University of Agriculture and Life Sciences, Budapest, Hungary

*Correspondence:

Vera TAKÁCSNÉ ZAJACZ

Takacsne.Zajacz.Vera@uni-mate.hu

Received: 31 May 2021; **Accepted:** 11 June 2021; **Published:** 30 June 2021

Abstract: The increasing urbanization process of the last decades has resulted in negative impacts and changes in the quality of the urban environment, as reflected in mortality and morbidity data (Páldy, 2018). The quality of the environment, the urban climate, the increased frequency and duration of extreme weather events, ultimately threaten human well-being. To design and build liveable cities, the quality of the urban environment must be improved, and improving micro- or local climate is an important factor in this. Increasing the proportion and quality of biologically active surfaces, i.e. the ecosystem services provided by green spaces, is one of the most effective tools for urban conditioning and enhancing human well-being.

Determining the proportions of the green area, the design of vegetation, the choice of pavements and micro-architectures all determine the microclimate of an open-space. This has been confirmed by a large body of research and implemented work, but it is also important for designers to make a preliminary prediction of the impact of any intervention on the climatic conditions of the design site. These predictions will help cost-effective designing to determine which intervention will result in climate change.

This research uses two specific examples to examine the effectiveness of each landscape designing tool and to show which designing tool produces what and how much climatic impact. For these studies, we used a climate modeling program (ENVI-MET), which runs simulations to infer the climate modifying effects of landscape planning tools.

In the course of the research, we have shown that the local climate of hospital gardens could be significantly influenced by favorable, environmental-friendly paving, a higher green cover ratio, and a well-developed and sufficiently dense tree canopy, and various water features.

Keywords: urban microclimate, hospital gardens, ecosystem services of urban green infrastructure.

1. Introduction

As the world's population grows, the number and proportion of people living in cities is also increasing. Due to the increasing intensity of urban development, the city's changing radiation patterns, water balance, solar radiation, air currents and temperature

have a negative impact on the urban climate, which in turn has a negative impact on our environment and well-being. The urban planning professions, such as urban designers, architects, transport engineers and landscape

architects, are trying to respond to challenges posed by these changing conditions.

In cities, the area covered with vegetation, i.e. the vegetation and possibly the water surface, is able to compensate for negative climatic effects, improve the urban climate at least at local level, which is beneficial for the human environment, human comfort and well-being (Gulyás, 2009).

The aim of the research is to map and present the role of biologically active surfaces in improving urban climate, to show how green surfaces can modify the microclimate and the feeling of human comfort in an urbanized environment.

Among the land-use units that can significantly influence the urban microclimate are those with a high intensity of green spaces, such as forests, grasslands, reeds, urban green spaces, institutional areas with large green spaces, industrial and commercial areas and residential areas. The biologically active surfaces that are of great importance for the research should be supported by landscape architectural plans during the permitting process: green spaces, green space institutions, institutions with significant green space, i.e. institutional gardens (**Table 1.**).

Table 1. The relationship between park size and potential air temperature (Oke et al. 2017)

The park area (ha)	Average cooling effect (°C)	Range
500	2	~ 2 km
60	1,5	~ 1 km
0,5	1,5	~ 150 m
0,24	1-2	~ 20 m

The Covid19 pandemic has highlighted the need to improve human comfort in hospitals, as patients' recovery is greatly enhanced when they are comfortable. Thus, our research has also focused on these institutional areas, and has investigated the microclimate-modifying effects of landscape architecture in hospital gardens.

Hospital gardens are in a special position in the city. Even when the first hospitals were built, great emphasis was placed on the gardens surrounding the buildings, as they were also used for healing. The hospitals built in the 19th and 20th centuries, including those in Budapest, were surrounded by large gardens. Initially these green spaces were used as healing sites, but as motorisation progressed they became parking lots, yet they have remained the same size. They have more or less avoided fragmentation and development and still form uniform surfaces today. (Takácsné Zajacz 2020) However, their position in the

city has mostly changed, as the former peri-urban hospitals have been surrounded by the city, and now the mostly large green institutional gardens are located in the inner, green-deficient parts of the cities (**Fig. 1.**)

The local climate of gardens is basically determined by two specific urban meteorological processes: the formation of a cool island and the local park circulation due to the temperature difference. The vegetation, the pavement and the water surfaces are primarily responsible for the formation of the cool island. The formation of a cool island generates park circulation, which enhances the microclimate-modifying effect of the green surface, thus also having a beneficial effect on thermal sensation and human comfort (Oke et al. 2017).

In **Table 2.** the landscape architectural tools and their effects that can influence these meteorological processes and thus the microclimate of the area were collected:

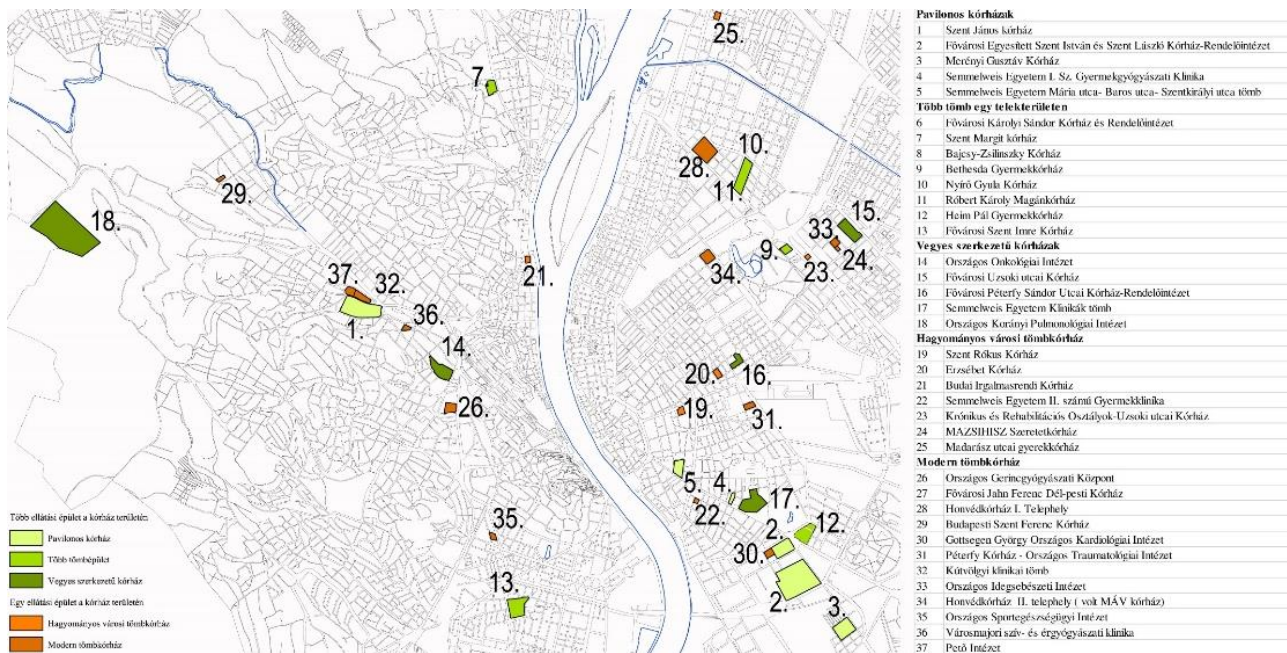


Fig. 1. Budapest hospitals (Takácsné Zajacz and Mezősné Szilágyi 2019)

Table 2. Landscape planning tools and their impact on local climate

	Impact on local climate	Possibility to intervene in climate improvement	Limitations, disadvantages and weaknesses of the intervention
Vegetation			
General	leaf area index (LAI), influences evaporation and heat removal	increase green area index	affect or limit the use of open spaces (e.g. lack or reduction of sunbathing lawns, natural ball fields)
trees	shading, reduces sky visibility, increases LAI thus promoting evaporation	60-65% increase in canopy cover	affect or limit the use of open spaces (e.g. lack or reduction of sunbathing lawns, natural ball fields)
	small-leaved species: lower canopy temperatures (Leuzinger et al. 2010)	mixed stock development	
	broad-leaved species: more shade, better use of rainwater (Hrotkó 2013)		
shrub	affects the flow of air through the park's air circulation system (park circulation - PC) (Unger 2010)		may impair local flow
	leaf area index (LAI), influencing evaporation and associated heat removal	LAI increases, evaporation increases	
lawn level	Leaf area index (LAI), influencing evaporation and associated heat removal	LAI increases, evaporation increases	
roof garden	controls incoming short-wave radiation, long-wave radiation	greening of flat roofs	can only be used on flat roofs, is expensive to build and

	from buildings, influences evaporation, reduces heating of the roof structure (Gerzson and Oláh 2012)		maintain intensively, and cannot be installed on all structures
greenwall	regulates incoming short-wave radiation, long-wave radiation from buildings, influences evaporation, vaporization, regulates wall temperature (Dezsényi et al. 2016)	designing green walls	supporting vegetation is costly and maintenance-intensive, and not feasible for all structures, and planting without supporting vegetation may face physical and population constraints
Pavement (Égerházi 2014)			
colour and material	affects long-wave radiation	increase albedo	dazzling cover in summer
construction	its rainwater retention capacity affects surface evaporation/evaporation	permeable pavement	more expensive
volume	affects long-wave radiation	quantitative reduction	a reduction in traffic space
Water surfaces			
	affects the humidity of the air	rehabilitation, establishment of new water surface	has an impact on a small surface area, is costly to build and maintain
Microarchitectures			
fences, walls	affects the airflow system in the park (Oláh, 2012)	none or less than 0,5 m	cannot be demolished everywhere for reasons of monument protection and townscape

2. Materials and methods

The aim of the research is to examine and prove how green areas and gardens created during landscape architecture participate in shaping local and microclimatic conditions, and whether they are able to influence the climatic conditions of the area. For this study, we have prepared 3-dimensional maps of the current and proposed or planned condition of the hospital gardens for better ecosystem services, and then we run climate simulations on these maps using a special program.

For this study, the microclimate modeling software ENVI-MET was used, which is able to simulate climatic conditions and their changes at a given time, under given meteorological conditions and for a given

geographical situation, using 3-dimensional models. The simulation program took into account short- and long-wave radiation, shading, evaporation of plants and surfaces, dynamic surface temperature and water and heat exchange in the soil. From the data, air temperature conditions, relative humidity, wind conditions and radiation conditions were determined and analyzed at different times. A biometeorological simulation program is also linked to the simulation program, which is used to run the data obtained to determine the thermal sensation and its variation, using the Physiologically Equivalent Temperature (PET) index.

As a sample area, we have chosen two hospitals in the city centre of Budapest, which are firmly embedded in the city and have now become practically part of the city centre:

- Szent Rókus Hospital - a classic urban hospital with two buildings, one large and one small courtyard, built in a closed structure;

- Péterffy Sándor Hospital - formerly a pavilion hospital, now a mixed structure hospital with a large block.

Szent Rókus Hospital (Takácsné Zajacz 2020)

The hospital opened in 1796 (**Fig. 2a.**). The 3-storey building accommodated patients from different social classes in nearly 300 beds. A small open-air reception area can be seen in the ornamental garden in the inner courtyard of the building complex, in front of the main entrance, as shown in contemporary depictions and in engravings and photographs from the turn of the century (**Fig. 2b.**). In the 20th century, the design and function of the garden changed, the enclosed front garden was transformed into a reception area, while the inner courtyard was extended with parking facilities at the expense of the ornamental garden (**Fig. 2c.**). By the 1970s, parking was added not only to the courtyard but also to the front garden.

In the 1990s, new buildings were built in the courtyard, and the ornamental garden was partially removed. (**Fig. 3b.**) The parking function was increased, which meant an increase in the size of the paved areas. The front garden has been redesigned over the last decade and, as in the 1830s, has been partially enclosed and closed off from the community (**Fig. 3c., Fig. 3d.**). The vegetation in the interior courtyard is typically single level, with only significant canopy cover and adequate canopy cover. The front yard vegetation is varied, with groundcovers and a variety of ornamental shrubs and trees.

Péterffy Sándor Hospital (Takácsné Zajacz 2020)

The first buildings of the hospital were constructed in the 1890s, with a one-storey brick pavilion design. Then, in two phases, between 1931-32 and 1940-42, a new 6-storey building was constructed, extending the full width of the garden. Several service buildings were added to the courtyard, which eliminated much of the garden between the pavilions.



Fig. 2. Szent Rókus Hospital: **a.** Map from 1867-72; **b.** Air photo 1972; **c.** Air photo 1995; **d.** Air photo 2021



Fig. 3. Szent Rókus Hospital: **a.** Therapeutic gymnastics area; **b.** Inner courtyard; **c.** Front garden; **d.** Dog run

The building process can be clearly followed on maps and aerial photographs.

The 1964 airphoto (**Fig. 4a.**) shows that there is an ornamental fountain in the courtyard, which is preserved in a photo documentation, but now only the basin of the fountain is visible (**Fig. 5b.**). In the early 2000s, the demolition of the service buildings did not increase the green area, but the area of the car parks. After the demolitions of 2006-2007, a recreation garden was created. In 2009 a new complex of buildings with underground parking was added to the courtyard, but unfortunately, this did not eliminate parking

surfaces. Moreover the parallel (**Fig. 4c.**) parking along the edge of the ornamental garden was replaced by perpendicular parking (**Fig. 4d.**), while parking between the pavilions was replaced by parking with crushed stone paving, further reducing the green area. (**Fig. 5c.**).

The whole garden is characterized by the fact that there is practically no shrub cover in the extensively managed, weedy lawns. However, the canopy cover is good, but the stand is partly old and neglected, and partly composed of invasive species along the margins.

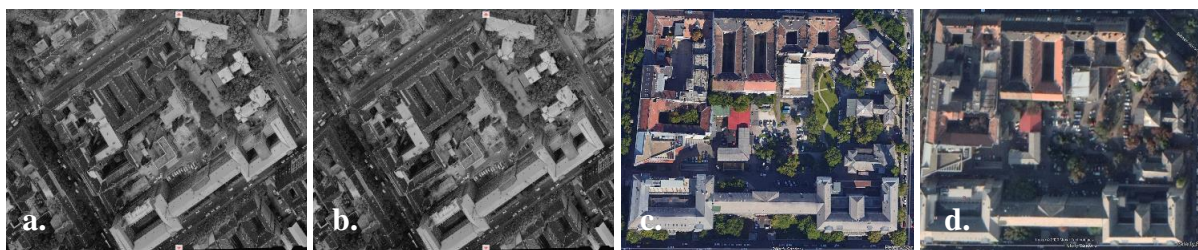


Fig. 4. Péterffy Sándor Hospital: **a.** Airphoto 1964; **b.** Airphoto 1972; **c.** Air photo 2016; **d.** Air photo 2017



Fig. 5. Péterffy Sándor Hospital: **a.** Plant container; **b.** empty fountain no longer in use; **c.** bench and paving

Simulation / Study

In the case of Rókus Hospital, the climatic impact of the ratio and intensity of green areas was modeled. In the conceptual design state, the effects of increasing the canopy cover, changing the type and amount of pavement, and creating an extensive roof garden were simulated using indicators of local climate and thermal comfort. The conditioning effect of the water surface and the fountain in the case of Péterffy Sándor Hospital was investigated, as

there are no such conditions in the area of the Rókus Hospital.

In ENVI-MET, the simulation was performed with the geographic data of the hospitals and with general meteorological conditions (22-34 °C, winds from NW 2.5 km/h) on August 1st. For both hospitals, heat maps and sections were analysed at 5 time points (8:00, 12:00, 13:00, 16:00, 20:00).

The simulation was also run for the original and the theoretical planned hypothetical state of the hospitals. Models

representing the 3-dimensional initial state were created from the air photo and plotted in a 2x2 m raster. The planned 3-dimensional model was carried out by enhancing the original building and space configuration in such a way that the changes to the landscape architecture in the hospital garden, as summarized in **Table 2.**, would have the most positive impact on the microclimate of the garden.

The following changes were made to the conceptual proposal (**Fig 6b.**, **Table 3.**):
The front garden and the hospital surroundings:

- Pavement reconstruction with a higher albedo material (asphalt (0,12)-concrete (0,48)) on the sidewalk around the building and in the forecourt
- Completion of the missing urban street trees

Internal courtyards:

- Increasing the green space index
- Create continuous green space
- Increase canopy cover
- Extensive roof garden
- Pavement reconstruction with a higher albedo (asphalt (0,12)-concrete (0,48))



Fig. 6. a. Original and **b.** planned model map of green surfaces and canopy cover

Table 3. The data of the models

	original whole area	original area Internal courtyards	planned whole area	planned area Internal courtyards
buildings	54%		54%	
paved surfaces	29 %	75 %	21 %	48 %
green space	17 %	23 %	25 %	50 %
canopy cover	17.5 %	35 %	30 %	68 %

The air temperature and thermal environment (PET) maps of the resulting models were analyzed and compared at the respective time points between the planned and

the original conditions, and then visualized using the Leonardo utility. We recorded 5 cross-sections of the area, where the different landscape architectural devices that play a

microclimate control role are clearly visible. We also analyzed the temperature and thermal variations plotted on the sections.

The differences between the heat maps and temperature maps allowed us to draw conclusions about the applicability and usefulness of general design principles, and the sections highlighted design guidelines for the use of specific landscape architectural tools.

3. Results and discussion

Study of the Rókus Hospital

The heat map plotted at five different points in time shows that the reduction of paved surfaces, the increase in green areas, the consolidation of green areas and the increase in cover reduce the air temperature in the area by 1 to 1.5 °C (Fig. 7.).

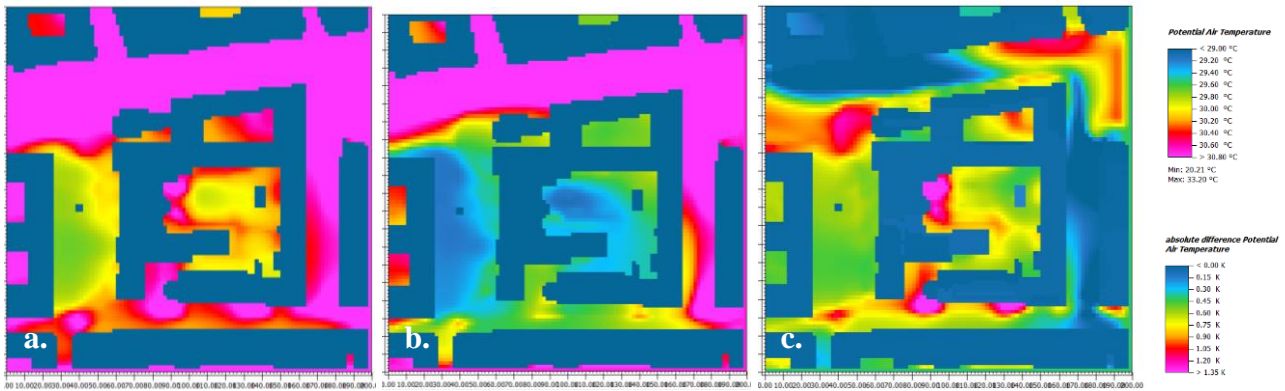


Fig. 7. a. Air temperature in the original and **b.** planned open space system; **c.** air temperature differences of original and planned situation

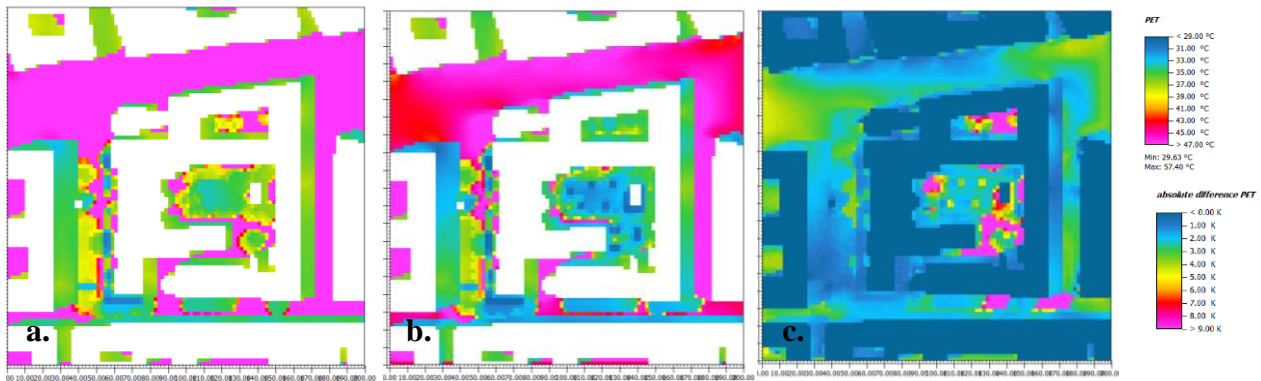


Fig. 8. a. PET in the original and **b.** planned open space system; **c.** PET differences of original and planned situation

Table 4. The temperature differences

	Air Temperature Difference	PET Difference
8:00	0.8 °C	22.01 °C
12:00	0.44 °C	20.88 °C
13:00	1.89 °C	23.20 °C
16:00	1.05 °C	21.20 °C
20:00	0.81 °C	1.71 °C

Other factors affecting the thermal comfort, such as air movement, radiation conditions and changes in relative humidity due to evaporation, had a much stronger influence on the PET value (**Fig. 8.**).

The temperature change in the area can reach 20-23 °C, depending on the time of day and the sub-area.

The changes are defined as the difference between the temperature at a given time, at a given unit area, simulated for the original state of the garden and the temperature simulated for the planned state of the garden. In all cases, this is a decrease and therefore a positive value for the result.

The largest changes in temperature and thermal sensation were observed around 1 p.m. during the hottest hours. The smallest change is measured in the evening hours; this is presumably due to the relatively large shading of the buildings, which has a significant effect on the thermal sensation (**Table 4.**) (Gulyás, 2009).

The effects of different landscape interventions can be illustrated by cross-sectional diagrams. Five cross-sectional heat maps, defined by the distribution of green areas, show the changes in temperature and thermal comfort conditions and the changes in temperature and thermal comfort (**Fig. 9.**).

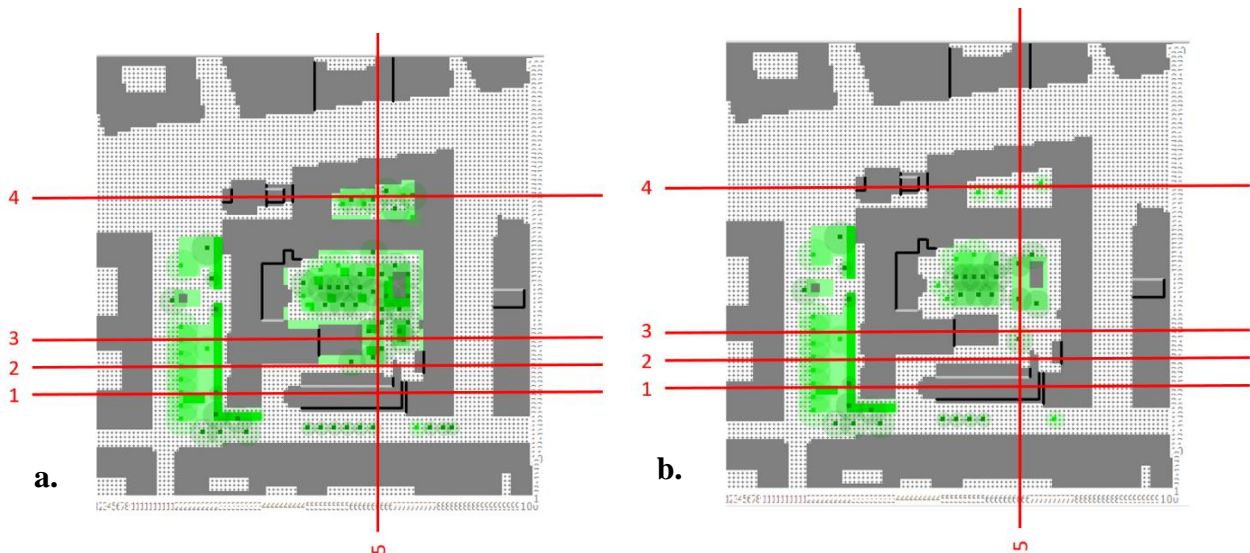


Fig. 9. a. Original and **b.** planned model maps with cross sections

We examined cases where only the quality and albedo of the pavement changed (section 1, 2), where new green space and extensive roof gardens were created (section 3, 4), and where the density of trees increased but no new canopy cover was established (section 5). Of course, other data can be read from these transects, such as the main role of trees in the horizontal shading of the building and its climate and thermal modification effects, and up to up the heights this effect reaches.

During the analysis of the cross-sections the following was found:

- with the change of the albedo of the paved surfaces, the air temperature decreased by about 0.5-1°C, and the thermal comfort decreased by only 1-2°C
- the extensive green roof did not meet expectations, with no significant change in either air temperature or thermal comfort (0.5-1°C)

- the replacement of the cover with a grass surface did not result in significant changes in temperature and thermal comfort either (0.5-1°C)
- where the pavement was replaced by 2-3 levels of vegetation, i.e. canopy cover and thus higher green cover intensity, a larger temperature difference (1-1.5 °C) and even more significant temperature difference (up to 20-23 °C) was observed
- there is practically no change in temperature and thermal comfort by thickening the canopy cover of the existing stand
- the shading and climate modification effect of the canopy close to the building is also felt at higher levels of the building, with a reduction of up to 20 °C in thermal comfort

AIR TEMPERATURE DIFFERENCE

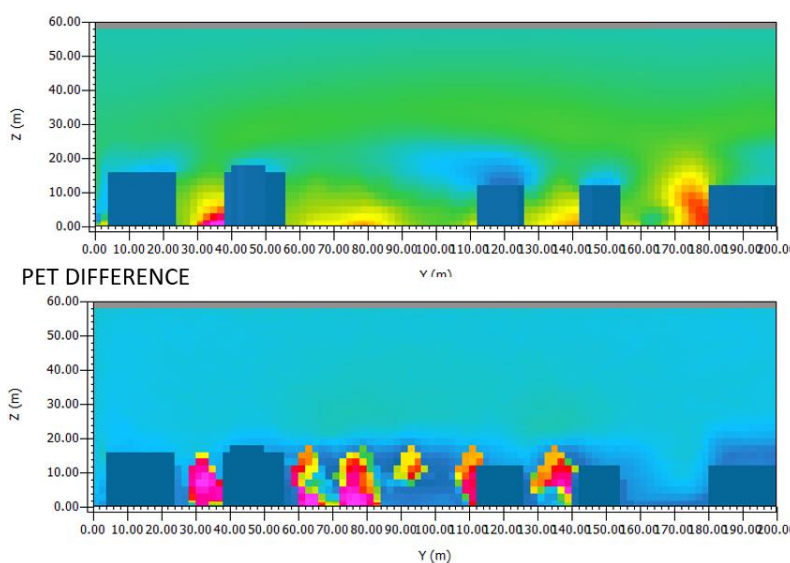


Fig. 10. Section 5

Péterfy Sándor Hospital

Models and simulations of the garden of Péterfy Sándor Hospital were also prepared for the study of the original and planned condition at the respective dates. Similar results were obtained for the two hospital gardens. The fountain in the garden of the Péterfy Street Hospital, which unfortunately is no longer functioning, provided a good opportunity to model the impact of the water surface. We "reconstructed" the fountain in the theoretical model design and examined the climate modifying effect of the moving water. Here, too, we analyzed both (potential air temperature, PET) heat maps, and a two-way

cross-sections. The relative humidity modifying effect of a working fountain has been shown to have a very large climate modifying effect, both horizontally and vertically; the moving water mass can reduce potential air temperature by up to 5.5°C (**Fig. 11., 12.**). However, the change in humidity does not cause such an extra change in thermal comfort; here, as in well-shaded areas, the temperature drop is around 22°C.

The climatic modification effect of the water surface depends to a large extent on the air movement, both vertically and horizontally, as the plume on the horizontal heat map shows the prevailing wind direction from the NW.

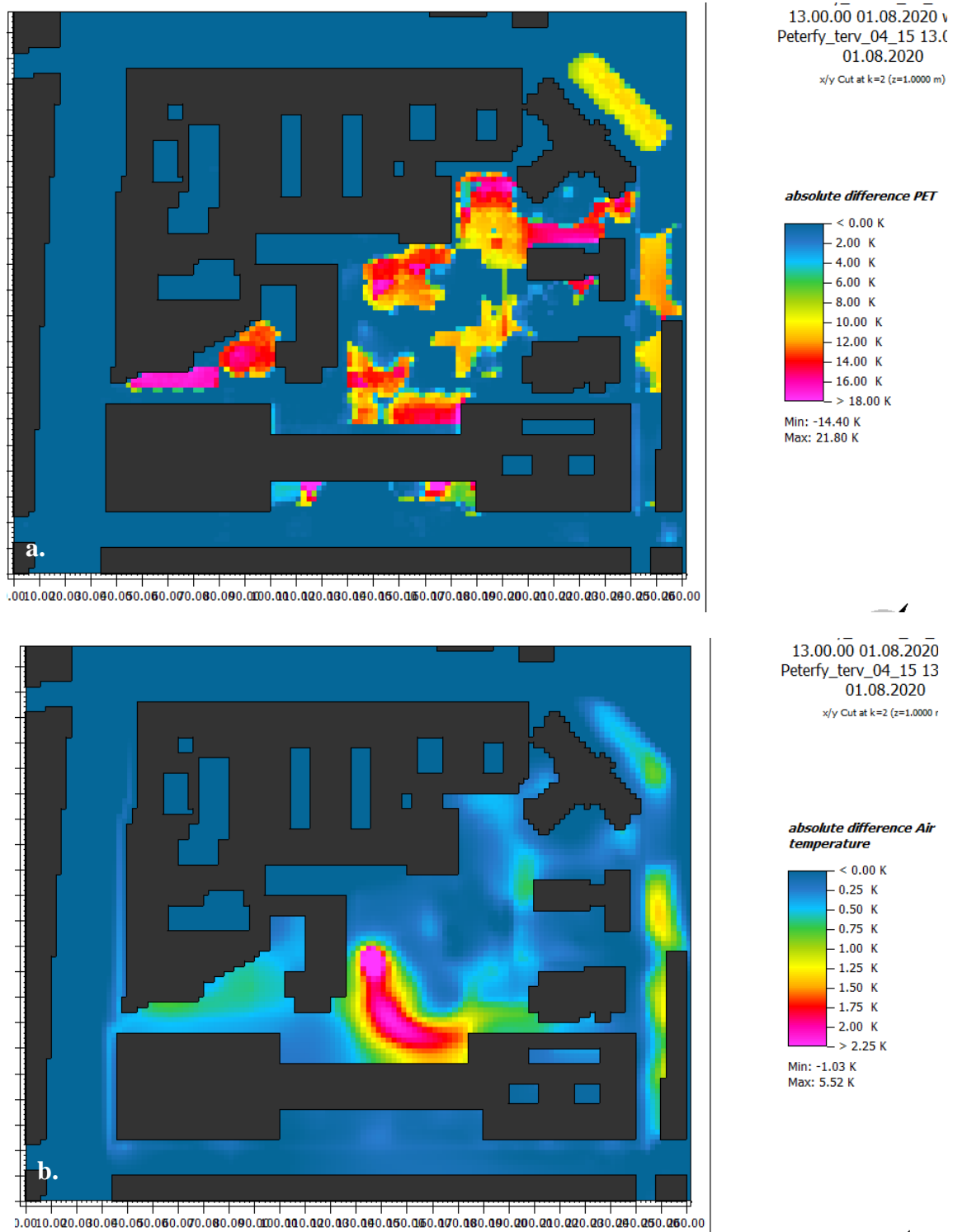


Fig. 11. a. PET in the original and planned open space system; **b.** PET differences of original and planned situation

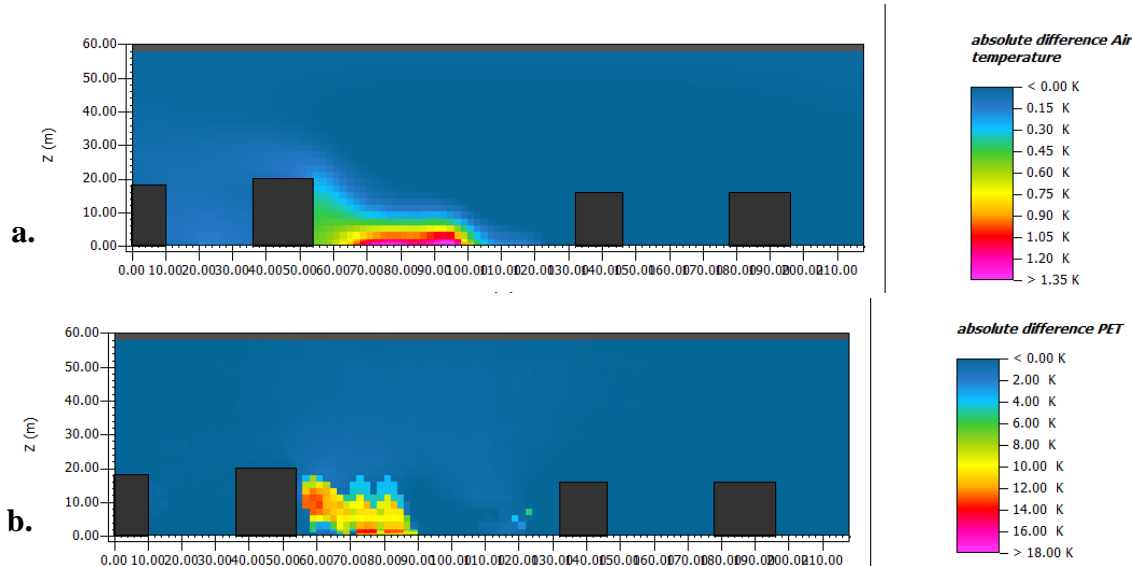


Fig. 12. a. Original, **b.** planned air temperature differences section and PET differences section

Conclusions

The simulations have shown that landscape architecture can have a significant influence on the micro- or local-climatic conditions of hospital gardens.

However, the 2x2 m scale of the used model does not provide an answer to the effectiveness of all landscape architectural tools in influencing the microclimate in how and how they affect it, so it was not possible to simulate the effect of fences, retaining walls and other micro architectural features, nor to isolate the effect of individual tree species with different leaf area indices and evaporative capacities.

However, the effects of changes in green area, cover and canopy cover, the choice of paving types and the appearance of water surfaces on the climatic conditions of the area were clearly observed. However, the extensive roof garden did not cause significant changes, so its role in the local climate is debatable. Although the building has a thermal insulating effect in terms of energy, its value for the ecology of the settlement is questioned. This raises the question of reconsidering the inclusion of the proportion of extensive green

roofs in the green space index. Further research should also examine the impact of more intensively planted and maintained green roofs.

Further studies should be carried out to clarify the issues raised, and the ENVI-MET program could be used for this purpose, as it is capable of simulating climatic conditions in a grid of up to 0.5 m x 0.5 m. This allows for more detailed studies, even of selected sub-areas, to map the role of certain plants and micro architectures in the microclimate.

Acknowledgement

I would like to thank my supervisor, Prof. Kinga Szilágyi for her immense patience, lots of useful advice, ideas and help, which made my participation in the conference possible.

Supported by the ÚNKP-2020-3-II New National Excellence Program of the Ministry for Innovation and Technology from the source of the National Research, Development and Innovation Fund.

Conflict of interest

The authors declare no conflict of interest.

References

1. Dezsényi P, Pataky R, Csibi K, et al (2016) ZÖLDHOMLOKZATOK Függőleges zöldfelületek tervezésének, kivitelezésének műszaki és kertészeti útmutatója, Budapest Főváros Városháza Tervező Kft. Budapest
2. Gerzson L, Oláh A (2012) A zöld építészet tájépítészeti vonatkozásai, eszközrendszere. 4D Tájépítészeti és Kertművészeti folyóirat
3. Gulyás Á (2009) Humán bioklimatológiai értékelések különböző léptékű megközelítésben, 2009th edn. SZTE TTIK Éghajlattani és Tájföldrajzi Tanszék, Szeged
4. Hrotkó K (2013) Városi fák környezeti hasznának vizsgálata. <https://docplayer.hu/43293800-Varosi-fak-kornyezeti-hasznanak-vizsgalata-dr-hrotko-karoly.html>
5. Oláh A (2012) A Városi beépítettség és a felszíntípusok hatása a kisugárzási hőmérsékletre. Budapesti Corvinus Egyetem, Tájépítészeti Kar, Kert- és Szabadtervezési Tanszék, Budapest
6. Páldy A (2018) Magyar Tudomány 2018/9 - A klímaváltozás hatása egészségünkre és az egészségügyre Magyarországon - MeRSZ. https://mersz.hu/dokumentum/matud__307. Accessed 7 Jun 2021
7. Unger J (2010) A városi hősziget-jelenség néhány aspektusa. Szeged
8. Égerházi LA (2014) Városi közterületek komplex humán-bioklimatológiai értékelése és annak várostervezési vonatkozásai szegedi példák alapján. <http://doktori.bibl.u-szeged.hu/id/eprint/2223/>. Accessed 11 Mar 2021
9. Leuzinger S, Vogt R, Körner C (2010) Tree surface temperature in an urban environment. *Agricultural and Forest Meteorology*. <https://doi.org/10.1016/j.agrformet.2009.08.006>
10. Oke TR, Mills G, Christen A, Voogt JA (2017) *Urban Climates*. Cambridge University Press
11. Takácsné Zajacz V (2020) A kórházkeretek funkcióváltozásának elemzése budapesti kórházkeretek példáján. *Ifjú Tehetségek Találkozója* 3808–401
12. Takácsné Zajacz V, Mezősné Szilágyi K (2019) Kórházkeretek ökoszisztéma szolgáltatása - különös tekintettel a településökológiai és zöldhálózati adottságok javítására. *Tájak működése és arculata*, 349-353.

THE EFFECT OF DIFFERENT SUBSTRATE ON THE MORPHOLOGICAL CHARACTERISTICS OF HUNGARIAN *TAGETES PATULA* CULTIVARS

Máté ÖRDÖGH^{1*}

^{*1}Department of Floriculture and Dendrology, Urban Planning and Garden Art, Institute of Landscape Architecture, Hungarian University of Agriculture and Life Sciences, Budapest, Magyarország

*Correspondence:
ordogh.mate@uni-mate.hu

Received: 31 May 2021; **Accepted:** 11 June 2021; **Published:** 30 June 2021

Abstract: The aim of this trial was to find the optimal substrate (sand, peat and 1:1 mixture of them) for germination and growing of *Tagetes patula* 'Robusza Kénsárga', 'Vénusz' and 'Tigris', with the use of 40 seeds according to substrates and cultivars in nine groups. Germination and survival ratio, plant height, root length, flower number and –diameter were examined. Almost all seeds germinated successfully, and the highest surviving was around 80% in case of peat + sand, and the lowest (50%) when plants grown in pure sand. The latter substrate resulted the longest roots (especially in the groups of 'Tigris') and all cultivars (particularly 'Vénusz') reached the lowest height with the use of this soil. On the other hand, peat effected the shortest roots, tallest specimens, most flowers of every cultivars. In case of flower number, there were significant differences between 'Tigris' (with averagely 58-70 flowers) and the other two types (23-39 flowers), irrespectively of the substrates. 'Vénusz' developed the smallest flower heads (maximum 3.5 cm) in all cases; the other cultivars produced at least 4 cm inflorescences. The lowest plant values experienced with the use of sand and the best results on peat.

Keywords: *Tagetes patula*, substrates, germination, plant height, rooting, flowering.

1. Introduction

Tagetes patula cultivars are one of the most popular annual ornamental bedding or balcony plants with typical flatted or half-globular flower head, a special inflorescence including „petal” shaped ray and smaller, circle formed disc flowers, which structures is typical of nearly all members of the Asteraceae family (Udvardy, 2008). These *Tagetes* varieties usually grow as compact, small plants with short stems and low (15-45 cm) height (Howe and Walters, 1990). Several flower colours (yellow, orange, red, two-coloured, marbled etc.) and types (simple, half- or full) are available, thanks to the crossbreeding of certain

species as *T. patula*, *T. erecta*, *T. tenuifolia*, *T. filifolia* and *T. lucida*. Most of them are densely branched, shrub-liked herbaceous plants (originated from northern part of South America and south-western regions of the USA) with pinnately lobed, deeply serrated, aromatic; glandulous leaves (Schmidt, 2002; Adams, 2004). Certain taxa (especially *T. erecta*) are applicable as medicinal plant, essential oil of the flowers contains antioxidants (Gutiérrez et al., 2006), and presence of flavonoids, tannins, saponins, carotenoids in *Tagetes* species have been reported (Riaz et al., 2013). Extracts of herbs

has been applied against respiratory problems (cold, bronchitis) and decoction of florets, leaves used as treatment of muscular, bone and abdominal pains, skin, kidney and eye diseases. Curative products of these annuals has diuretic, carminative effects (Maity et al., 2011; Dixit et al., 2013; Kadam et al., 2013; Manisha et al., 2013) or beneficial to reduce high levels of cholesterol and hypertension (Raghuveer et al., 2011). Additionally, examinations on different taxa of *Tagetes* genus proved their insecticidal effects; which reduced populations of certain insects such as mosquitos (Marcia et al. 2011; Nikkon et al., 2011), moreover, nematodes (Kiranmai et al., 2011). Hungarian cultivars (bred by Zoltán Kováts) usually produce bright, durable flowers in large quantities during whole summer and September-October (until the first frosty days) and tolerates unfavourable especially drought conditions. In this particular case (as sowing trial), some of these cultivars were used, such as the yellow flowered, medium sized (around 40 cm tall) 'Robusztá Kénsárga', the orange coloured, smaller (25-30 cm) 'Vénusz' and 'Tigris', an exceed, upright (70-80 cm) type with yellow and red striped flowers, as shown in **Fig. 1**. (Tillyné and Honfi, 2011; Szabó, 2020).

Several substrates can be used for plant propagation and growing. One of the cheapest is sand, but (especially comparing with peat)

certain disadvantages (e.g. heavier weight, less porous structure) often give us difficulties during sowing, cutting and plant care. Mixtures of sand + peat (with 1:3 to 3:1 ratio) had better physical and chemical parameter, which usually stimulate effectively plants' development, mainly rooting (Schmidt and Tóth, 1996). Properly selected substrates are one of the main factors affecting growth of plants, and optimal media have large water capacity, high porosity and durable, stabile structure (Fascella, 2015). In horticultural production, peat or peat-coconut based substrates are highly used (especially for the cultivation of bedding and balcony plants), however, these substrates can be substituted by cheaper soils (Dobrowolska and Janicka, 2014).

2. Materials and methods

Three In the first decade of May 2019, seeds (120 pieces per cultivar, originated from Fruit Culture Research and Development Institute, Budapest and Érd, Hungary) were sown into plug trays (with 4 x 4 cm cells) filled with fluvial sand (collected from the river Tisza), peat (marked as TS2, Klasmann-Deilmann, Germany) and 50-50% mixture of these substrates.

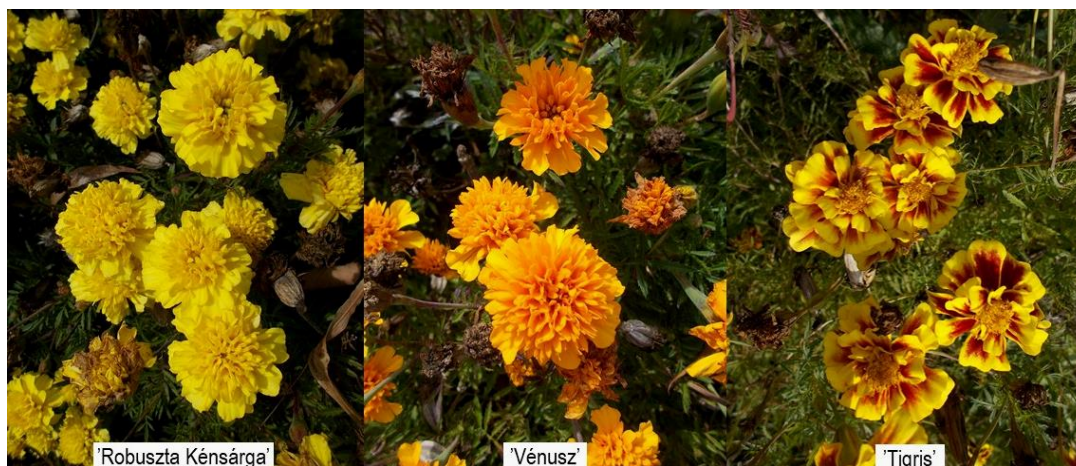


Fig. 1. Hungarian *Tagetes patula* cultivars with different flower colours

Each groups contain 40 seeds according to the three Hungarian cultivar and substrates:

1. group: 40 'Vénusz' seeds sown into sand
2. group: 40 'Robusztá Kénsárga' seeds sown into sand
3. group: 40 'Tigris' seeds sown into sand
4. group: 40 'Vénusz' seeds sown into 50-50% sand+peat
5. group: 40 'Robusztá Kénsárga' seeds sown into 50-50% sand+peat
6. group: 40 'Tigris' seeds sown into 50-50% sand+peat
7. group: 40 'Vénusz' seeds sown into peat
8. group: 40 'Robusztá Kénsárga' seeds sown into peat
9. group: 40 'Tigris' seeds sown into peat

At the end of May, all germinated specimens were replanted into plastic pots measuring 10 cm over (with the same substrates). Until planting out to open field, young plants were grown in unheated, unlit polytunnel without chemical pest control and fertilization. From germination to the end of life, different parameters such as germinate and survival ratio, plant height, root length, flower number and flower diameter were measured (**Fig. 2**).

Data were evaluated by Ropstat statistical software (Vargha, 2002, 2008). An analysis of variance (ANOVA) was conducted to calculate the statistical significance of all data presented. In cases of significant differences, means were separated by Tukey's test at $p < 0.1$, $p < 0.05$.



Fig. 2. Examination of root length and flower diameter

3. Results and discussion

3.1. Germination rate

Four days after sowing on 12th May, first seedlings ('Robusztá Kénsárga') were found on sand + peat and further four days following, all of them sprouted but only on pure peat (**Fig. 3**). In case of the other cultivars and substrates, 1-3 seed did not germinated, so, most of them successfully start their life, irrespective of the soils/cultivar (excepting 'Vénusz' seeds in sand: only 35 of them germinated well). In another study, *Tagetes erecta* seeds germinated

similarly fast, within 5-8 days (Kadam et al., 2012), but other taxa, for example *T. caracasana* required longer period (3 weeks) and reached only 61-69 % germination both in greenhouse and laboratory (Herrera-Moreno et al., 2013). *T. minuta* sprouted completely in 10-15 days with variable values (from 50 to 83%) depending on the culture environments, usually special, controllable sowing conditions (Petri dishes, filter papers) resulted higher percentages than in case of use pots and solid substrates such as sand (Ferreira et al., 2001; Singh et al., 2003).

3.2. Number of survived plants

Until 30th November (when first frost days destroy all plants), the highest plant number reduction (16-16 specimens) was obtained in case of 'Robusztá Kénsárga' and 'Tigris' groups on 100 % peat or also pure sand. The latter soil resulted similarly strong decrease of 'Vénusz' plant number; overall, this substrate negatively affected all *Tagetes patula* cultivars' survival, because of the bad water storage (after planting out, all groups were grown without

irrigation, so as to ascertain, which is the best drought tolerant cultivar). At the same time, combination of 50% peat and 50% sand enhanced survival ratio: only 7-9 individuals died before flower production, considering all cultivars (**Fig. 4**).

3.3. Plant height

Plants reached lower height on pure sand (in case of every groups) and 100% peat eventuated the largest growth (**Fig. 5**).

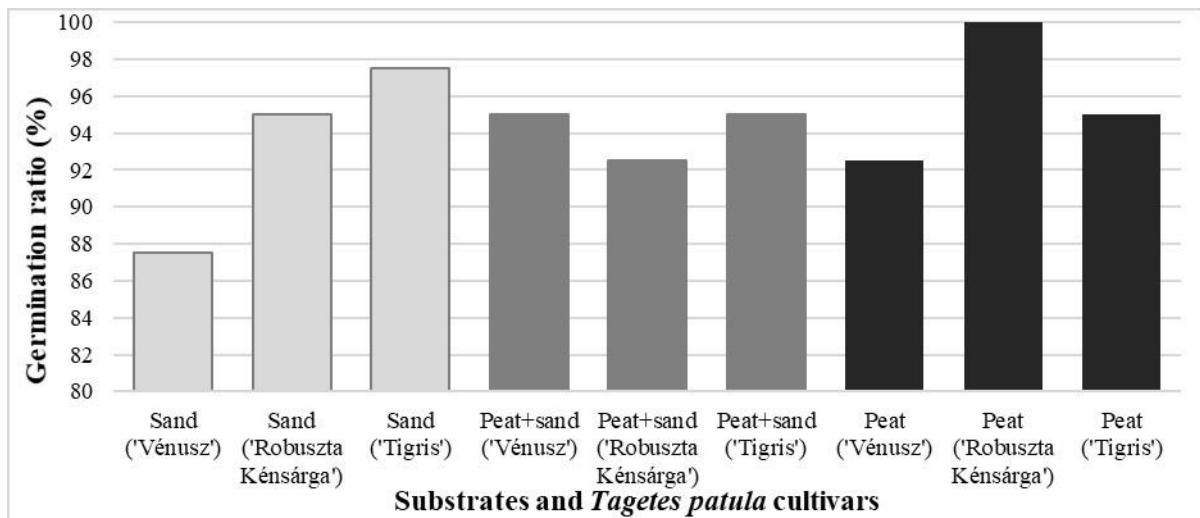


Fig. 3. Germination of *Tagetes patula* cultivars on different substrates (8 days after sowing)

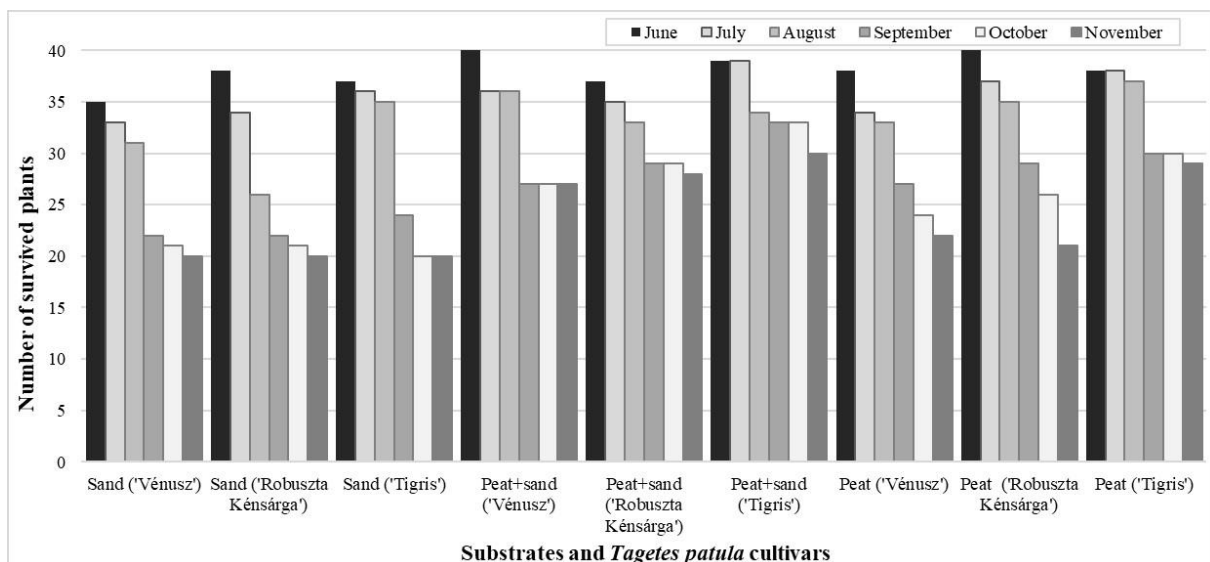


Fig. 4. Number of survived plants of *Tagetes patula* cultivars on different substrates (June-November 2019)

In another study of investigating the effect of various substrates (for example compost, flower soil, peat-coconut, peat TS1) on the development of *T. erecta* 'Marvel Mixture', 'Taishan Orange' and *T. patula* 'Durango Red' and 'Bonanza Flame', results showed that all specimens grown in peat TS1 had longer, thicker stems and larger height (Maślanka and Magdziarz, 2017).

On the other hand, cultivars (as an important factor) influenced average plant height (the highest was 'Tiger' with almost 60 cm size and the lowest was 'Vénusz', which grown not more than 22 cm on peat and 18 cm on sand. 'Robusztá Kénsárga' reached middle values (peat: almost 35 cm, sand: not more than 23 cm). Significant differences detected mainly between the cultivars, even on the same substrates. Considerable variances were also observed between 'Super Giant' and 'Inca F1' *T. erecta* cultivars when plants cultured in the same medium (1:1:1 mixture of sand, silt and leaf compost); the latter variety became taller and produced longer shoots (Riaz et al, 2013).

Comparing water-stressed (non-irrigated) stocks of *T. erecta*, *T. patula* and *T. tenuifolia*, Romanian and Hungarian, cultivars on 2:1:1 peat, vermiculite and perlite, great differences were recorded among not only species but also cultivars. Especially Hungarians (*T. patula* 'Orion' and 'Színkeverék', *T. erecta* 'Alacsony Citromsárga' and 'Aranysárga', *T. tenuifolia* 'Sárga') developed much shorter shoots with lower height in dry conditions (Cicevan et al., 2016).

3.4. Estimated spread of root system

In order to determine a rough degree of rooting (without serious root damages during repotting and examination of fragile plants' roots), estimated values (percentages) were ascertained according to the spread of root system inside the substrate. Thus, plants has the smallest results (20-45%) on sand and the largest values (50-85%) on peat. Comparing the cultivars, 'Vénusz' produced the least and 'Tigris' developed the greatest root system, irrespective of the substrate type (Fig. 6).

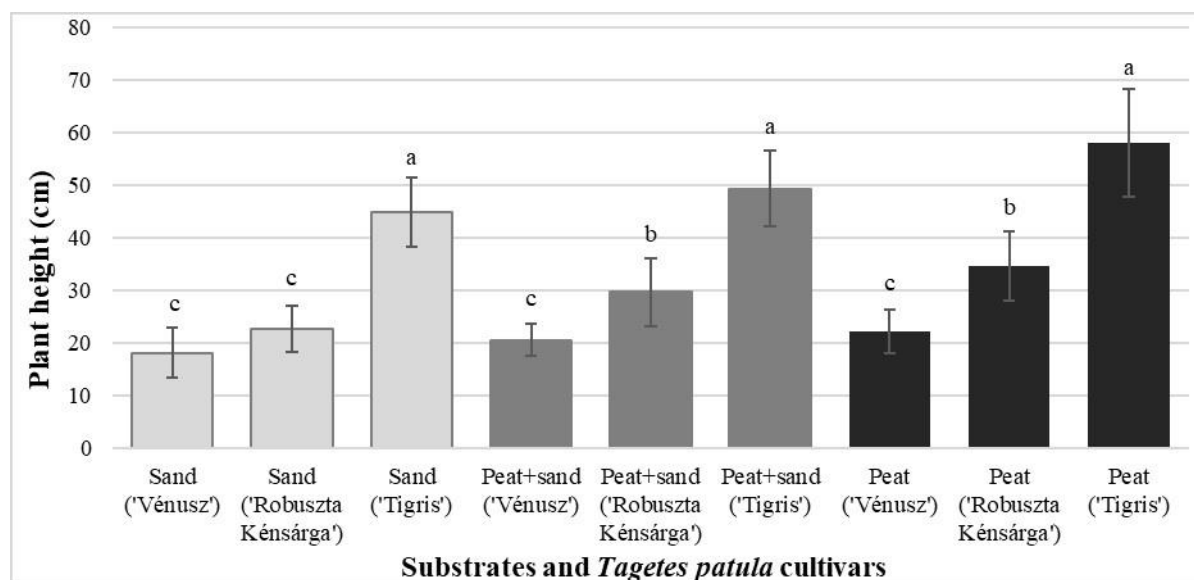


Fig. 5. Plant height of *Tagetes patula* cultivars on different substrates (November 2019)

3.5. Length of roots

Significantly, the longest roots were found on plants which germinated and grown on pure sand, and 100% peat resulted the shortest ones. Also considerable differences were observed between the cultivars; 'Tigris' plants developed the longest (longer than 20 cm) and 'Vénusz' produced the shortest (15.27 cm) roots with the

use of sand (**Fig. 7**). Additionally, we noticed inverse proportion between the length and estimated spread, therefore, poorly rooted plants (with smaller root system) usually created longer roots (chiefly in 100% sand) and plants with strong, well-developed root ball has shorter ones (mainly with the use of pure peat).

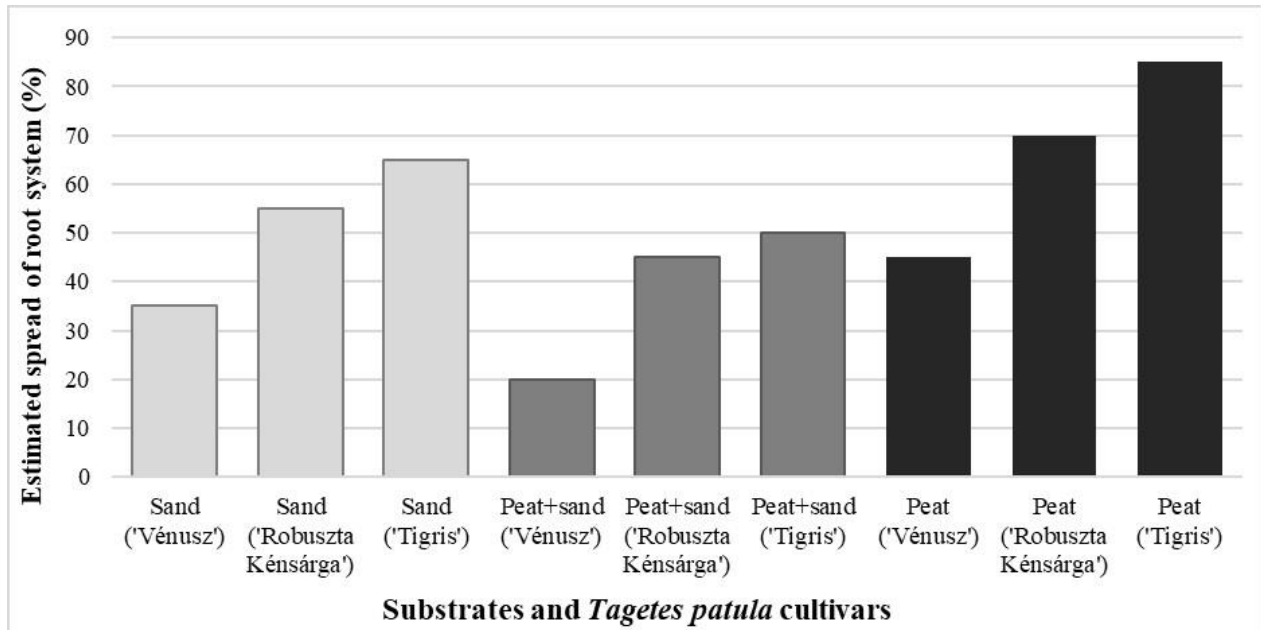


Fig. 6. Estimated spread of root system of *Tagetes patula* cultivars on different substrates (May 2019)

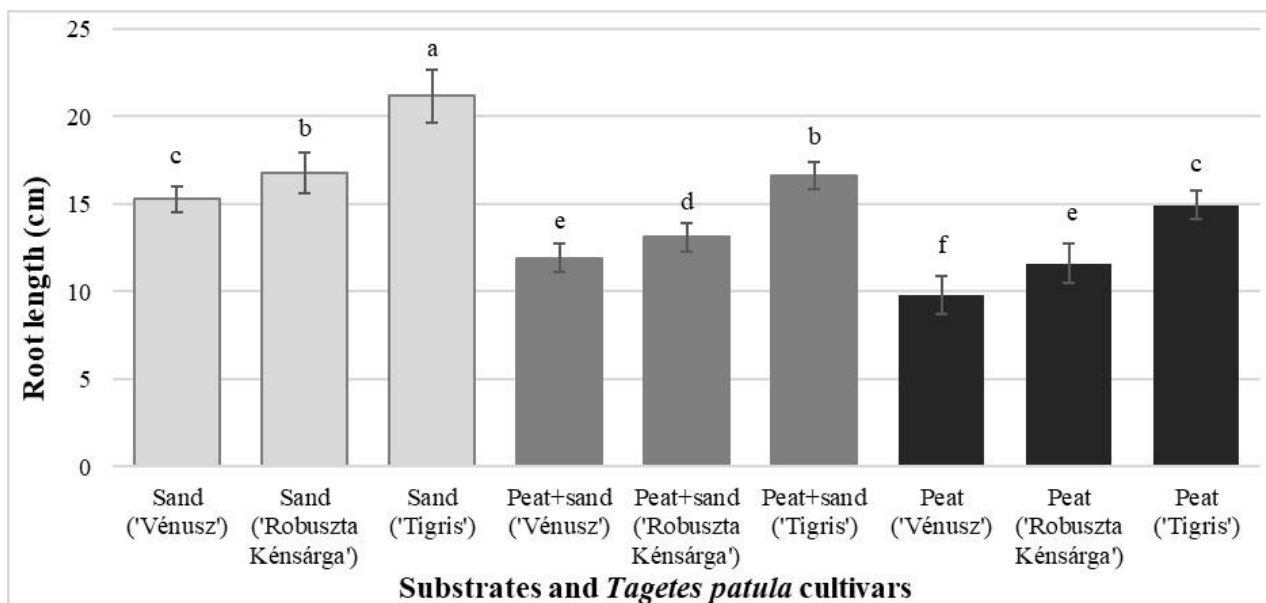


Fig. 7. Root length of *Tagetes patula* cultivars on different substrates (May 2019)

3.6. Number of flowers

The first full-blown flower was found at the beginning of July in the 'Robusztá Kénsárga' stock grown on peat, and 'Tiger' and 'Venus' groups which also cultivated on the same substrate opened second. Sand-grown 'Robusztá Kénsárga' and 'Vénusz' plants produced their first flower at the latest. In the case of average time from the sowing to the first flowers, 'Robusztá Kénsárga' had the shortest period (61 days) and 'Vénusz' required the longest time (65 day). It is worth notify that the latter cultivar developed the shortest roots with the smallest root systems, which possibly affected negatively the beginning of flowering and plant height, however, in another study, late flowering *T. patula* cultivars ('Flame', 'Yellow') usually became higher (Neri et al., 2012). The times of appearance of the first flowers and DAS (Day After Sowing) values were summarized in **Table 1**.

Flower number examined monthly, from early August to early November. In the first measurement, groups of 'Robusztá Kénsárga' cultivated on peat and 50-50% peat + sand showed the most flowers, but from the second monitoring (and regardless of the medium) the highest growing 'Tiger' stocks gave the largest number (70.8), specifically on peat. This tendency remained until the end of the plant life cycle in November (the number of flowers increased steadily in all groups). Comparing the cultivars, 'Vénusz' developed the fewest flowers, not even averaging 25 pieces when

using peat. Plants produced the fewest flowers on sand, in all studies and for all three varieties (**Fig. 8**). Statistical evaluation of the obtained data revealed that the difference between cultivars could be considered significant even in the case of the same substrate, although the number of flowers of the same cultivar in different media did not differ significantly. The number of flowers increased especially in October and November, but their diameter decreased mainly the latter month.

Examining other *T. patula* cultivars (in study of Neri et al., 2012), there was positive coherence between flower numbers and the beginning of flowering, thus, earlier blooming cultivars ('Orange', 'Spry') developed more flowers and later varieties ('Flame', 'Yellow') had fewer. In the present instance, although 'Vénusz' flowered at the latest and produced the least numbers of flowers, but then again, the earliest 'Robusztá Kénsárga' had middle values.

3.7. Flower diameter

At the first flower-measurement (in August), the largest diameter was obtained in the 'Tiger' group grown on peat (3.85 cm) and the smallest in the case of 'Vénusz' stocks on sand or peat (2.75 cm). By the way, the latter cultivar gave the lowest values (usually less than 3.3 cm) in every time and media. At the second occasion (in September), 'Tiger' developed the largest sized flowers (4.36 cm, on sand) and the next month (on the same substrate) 'Robusztá Kénsárga' produced the biggest ones (4.2 cm).

Table 1. Appearance of the first opened *Tagetes patula* flowers and DAS values

Cultivar name	'Robusztá Kénsárga'			'Vénusz'			'Tigris'		
Substrate	Sand	Peat + sand (1:1)	Peat	Sand	Peat + sand (1:1)	Peat	Sand	Peat + sand (1:1)	Peat
Date of 1st flower	20 th July	15 th July	2 nd July	20 th July	20 th July	10 th July	15 th July	15 th July	10 th July
DAS	69	64	51	69	69	59	64	64	59
DAS (average)	61			65			62		

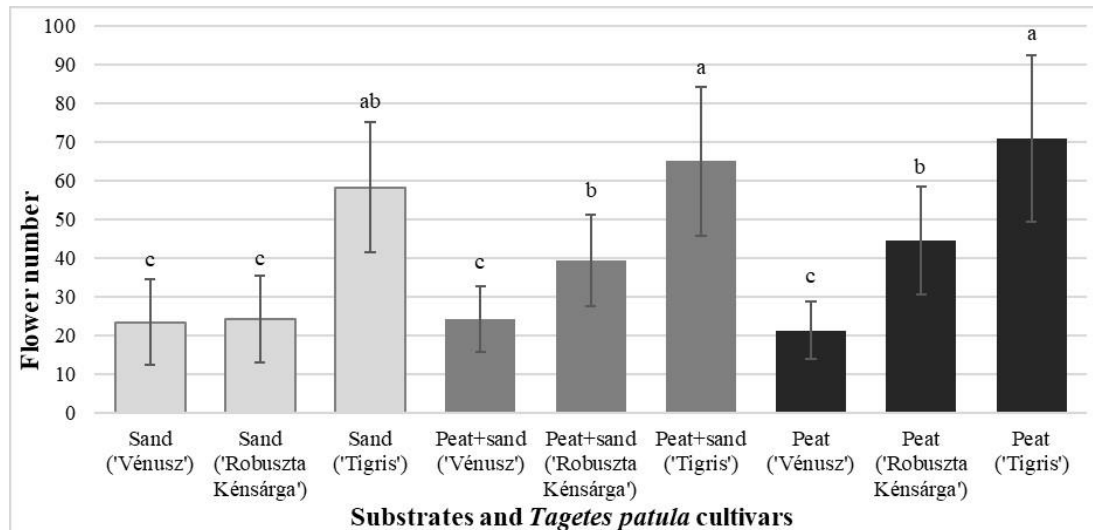


Fig. 8. Flower number of *Tagetes patula* cultivars on different substrates (November 2019)

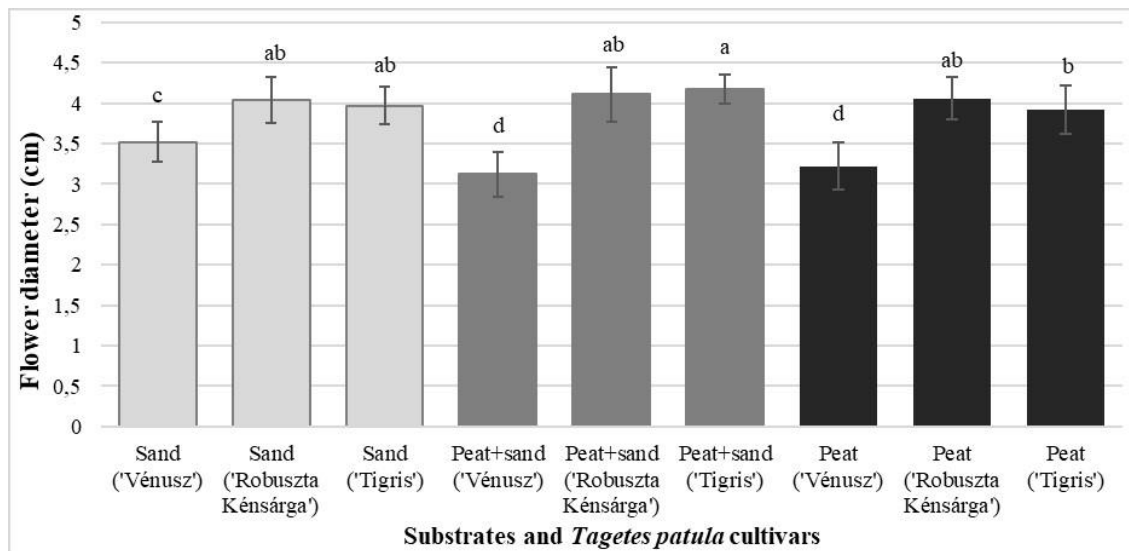


Fig. 9. Flower diameter of *Tagetes patula* cultivars on different substrates (November 2019)

In the last measurement (in November), 'Tiger' was again in first place, however, the maximum size was only 4.17 cm (on peat + sand medium). So in general, 'Tiger' developed flowers with the largest (and 'Vénusz' with the smallest) diameter (**Fig. 9**). The flower size of 'Robusztá Kénsárga' decreased from October to November, while in case of 'Vénusz', increased in all groups over the same period. Statistical evaluation of the flower data have shown that the latter cultivar developed significantly smaller flowers compared to the other two varieties in the same media.

4. Conclusions

The use of pure sand resulted the lowest survival values (in case of all cultivars), only half of the plants (20 specimens of 40) remained in the stock planted into this media. The rate of decrease in the number of individuals (if all three cultivars are included) was the smallest in the plants grown in the peat + sand mixture, not more than 7 or 9 individuals. Therefore, combination of these substrates proved to be more favorable, and sand was the least suitable.

Groups sown in the sand had the longest (and the least expanded) and the shortest (at once the densest) roots in the peat. There were also (and significant) differences between substrates and cultivars; ‘Venus’ produced the weakest (shortest, sparsely branched) and ‘Tiger’ had the strongest (longest and thickest) roots. Overall, the length of the roots and their density inversely related to each other.

Plants that developed on sand (regardless of cultivar) became shorter than which grown on peat + sand or even more peat (the latter resulted the tallest specimens). The effect of cultivar was also important: ‘Tiger’ was the highest and ‘Venus’ the lowest variety, in all substrates. The first flower opened in the ‘Robusza Kénsárga’ stock grown on peat, and the other two varieties also started to bloom earlier on the same substrate. There were also significant differences between cultivars when using the same medium, ‘Vénusz’ developed the least and ‘Tiger’ the most flowers. On the other hand, the substrate type also influenced the number of flowers, thus, pure sand resulted the fewest ones, at each cultivars. Flower diameter was the smallest in the case of ‘Vénusz’ (in all media cases), and ‘Tiger’ developed the largest flowers. However, as far as the substrate is concerned, it was not evident in the flower diameters of everyone. The role of a given plant variety can generally be considered more important than the type of medium, but if we have choice, peat, even more cheaper mixture of peat + sand is more suitable, as the weakest root systems, lowest plants, least flowers have developed as a result of sand, regardless of variety.

Conflict of interest

The author declare that the research was conducted in the absence of any commercial or financial relationships that could be construed as a potential conflict of interest.

References

1. Adams D W (2004) Restoring American Gardens: An Encyclopedia of Heirloom Ornamental Plants, 1640-1940. Portland: Timber Press.
2. Cicevan R, Hassan MA, Sestras AF, Prohens J, Vicente O, Sestras RE, Boscaiu M (2016) Screening for drought tolerance in cultivars of the ornamental genus *Tagetes* (Asteraceae). PeerJ 4:e2133; DOI:10.7717/peerj.2133
3. Dixit P, Tripathi S, Verma NK (2013) A brief study on marigold. Int Res J Pharm 4:43-48.
4. Dobrowolska A, Janicka A (2014) Changes in the chemical composition of organic media used in cultivation of garden horned violet (*Viola cornuta* L.) from the Patiola F1 group. J Elem 19(4):959-976.
5. Gutiérrez PRM, Luna HH, Garrido SH (2006) Antioxidant activity of *Tagetes erecta* essential oil. J. Chile Chem Soc 51(2):883-886.
6. Ferreira AG, Cassol B, Galli S, Da Silveira TS, Stival AL, Andreoli SA (2001) Germinação de sementes de *Asteraceae* nativas no Rio Grande do Sul, Brasil. Acta Bot Bras 15:231-242.
7. Herrera-Moreno AM, Carranza CE, Chacón-Sánchez MI (2013) Establishment of propagation methods for growing promising aromatic plant species of the *Lippia* (Verbenaceae) and *Tagetes* (Asteraceae) genera in Colombia. Agronomía Colombiana 31(1):27-37.
8. Howe TK, Walters WE (1990): Evaluation of Marigold cultivars as bedding plants, spring and fall 1989. Proceedings of the Florida State Horticultural Society 103: 332-337.
9. Kadam PV, Bhingare CI, Sumbe RB, Nikam RY, Patil MJ (2013) Pharmacocognostic, physicochemical and

- phytochemical investigation of *Tagetes erecta* Linn flowers (*Asteraceae*). J Biol Sci Opin 1(1):21-24.
10. Kiranmai M, Kazim SM, Ibrahim M (2011) Combined wound healing activity of *Gymnema sylvestre* and *Tagetes erecta* Linn. Int J Pharmaceut Appl 2(2):135-140.
11. Maity N, Nema NK, Abedy MK, Sarkar BK, Mukherjee PK (2011) Exploring *Tagetes erecta* Linn flower for the elastase, hyaluronidase and MMP-1 inhibitory activity. Journal of Ethnopharmacology 137(3): 1300-1305.
12. Manisha RL, Shaik R, Satyanarayana B (2013) Evaluation of anxiolytic activity of flowers of *Tagetes erecta* Linn (*Asteraceae*) in rats. J Appl Pharmaceut Sci 39(12):75.
13. Maślanka M., Magdziarz R (2017) The influence of substrate type and chlormequat on the growth and flowering of marigold (*Tagetes* L.). Folia Horticulturae 29(2):189-198.
14. Marcia M., Marques M, Selene M (2011) Larvicidal activity of *Tagetes erecta* against *Aedes aegypti*. J Am Mosq Contr Assoc 27(2):156-158.
15. Nikkon FM, Habib MR, Saud ZA (2011) *Tagetes erecta* Linn and its mosquitocidal potency against *Culex quinquefasciatus*. Asian Pac J Trop Biomed 1(3):186-188.
16. Neri FCS, Jr. Usberti JA, Usberti R, Paiva PDDO (2012) Morpho-agronomic trait comparisons among *Tagetes patula* L. cultivars. Ornamental Horticulture 18(1):85-90.
17. Riaz A, Younis A, Taj AR, Karim A, Tario U, Munir S, Riaz S 2013 Effect of drought stress on growth and flowering of marigold (*Tagetes erecta* L.). Pak J Bot 45(S1):123-131.
18. Raghuvver R, Sreeja K, Sindhuri T, Kumar SA (2011) Antihyperlipidemic effect of *Tagetes erecta* in cholesterol fed hyperlipidemic rats. Der Pharmacia Lettre 3(5):266-270.
19. Schmidt G (2002) Növényházi dísznövények termesztése. Mezőgazda Kiadó, Budapest
20. Schmidt G, Tóth I (1996) Díszfaiskola. Mezőgazda Kiadó, Budapest
21. Singh V, Singh B, Kaul VK (2003) Domestication of wild marigold (*Tagetes minuta* L.) as a potential economic crop in western Himalaya and north Indian plains. Econ Bot 57(4):535-544.
22. Szabó M (2020) Magyar nemesítésű egynyári virágfajták. Katiötletek Nyomdai Ötletgyár, Szeged
23. Tillyné Mándy A, Honfi P (2011) Növényházi dísznövénytermesztés. Budapesti Corvinus Egyetem, Kertészettudományi Kar, Dísznövénytermesztési és Dendrológiai Tanszék, Budapest
24. Udvardy L (2008) A kertészeti növénytan növényismereti kompendiuma. Budapesti Corvinus Egyetem, Kertészettudományi Kar, Budapest
25. Vargha A (2002) Független minták egyszempontos összehasonlítása új rangsorolási eljárások segítségével. Statisztikai Szemle 80(4):328-353
26. Vargha A (2008) Új statisztikai módszerekkel új lehetőségek: a ROPstat a pszichológiai kutatások szolgálatában. Pszichológia 28(1):79-100.

INCLUSION COMPLEX OF GEDUNIN-2-HYDROXYPROPYL- β -CYCLODEXTRIN PREPARED BY KNEADING AND FREEZE-DRYING METHODS: SYNTHESIS AND STRUCTURAL CHARACTERIZATION

Mary Olufunmilayo OLOGE^{1*}, Adedibu Clement TELLA², Olubunmi ATOLANI², Olajire Aremu ADEGOKE³, Olusegun George ADEMOWO^{1,4}

¹Department of Pharmacology and Therapeutics, P.M.B.1515, University of Ilorin, Ilorin, Nigeria

²Department of Chemistry, P.M.B.1515, University of Ilorin, Ilorin, Nigeria

³Departments of Pharmaceutical Chemistry, P.M.B.1515, University of Ilorin, Ilorin, Nigeria

⁴Institute for Advanced Medical Research and Training, University of Ibadan, Ibadan, Nigeria

*Correspondence:

Mary Olufunmilayo OLOGE

funmiologe@yahoo.com

Received: 21 May 2021; **Accepted:** 16 June 2021; **Published:** 30 June 2021

Abstract: The potential application of gedunin, a pharmacologically active limonoid, is limited in medicine because it has poor aqueous solubility. This study was aimed at preparation and characterization of an inclusion complex of gedunin and 2-hydroxypropyl- β -cyclodextrin (HBD) to increase the solubility in aqueous solvents and thus enhance the possibility of pharmaceutical formulation and oral administration of gedunin. Inclusion complex of gedunin isolated from *Entandrophragma angolense* heartwood with 2-hydroxypropyl- β -cyclodextrin (HBD) was prepared using freeze-drying and kneading methods. The gedunin-2-hydroxypropyl- β -cyclodextrin complex (GCD) was characterized using elemental analysis, Fourier-transform infrared spectroscopy (FT-IR), ¹H nuclear magnetic resonance (¹H-NMR) and X-ray diffraction analysis (XRD). Elemental analysis indicated that gedunin and HBD formed 1:1 stoichiometric inclusion complex. Results of FT-IR indicated that gedunin was stabilized in HBD cavity by intra-molecular hydrogen bonds and van der Waals forces. ¹H-NMR revealed that the entire gedunin molecule was not trapped into the core of the HBD. Nevertheless, the fraction trapped may be sufficient to enhance the apparent solubility of gedunin. XRD results showed the formation of new solid crystalline phase. The results obtained by different characterization techniques clearly indicated that both kneading and freeze-drying methods led to inclusion complex formation which may enhance oral administration of gedunin.

Keywords: Gedunin, 2-hydroxypropyl- β -cyclodextrin, inclusion complex, spectroscopy.

1. Introduction

Cyclodextrins (CDs) are non-toxic macrocyclic biodegradable oligosaccharides which contain at least 6 D-(+) glucopyranose units attached by α -(1, 4) glucosidic bonds. They have a relatively hydrophobic central cavity and a hydrophilic outer surface. The CDs and their derivatives have the capability to

form non-covalent inclusion complexes both in solution and in solid state with a wide variety of guest molecules of appropriate shape and size (Jansook et al., 2017; Wankar et al., 2020). The most common pharmaceutical application of cyclodextrins is to enhance drug solubility in aqueous solutions (Gowardhane et al., 2014;

Jambhekar and Breen, 2016). Drug bioavailability is expected to improve through enhancement of the solubility and dissolution rate. Cyclodextrins are considered to have advantage over organic solvents as solubilizers, in terms of toxicology and kinetics of solubility enhancement (Stella and He, 2008). Gedunin (**Fig. 1.**) is a limonoid that is common to the Meliaceae plant family (MacKinnon et al., 1997). This limonoid is potent *in vitro* against *Plasmodium falciparum* but it has limited *in vivo* activity against *Plasmodium berghei*. This has been partly attributed to poor solubility and low uptake (due to its lipophilicity), first pass metabolism by intestinal cytochrome P-450 enzymes of the small intestines (which reduce its plasma levels) and hydrolysis to its inactive and unstable metabolite, 7-deacetylgedunin

(Omar et al., 2003). Additionally, its short half-life and poor solubility in water have limited its application in medicine.

Complexation with cyclodextrins is expected to ease oral administration of gedunin thus increasing its pharmaceutical applications because the lack of water solubility reduces the flexibility for drug formulation and administration.

2-hydroxypropyl- β -cyclodextrin (HBD) (**Fig. 2.**) is the most widely used cyclodextrin derivatives in current scientific researches and in the industry because it has excellent inclusion properties for many compounds, is less toxic, safe, and an effective drug carrier (Srivalli and Mishra, 2016; Carneiro et al., 2019). It is mainly used in food, pharmaceutical and cosmetics industries.

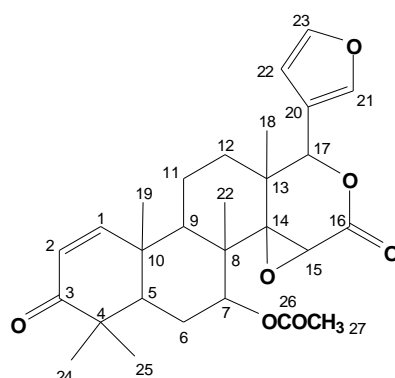


Fig. 1. Gedunin

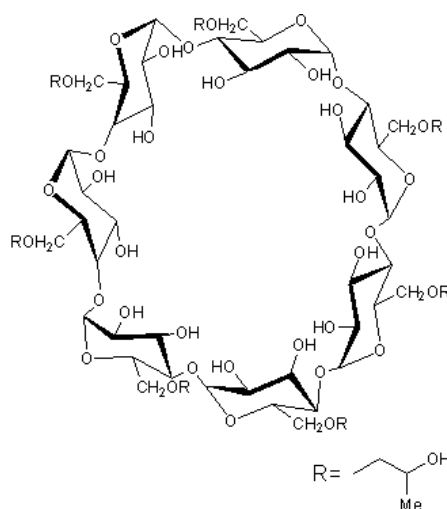


Fig. 2. 2-hydroxypropyl- β -cyclodextrin (HBD)

We have previously reported a stoichiometric ratio of 1:1 for inclusion complex formation between gedunin and HBD (Ologe et al., 2016). A survey of literature on inclusion complexes revealed that no inclusion complex between gedunin and HBD has been reported to date. In this study, isolation and preparation of gedunin from *Entandrophragma angolense* Welwitsch C.D.C (Meliaceae) heartwood was carried out and the inclusion complex containing gedunin as guest and HBD as host was prepared by freeze-drying and kneading methods.

2. Materials and methods

2.1. Spectroscopic methods

All reagents were purchased from Sigma-Aldrich and were used without further purification. Infra-red spectra were obtained from the samples in the form of potassium bromide (KBr) pellets using FTIR 8400s Spectrometer (Shimadzu, Japan). The analyses of carbon, hydrogen, and nitrogen were carried out on a Perkin-Elmer 240°C series elemental analyzer (Germany). For the Nuclear Magnetic Resonance (NMR) experiments, the sample was dissolved in either deuterated DMSO or chloroform and the ^1H -NMR and ^{13}C -NMR spectra for all samples were recorded at 600 MHz on Bruker Avance NMR spectrometer (U.S.A). Powder X-ray diffraction (PXRD) patterns were recorded on a scintag PADS diffractometer (Scintag, Santa Clara, CA) using Cu K α radiation ($\lambda = 1.54059 \text{ \AA}$, voltage of 40 kV and 25 mA current). Each sample was analyzed between 4.0 to 40.0 (2 θ) range with a total scan time of 4.0 min.

2.2. Preparation and Isolation of Gedunin

Gedunin was isolated from *Entandrophragma angolense* Welwitsch C.D.C (Meliaceae) heartwood using the modified procedure of Akisanya et al (1961) and Okhale

et al (2012). Briefly, 100g of powdered heartwood of *E. angolense* was extracted with 400 ml of n-hexane by solvent extraction at 60°C for 48 h. The extract was vacuum filtered with Whatman No. 1 filter paper. The filtrate was concentrated under vacuum with rotary evaporator at 40°C to 100 ml and allowed to stand in the dark for 24 h during which gedunin crystallized out. The isolation of pure gedunin from Crude crystal was done by thin layer chromatography (TLC) using authentic gedunin sample as reference. The crude crystals were further purified by column chromatography, preparative thin layer chromatography (PTLC) and recrystallization with methanol in order to isolate the pure shining white crystals.

Gedunin ($\text{C}_{28}\text{H}_{34}\text{O}_7$; **Fig. 1.**): Yield: 0.92 %, Mp. = 219°C, M.wt = 482 g/mol Anal. Calc. for $\text{C}_{28}\text{H}_{34}\text{O}_7$ (%): C, 69.71; H, 7.05; O, 23.24 Found %: C, 68.71; H, 6.68; O, 20.54; IR(KBr, v/cm^{-1}): 2960, 1731, 1435, 1255, 1233, 1048, 1024, 875, 796, 698, 627, 604, 400; Rf = 0.68 . IR (KBr) V_{max} : 2960 (C-H Str), 1731 (C=O), 1435, 1373 (C=C), 1255 (C-O-C), 1047, 1048 (C-O) cm^{-1} ; ^1H NMR (600 MHz, CDCl_3) δ (ppm) as shown in **Table 1** and **Figure 2**. ^{13}C NMR (CDCl_3) δ (ppm): 203.9 (C-3), 169.9 (7-acetyl CO), 167.4 (C-16), 156.9 (C-1), 143.1 (C-23), 141.2 (C-21), 126.0 (C-2), 120.4 (C-20), 109.8 (C-22), 78.2 (C-17), 73.2 (C-7), 69.7 (C-14), 56.8 (C-15), 44.0 (C-5), 42.6 (C-4), 40.0 (C-8), 39.5 (C-10), 46.0 (C-13), 38.7 (C-9), 27.1 (C-24), 26.0 (C-12), 23.2 (C-6), 21.1 (C-19), 21.0 (C-27, 7-acetyl CH_3), 19.7 (C-25), 18.31 (C-26), 17.7 (C-18), 14.9 (C-11).

2.3. Preparation of gedunin-2-hydroxypropyl- β -cyclodextrin complex (GCD)

The preparation of solid complexes of gedunin and HBD were performed by kneading and freeze-drying methods using a molar ratio of 1:1 based on the results of the stoichiometric ratio determination (Ologe et al., 2016).

2.3.1. Kneading method

The required quantities of gedunin and HBD were weighed accurately in a ratio of 1:1. Product from the kneading method was obtained by adding small amount of ethanol: water (1:5) to HBD placed in a glass mortar, the two were mixed to obtain a homogeneous paste. Gedunin was slowly added and the mixture was kneaded for 60 min. During the process, few drops of the ethanol: water was introduced to maintain a suitable consistency. The resulting paste was dried in an oven at 70 °C for 3 days. The dried complex was pulverized into a fine powder using 100 µm mesh sieve.

Yield: 69.6 %, Mp. = 254°C, M.wt = 1852g/mol Anal. Calc. for C₈₂ H₁₃₂ O₄₆ (%): C, 53.17; H, 7.1; O, 39.7% Found %: C, 52.20; H, 6.79; O, 39.52 ; IR (KBr, ν/cm⁻¹): 3335br(O-H), 2936m(C-H), 1739(C=O), 1668m(H-O-H bending), 1457(C=C), 1234m (C-O-C), 1025 (C-O)

2.3.2. Freeze-drying method

The complex was prepared by mixing gedunin and HBD, 1:1 molar ratio using freeze-drying method. Equimolar amount of the drug dissolved in 95% ethanol was added to the HBD in distilled water. The suspension was shaken at 37 °C for 6 h. The resulting solution was kept in a -20 °C freezer and lyophilized in a freeze-dryer (LTE Lyotrap Plus, UK) for 24 h.

Yield: 69.3 %, Mp. = 255°C, M.wt = 1852g/mol Anal. Calc. for C₈₂ H₁₃₂ O₄₆ (%): C, 53.17; H, 7.1; O, 39.7% Found %: C, 52.23; H, 6.89; O, 39.60 ; IR (KBr, ν/cm⁻¹): ; IR (KBr, ν/cm⁻¹): 3330br(O-H), 2935m(C-H), 1737(C=O), 1667m(H-O-H bending), 1457(C=C), 1239(C-O-C), 1024s(C-O)

3. Results and discussion

Gedunin was isolated from the *Entandrophragma angolense* Welwitsch C.D.C (Meliaceae) heartwood. Elemental analysis, Melting points (**Table 1.**) and the combined spectra FT-IR (**Table 2.**), ¹H and ¹³C NMR data of isolated compound conformed with literature reports (Connolly et al., 1967; Taylor, 1974; Hofer et al., 2009) and were used to establish the structure as gedunin (C₂₈H₃₄O₇). The infrared spectrum (**Fig. 5a**) exhibited peak at strong peak at 1731 cm⁻¹ which corresponds to the carbonyl of the α, β – unsaturated ketone of ring A lactone ring. The broadness of the α, β – unsaturated carbonyl was apparently due to the contribution from the carbonyl of the lactone and acetate. The β-substituted furan ring exhibited peaks at 1435 and 796 cm⁻¹ while the C-O-C of the ether was recorded at 1253 and 1232 cm⁻¹. Putting all the data together, the compound (**Fig. 1.**) was unambiguously established as tetranortriterpenoid, a special class called limonoid precisely as gedunin or 16,17-Seco-24-nor-5α,13α,14β,17α-chola-1,20,22-trien-16-oic acid, 14,15β:21,23-diepoxy-7α,17-dihydroxy-4,4,8-trimethyl-3-oxo-16,17-lactone, acetate.

Precisely, the ¹H NMR exhibited resonance at attributable to β-substituted furan, ring A 1-en-3one, an α, β – unsaturated lactone and acetate at C-7 and five tertiary methyl signals which are consistent with the basic structural skeleton of gedunin. The signals at H-15 and H-17 which corresponds to δ 3.49 and 5.58 ppm respectively are additional characteristic signals of gedunin (Ohochuku and Powell, 1966). The relatively downfield shift of the H-17 was apparently due to the coupling with allylic proton of the furan on ring E while the H-15 with 14, 15 – epoxide has no close neighbouring proton for such coupling. Equally, this is partly responsible the more sharp singlet observed for H-15.

Similarly, five characteristic methyl shifts between δ 1.12 - 1.22 ppm corresponding to H-18, 19, 20, 24, and 25 respectively were observed. The ^{13}C NMR data showed (**Fig. 2.**) distinct 28 signals. Three carbonyls signals at δ 203.9, 167.4 and 169.9 ppm which corresponded to C-3, C-16 and C-26 were observed while the other quaternary carbons (C-4, C-8, C-10, C-13, C-14, C-15 and C-20) were all observed as stated *ab initio*. The epoxide C-14 and C-15 were also distinctly observed at δ 69.7 and 56.8 ppm.

Two principal methods were adopted in the preparation of the formulation; kneading and freeze-drying techniques. Thus two products (inclusion complexes) were formed and were characterized using elemental analysis, melting point, FT-IR, ^1H NMR spectroscopies and PXRD. The Melting point and % of C, H and O are given in **Table 1**. Based on the analytical data and the molecular formula assigned, the complexes revealed 1:1 mole ratio which corresponded well to general formula $\text{C}_{82}\text{H}_{132}\text{O}_{46}$.

The obtained values of the elemental analysis were very much similar to the calculated values and indicate the complexes are fairly pure. The complexes are non-hygroscopic solids with melting points higher than the starting materials. An initial study on behavior of gedunin, HBD and GCD in various solvents showed that gedunin and its complexes had sharp electronic absorption spectra bands in acetate buffer of pH 3.50 (Ologe et al., 2016). This implies that the interaction with an acid allowed for the formation of discrete bonds. The discrete sharp bands imply the complex is not involved in extensive solute-solvent interactions that usually produce band broadening in UV spectrum. The presence of an acidic medium also aids ionization of cyclodextrin due to their basic pKa values. The formation of very sharp bands between gedunin and HBD in acetate buffer led to the adoption of acetate buffer as the medium for the spectrophotometric titrations of the two compounds as previously reported (Ologe et al., 2016).

Table1. Analytical data of Gedunin and Inclusion complexes synthesized by both methods

Gedunin/ Complexes	Molecular formula	M. wt (g/mol)	Melting point ($^{\circ}\text{C}$)	C H O % found(calculated)
Gedunin	$\text{C}_{28}\text{H}_{34}\text{O}_7$	482.5	219	C, 68.71(69.71) H, 6.68 (7.05) O, 20.54(23.24)
GCD(Kneading)	$\text{C}_{82}\text{H}_{132}\text{O}_{46}$	1852	254	C, 52.20(53.17) H, 6.79 (7.10) O, 39.52(39.7)
GCD(Freeze-drying)	$\text{C}_{82}\text{H}_{132}\text{O}_{46}$	1852	255	C, 52.23 (53.17) H, 6.89 (7.10) O, 39.60(39.7)

3.1. Infra-red spectra

Figure 3 shows comparison of the infrared spectra for gedunin, HBD, GCD (kneading) and GCD (freeze-dried). **Table 2** shows comparison of the selected FT-IR data of the HBD and inclusion complexes; comparison of

selected FT-IR data of gedunin and inclusion complexes is shown in **Table 3**. The frequencies for gedunin observed at 2960, 1731, 1435, 1255, 1048 cm^{-1} correspond to $\nu(\text{C-H})$, $\nu(\text{C=O})$, $\nu(\text{C=C})$, $\nu(\text{C-OC})$, $\nu(\text{C-O})$ respectively. Meanwhile, the frequencies for

HBD recorded at 3320, 2928, 1642, 1231, 1022 cm^{-1} were assigned to $\nu(\text{O-H})$, $\nu(\text{C-H})$, $\nu(\text{H-OH})$ bending, $\nu(\text{C-OC})$ and $\nu(\text{C-O})$ respectively. The FT-IR spectra of the GCD inclusion complexes were identical to that of HBD instead of gedunin due to the less amount of gedunin in the complex. This finding was in agreement with the results of other researchers (Subramaniam et al., 2010; Yuan et al., 2012). It can be observed in **Table 2** that the bands at 3320 and 2928 cm^{-1} for pure HBD were shifted to higher wavenumber ~ 3330 and 2935 cm^{-1} for the inclusion complex due to the formation of intramolecular O-H---O hydrogen bonds and presence of van der Waals forces that stabilize gedunin in the cavity of HBD (Sambasevan et al., 2013). The absorption bands at 1435 due to $\nu(\text{C=C})$ in gedunin shifted to higher frequency ~ 1457 cm^{-1} for both complexes, in addition $\nu(\text{C=O})$ band at 1731 in gedunin also shifted to higher wavenumber at

~ 1737 cm^{-1} , this indicates the formation of complex between guest and host. When complexation occurs, the peaks can change position, diminish or even disappear (Corti et al., 2007.; Hui et al., 2020), thus the disappearance, decreased intensity and change in position of some gedunin absorption bands, in the GCD spectra, point to formation of a complex between the guest and host. The modification of some of the bands representing the guest molecule is indicative that only part of the molecule has been encapsulated by the cyclodextrin. The portion that has not been complexed is responsible for the presence of any unchanged bands (Yang et al., 2008). The presence of two unchanged bands (C=O and C=C) in the kneading and freeze-dried complex shows that the gedunin molecule is not totally encapsulated in HBD. This is in line with the NMR analysis.

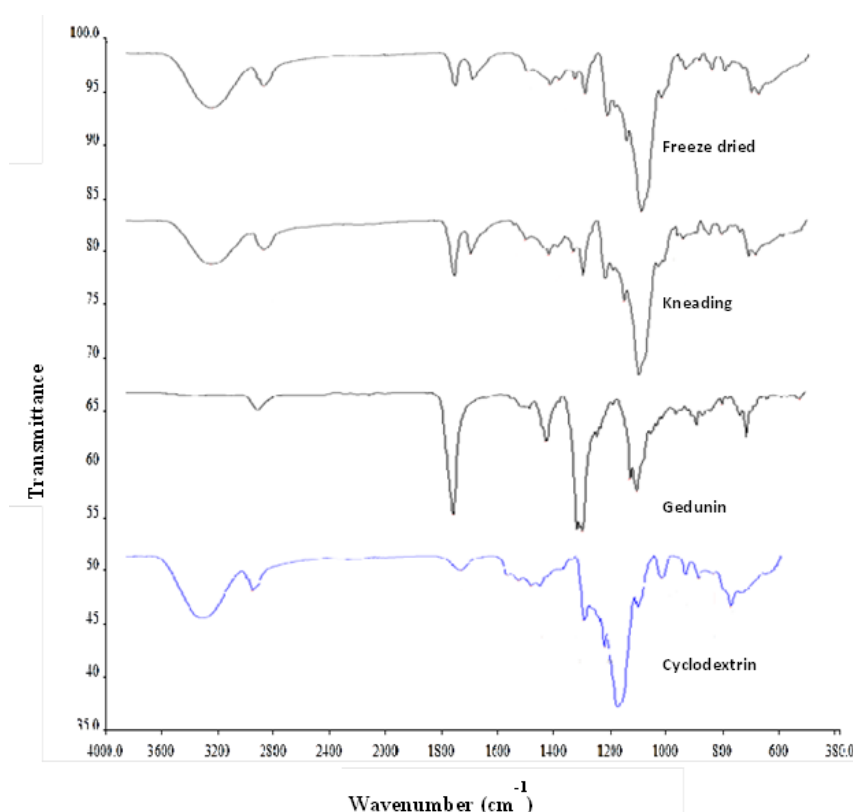


Fig. 3. Infrared spectra of 2-hydroxypropyl-cyclodextrin (HBD), gedunin, GCD (kneading), GCD (freeze-dried)

Table 2. Comparison between FT-IR spectra of HBD and Inclusion complexes (kneading and freeze-dried)

Functional group	HBD	Inclusion complex (Kneading)	Inclusion complex (Freeze- dried)
v(OH)	3320br	3335	3330 br
v (C-H)	2928	2936m	2935m
v (H-O-H) bending	1643s	1668s	1667s
v (C-OC)	1231s	1234s	1239s
v (C-O)	1022s	1025m	1024m

Note: br = broad, m = medium, s = strong, w = weak

Table 3. Comparison between FT-IR spectra of Gedunin and Inclusion complexes (kneading and freeze-dried)

Functional group	Gedunin	Inclusion complex (Kneading)	Inclusion complex (Freeze- dried)
V(O-H)	-	3335br	3330br
V(C-H)	2960w	2936m	2935 m
V(C=O)	1731s	1739m	1737m
V(C=C)	1435m	1457 m	1457 m
V(C-OC)	1255s	1234s	1239s
V(C-O)	1048s	1025m	1024m

Note: br= broad, m= medium, s= strong, w= weak

3.2. NMR Spectra

In order to study the principal structural changes occurring in the gedunin molecule, the ^1H and ^{13}C NMR spectra (**Fig. 4.**) were recorded. In addition, the ^1H -NMR spectra of both the kneaded and freeze-dried products were recorded (**Fig. 5.**). **Table 4** shows the proton signals for gedunin, kneaded and freeze-dried complex with HBD. NMR spectroscopy has been widely used to investigate cyclodextrin inclusion complexes (Floury et al., 2016). A cursory look at the differences between the major protons of complexed gedunin relative to that of the intact gedunin shows similar magnitude between the proton signals. However, looking at the intensities of the signals for the freeze-dried sample and considering that the kneaded samples (**Fig. 5.**) were prepared in the same mole fraction as the freeze-dried, the latter had all proton signals

with higher intensities than the kneaded samples. From **Table 4**, it is also evident there is not much difference in the proton signals of both the kneaded and freeze-dried products. From the columns on the subtraction of the chemical shift values from that of intact gedunin, very similar differences were produced in the signals obtained for both formulated products. Very close values were particularly obtained for protons on carbon numbers 4, 8, 18 and 22.

Some of the protons experienced a significant shielding effect in which the proton signals obtained for the complex had lower chemical shifts values compared to gedunin alone. This implies that such protons must be within the core of the complex and those exposed to the outside were found to be deshielded (i.e. possessing higher chemical shift values than the intact gedunin moiety).

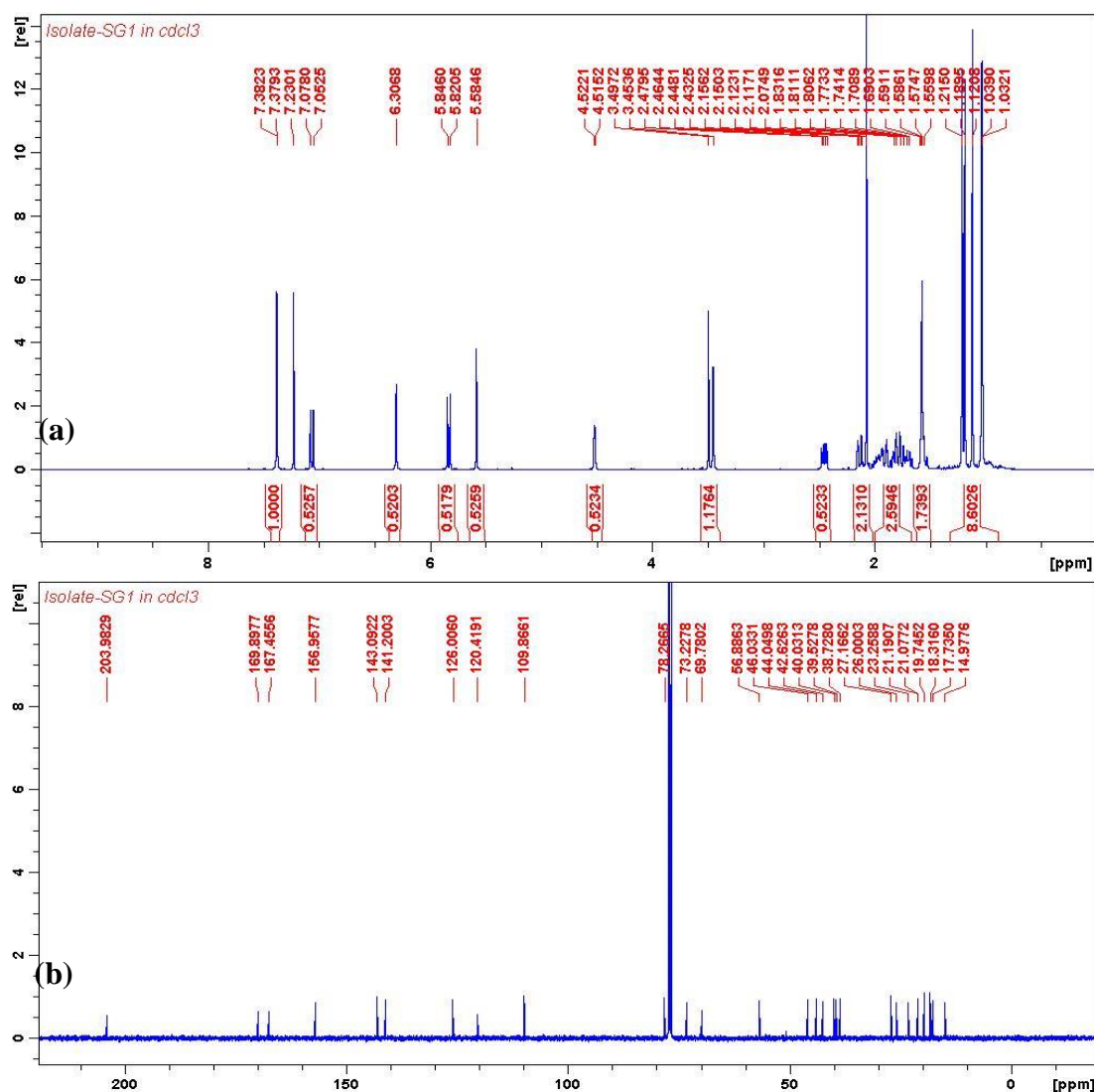


Fig. 4. (a) ^1H NMR and (b) ^{13}C NMR for gedunin in deuterated Chloroform

Shielding implies that the protons are held in a more magnetically enriched environment and hence a stronger amount of energy is required to bring them into resonance. Functional groups within the gedunin molecule that is involved in the binding of gedunin through hydrophobic interaction in the interior of the HBD molecule will shield the protons from the environment generating low chemical shift values.

From **Table 4**, some of the protons that experienced shielding are those on Ring A (proton numbers 2 and 4); Ring B (protons numbers 5, 6, 8 and 9); Ring C (proton numbers 11, 12 and 13) and Ring E (proton number 19). A small shielding effect was

observed for proton number 18 on ring D with the freeze-dried product was which actually deshielded in the kneaded proton, this thus appears insignificant for the consideration of the complex formation. This is the evidence of the guest inclusion in the cyclodextrin cavity (Schneider et al., 1998; Shah et al., 2010). Some of the protons experiencing deshielding are notably those near the few mildly polar functional groups and thus these may be at the outer portion of the cyclodextrin. The classical protons that seem to point to the positioning of the gedunin in the hydrophobic core of the complex are those on Rings A and B as well as proton 19 on Ring E.

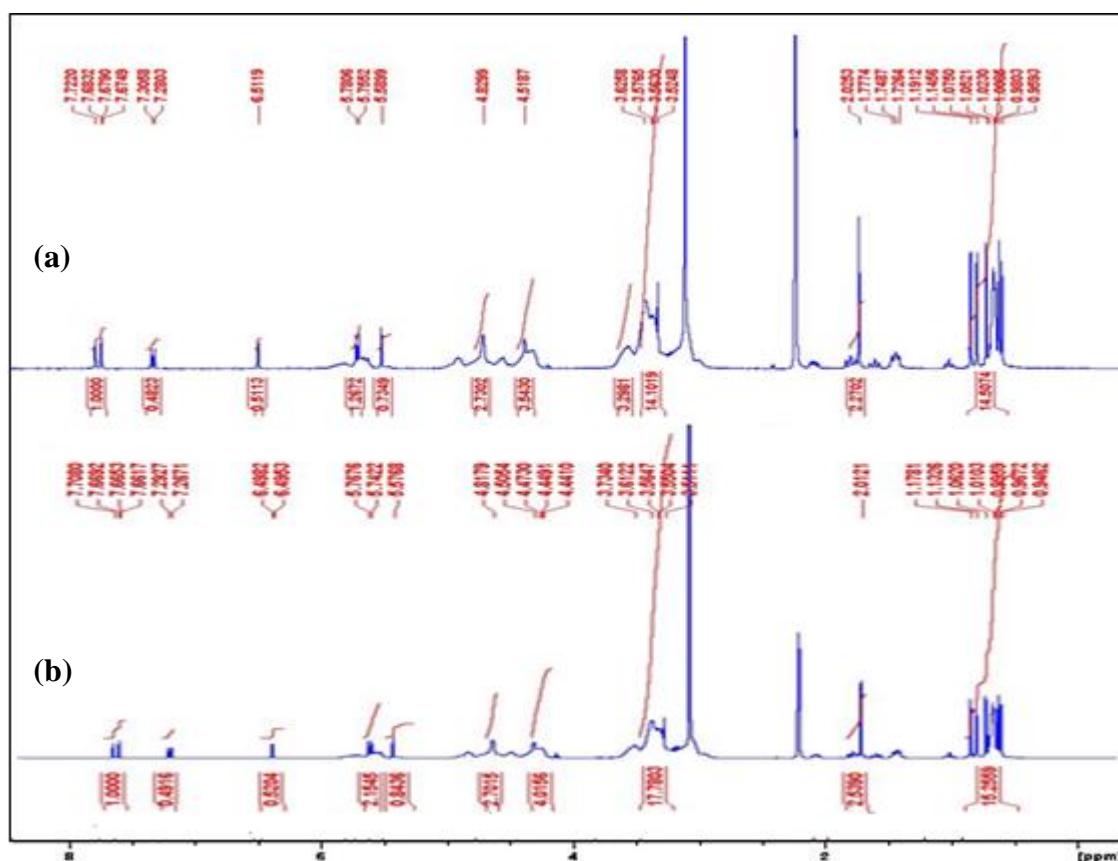


Fig. 5. ^1H NMR spectrum for GCD prepared by (a) kneading method; (b) freeze-dried method

There thus seem to a conformation that permit the Rings A and B and part of Ring E to be positioned in the core of HBD while Rings C and D are at the outer region alongside the remaining portions of Ring E. The few exceptions to this submission are those protons on Ring C (C-11) which experienced slight shielding especially the axial protons and the C-13 methyl protons which are also out of plane with the ring. The positioning of these two protons may actually contribute to their being shielded when the molecule undergoes a twisting to fit into the hydrophobic core of HBD.

In summary, the presence of shielded protons has justified the formation of an inclusion complex between HBD and gedunin and the observance of deshielded protons points to the idea that not the entire gedunin molecule is trapped into the core of the complex (Cabral and Pugh., 1990; Celin and

Nagarajan., 2014). Nevertheless, the fraction trapped may be sufficient to enhance the apparent solubility of gedunin. Biopharmaceutics Classification System (BCS) is a scientific tool used for classifying drugs based on their aqueous solubility and intestinal permeability characteristics. In general, formulation techniques that increase aqueous solubility of Class II and Class IV drugs without decreasing their lipophilicity will enhance their absorption through biological membranes (Loftsson et al., 2005). Gedunin can be regarded as a class II (low solubility and high permeability) compound on the BCS because of its lipophilicity. Thus, the complexation between gedunin and HBD should have a positive effect on the absorption of gedunin after oral administration.

Table 4. Proton Chemical Shifts values for GCD compared with gedunin alone

C/H no.	$\delta(^1\text{H})$ –Gedunin	$\delta(^1\text{H})$ –GCD (Kneaded)	$\delta(^1\text{H})$ –GCD (Freeze dried)	Difference between δ of gedunin and GCD (Kneaded)*	Difference between δ of gedunin and GCD (Freeze- dried)*
Ring A					
1	7.065(1H, <i>d</i>)	Not detected	Not detected		
2	5.8333 (1H, <i>dd</i>)	5.7679 (<i>d</i> , <i>J</i> =10.16 Hz)	5.7549 (<i>d</i> , <i>J</i> =10.16 Hz)	+0.0654	+0.0784
3					
4(methyl groups)	1.2224 (6H)	1.0521	1.0620	+0.1703	+0.1604
Ring B					
5	1.2335 (1H) 1.54-1.566 (2H)	1.0750 1.1456	1.0620 1.1326	+1.1585 +0.4204	+0.1715 +0.4334
6 (methyl group on acetyl substituent)	2.0820 (3H)	2.0253	2.0121	+0.0567	+0.0699
6	3.48 (1H)	3.5725	3.5111	-0.0925	-0.0311
7 (Methyl group – endocyclic)	1.1279 (3H)	1.1456	1.1326	-0.0177	-0.0047
8 (endocyclic)	1.5405 (1H)	1.1912	1.1781	+0.3493	+0.3624
9 (methyl group)	1.2335 (3H)	1.0750	1.0620	+0.1585	+0.1715
10	1.5988 (1H)	1.7508	Not detected	-0.152	-
Ring C					
11	1.2335 (Axial) 1.5660 (Equatorial) [2H]	1.0750 1.7508	1.0620 Not detected	+0.1585 -0.1848	+0.1715 -
12	1.2335 (Axial) 1.5405 (Equatorial) [2H]	1.0750 1.7508	1.0620	+0.1585 -0.2103	+0.1715
13			Not detected		-
C-13 methyl group	1.1279 (3H) – methyl protons	1.0750	1.0620	+0.0529	+0.0659
Ring D					
14					
15	3.4972 (1H, <i>s</i>)	3.6258	3.6122	-0.1286	-0.1150
16					
17	5.5846 (1H, <i>s</i>)	5.5899	5.5768	-0.0053	+0.0078
Ring E					

19	7.3808 (1H, d)	7.2931 (d, $J=10.2$ Hz)	7.2799 (d, $J=10.24$ Hz)	+0.0877	+0.1009
20	6.3068 (1H, s)	6.5119 (s)	6.4968 (weak splitting, $J=1.16$ Hz)	-0.2051	-0.91
21					
22	7.0653 (1H, dd)	7.6898 (dd, $J=18.84$ and 1.68 Hz)	7.6761 (dd, $J=18.52$ and 1.56 Hz)	-0.6245	-0.6108
18 (methyl)	1.1279(3H) CH ₃	1.0750	1.0620	+0.0529	+0.0659
19	1.2335(3H)	1.0750	1.0620	+0.1585	+0.1715
20 (methyl)-endocyclic)	1.1279(3H)	1.1456	1.1326	-0.0177	-0.0047
24,25(2-methyl group)	1.2224(6H)	1.0521	1.0620	+0.1703	+0.1604
26,27(OCOCH ₃)	2.0820(3H)	2.0253	2.0253	+0.0567	+0.0699

Note: *a*Integrals in parenthesis; s=singlet; d=doublet; dd=doublet of doublet; *positive sign (proton shielded relative to gedunin), negative sign denotes deshielding

3.3. Powder X-ray diffraction (PXRD)

Figure 6 shows the PXRD patterns of gedunin, HBD and GCD obtained *via* kneading and freeze-drying. Gedunin displayed some distinct peaks at $2\theta = 6.98, 12.40, 18.85, 24.78, 25.58$ and 27.71 which are absent in GCD due to complexation. The PXRD diffraction patterns of the complexes are completely different from starting materials. New diffraction peaks in the spectrum and the shift of the representative guest molecule peaks as well as the changes in their relative intensity confirm the formation of a new solid phase and complexation (Mura, 2015). Quantitative estimation of the 2θ PXRD patterns of GCD (kneading) and GCD (freeze-dried) revealed

that the major peaks in the PXRD patterns of GCD (kneading) were observed at $2\theta = 5.64, 6.22, 8.22, 10.48, 12.37, 12.99, 13.71, 14.44, 15.44, 16.15, 17.11, 18.66, 20.57$ and 21.11 while those of GCD (freeze-dried) were observed at $2\theta = 5.73, 6.17, 8.34, 10.38, 10.55, 12.33, 12.87, 13.69, 14.31, 15.49, 16.44, 17.06, 18.42, 20.64$ and 21.16 .

Powder X-ray diffractometry is an appropriate procedure for establishing the molecular state of an inclusion complex (Singh et al., 2010). The closeness of 2θ values for GCD prepared by the different method in the PXRD analysis strongly implies that the two methods (freeze-drying and kneading) produced similar complexes.

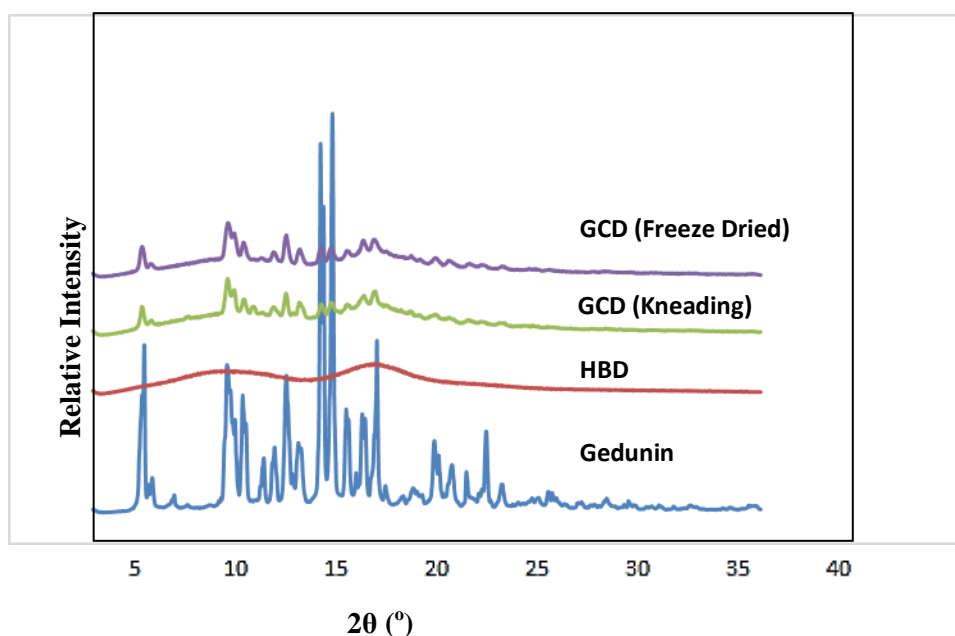


Fig. 6. Powder X-ray diffraction patterns of Gedunin, HBD, GCD (kneading) and GCD (freeze-dried)

3.4. Comparison of the methods (Kneading and Freeze-drying methods)

The two methods had almost the same yield of ~69%. The freeze-drying method was completed within a shorter time of about 30 hrs as compared to kneading method which took 3 days to get the product. In addition, the freeze-drying may be a better method for the

preparation of the inclusion complex since the proton signals of the freeze-dried complex had higher intensities. (Veiga et al., 2001; Shah et al., 2010).

4. Conclusions

Pure Gedunin was successfully isolated and characterized to ascertain its structure. The inclusion complex of gedunin (GED) and 2-hydroxypropyl- β -cyclodextrin (HBD) was prepared using kneading and freeze-dried methods. The complexes were characterized using elemental analysis, FT-IR, ^1H NMR and PXRD. These characterization methods support inclusion complex formation. The entire gedunin molecule was not trapped in the cyclodextrin cavity but the partial entrapment may be sufficient to improve the aqueous solubility of the complexes thus increasing possibility of pharmaceutical formulation and oral administration of gedunin. The studies revealed that freeze-dried method presents higher efficiency in terms of shorter time of preparation compared to kneading method especially for large scale industrial production. This makes the complexes potential therapeutic agents suitable for subsequent applications.

Acknowledgement

Author appreciates the Staff Development Award from University of Ilorin, Ilorin, Nigeria which led to the execution of part of the study.

Conflict of interest

The authors declare that the research was conducted in the absence of any commercial or financial relationships that could be construed as a potential conflict of interest.

References

1. Akisanya A, Bevan CW, Halsall TG, Powell JW, Taylor DAH (1961) West African Timbers, Part IV, Some Reactions of Gedunin. *J Chem Soc* 3705-3708.
2. Cabral Marques HM, Pugh WJ (1990) Studies of cyclodextrin inclusion complexes II. Molecular modeling and ^1H -NMR evidence for the salbutamol- β -cyclodextrin complex. *International Journal of Pharmaceutics*. 63(3): 267-274.
3. Carneiro SB, Costa Duarte FÍ, Heimfarth L, et al. (2019). Cyclodextrin–drug inclusion complexes: *in vivo* and *in vitro* approaches. *Int J Mol Sci* 20:642.
4. Celin TS, Nagarajan S (2014) Inclusion complexation of 2-aminopyrimidines with β -cyclodextrin, physico-chemical and nuclear magnetic spectroscopic studies. *Materials Science-Poland* 32(1): 39-44.
5. Connolly JD, McCrindle R, Overton KH, Warnock WDC (1967) Tetranortriterpenoids- III; 6-Hydroxy and 6-acetoxy-methyl angolensate from heartwood of *Khaya grandifoliola*. *Tetrahedron* 23: 4035 - 4039.
6. Corti G, Capasso G, Maestrelli F, Cirri M, Mura P (2007) Physical-chemical characterization of binary systems of metformin hydrochloride with triacetyl- β -cyclodextrin. *J Pharm Biomed Anal* 45: 480-486.
7. Floury M, Landy D, Ruellan S, Auezova L, Greige-Gerges H, Fourmentin S (2016) Determination of formation constants and structural characterization of cyclodextrin inclusion complexes with two phenolic isomers: carvacrol and thymol. *Beilstein J Org Chem* 12: 29–42. doi:10.3762/bjoc.12.5
8. Gowardhane AP, Kadam NV, Dutta S (2014) Review on Enhancement of Solubilization Process. *American Journal of Drug Discovery and Development* 4: 134-152.
9. Hofer M, Greger H, Mereiter K (2009) 6 α -Acetoxygedunin. *Organic compounds, Acta Crystallographica Section E*. E65, o1942–o1943.
10. Hui BY, Zain NNM, Mohamad S, Prabu S, Osman H, Raoov M (2020) A comprehensive molecular insight into host-

- guest interaction of Phenanthrene with native and ionic liquid modified β -cyclodextrins: Preparation and characterization in aqueous medium and solid state, *Journal of Molecular Structure* 1206: 127675.
<https://doi.org/10.1016/j.molstruc.2019.127675>.
11. Jambhekar SS, Breen P. Cyclodextrins in pharmaceutical formulations II: solubilization, binding constant, and complexation efficiency (2016) *Drug Discovery Today* 21(2): 363-368.
doi.org/10.1016/j.drudis.2015.11.016.
12. Jansook P, Ogawa N, Loftsson T (2017) Cyclodextrins: Structure, physicochemical properties and pharmaceutical applications. *International Journal of Pharmaceutics* 535: 272-284.
13. Loftsson T, Jarho P, Masson M, Jarvinen T (2005) Cyclodextrins in Drug Delivery. *Expert Opinion on Drug Delivery* 2(2): 335 - 351.
14. MacKinnon S, Durst T, Arnason JT, Angerhofer C, Pezzuto JM, Sanchez-Vindas PE, Poveda LJ, Gbeassor FM (1997) Antimalarial activity of Tropical Meliaceae extracts and Gedunin Derivatives. *Journal of Natural Products* 60: 336-341.
15. Mura P (2015) Analytical techniques for characterization of cyclodextrin complexes in the solid state: a review. *Journal of Pharmaceutical and Biomedical Analysis* 113(10): 226-238.
<http://doi.org/10.1016/j.jpba.2015.01.058>.
16. Ohochuku NS, Powell JW (1966) Nuclear Magnetic Resonance Spectroscopy, The Bandwidths of the Singlets in Gedunin and its Simple Derivatives. *Chemical communications London* 13: 422-423.
17. Okhale SE, Amupitan JO, Ndukwe IG, Oladosu PO, Okogun JI (2012) Synthetic modification of gedunin and comparative antibacterial activity of gedunin and 7-deacetoxy-7 α -hydroxygedunin potassium salt. *African Journal of Pure and Applied Chemistry* 6(14):183-189.
18. Ologe MO, Adegoke AO, Iwalewa EO, Ademowo OG (2016) Spectrophotometric studies of a novel Gedunin-2-Hydroxypropyl- β -cyclodextrin binary complex. *African Journal of Medicine and Medical Sciences* 45:159-169.
19. Omar S, Zhang J, MacKinnon S, Leaman D, Durst T, Philogene BJR, Arnason JT, Sanchez-Vindas PE, Poveda L, Tamez PA, Pezzuto JM (2003) Traditionally Used Antimalarials from the Meliaceae. *Current Topics in Medicinal Chemistry* 3: 133-139.
20. Sambasevan KP, Mohamad S, Sarih NP, Ismail NA (2013) Synthesis and Characterization of the inclusion Complex of β -Cyclodextrin and Azomethine. *Int J Mol Sci* 14: 3671-3682.
21. Schneider HJ, Hacket F, Rüdiger V, Ikeda H (1998) NMR studies of cyclodextrins and cyclodextrin complexes. *Chemical Reviews* 98(5): 1755-1785.
22. Shah MR, Sancheti PP, Vyas VK, Karekar PS, Pore YV (2010) Proton magnetic resonance (^1H NMR) spectroscopy and Physicochemical studies of Zaleplon-hydroxypropyl- β -Cyclodextrin inclusion compounds. *Drug discoveries and Therapeutics* 4(2): 70 -76.
23. Singh R, Bharti N, Madan J, Hiremath SN (2010) Characterization of Cyclodextrin Inclusion Complexes – A Review. *Journal of Pharmaceutical Science and Technology*. 2(3): 171-183.
24. Srivalli KM, Mishra B (2016) Improved aqueous solubility and antihypercholesterolemic activity of ezetimibe on formulating with hydroxypropyl- β -cyclodextrin and hydrophilic auxiliary substances. *AAPS PharmSciTech* 17:272-83.

25. Stella VJ, He Q (2008) Cyclodextrins. Toxicologic Pathology 36 (1):30-42.
26. Subramaniam, P, Mohamad S, Alias Y (2010) Synthesis and Characterization of the inclusion Complex Dicationic Ionic Liquid and β -Cyclodextrin. Int J Mol Sci 11: 3675 -3685.
27. Taylor DAH (1974) ^{13}C nuclear magnetic resonance spectra of some limonoids. Part I. The structure of procerin, an extractive from *Carapa procera*. J Chem Soc Perkin Trans1: 437–441.
28. Veiga F, Fernandes C, Maincent P (2001) Influence of the preparation method on the Physicochemical properties of Tolbutamide/Cyclodextrin binary systems. Drug development and Industrial pharmacy 27(6): 523- 532.
29. Yang X, Ke W, Zi P, Liu F, Yu L (2008) Detecting and identifying the complexation of nimodipine with hydroxypropyl- β -cyclodextrin present in tablets by Raman spectroscopy. J Pharm Sci 97: 2702-2719.
30. Wankar J, Kotla NG, Gera S, Rasala S, Pandit A, Rochev YA (2020) Recent Advances in Host–Guest Self-Assembled Cyclodextrin Carriers: Implications for Responsive Drug Delivery and Biomedical Engineering. Advanced Functional Materials 30: 1909049 (1-27).
31. Yuan C, Jin ZY, Xu XM (2012) Inclusion complex with hydroxylpropyl- β -cyclodextrin: UV, FTIR, ^1H NMR and molecular modeling studies. Carbohydrate Polymers 89(2): 492-496.



„George Emil Palade” University of Medicine, Pharmacy,
Science and Technology of Târgu Mureș
38 Gheorghe Marinescu Street, Târgu Mureș, 540139, ROMANIA
Telephone: +40-265-21 55 51; fax:+40-265-21 04 07

abmjourn@umfst.ro
www.abmj.ro